ABSTRACT

LLEWELLYN, NICHOLAS THOMAS. An Evaluation of the Rooftop PV and Solar Water Heating Systems at the NCSU Solar House. (Under the direction of Drs. Stephen D. Terry and Herbert M. Eckerlin).

The NCSU Solar House is a passive solar home on the campus of North Carolina State University. It has many features designed to make use of solar energy, including: a central sunspace, two Trombe walls, solar lighting fixtures, as well as many other energy-conserving details. This thesis aims to evaluate the current status of the two main active systems of the NCSU Solar House: the rooftop solar photovoltaic (PV) system and the solar water heating system (SWHS). Data pertaining to the performance of these systems has been collected over several months in 2018 and 2019. These data are used to observe patterns due to weather and seasons, calculate relevant performance parameters, as well as to compare house energy production and usage.

Based on the available data, the overall performance of the PV system is found to compare well with similar systems from the literature, with notes are made of underlying assumptions used in the analysis. Results show noticeable variations in performance for both systems attributable to both current weather conditions and season. Potential specific reasons for these results are presented alongside them.

Lastly, recommendations are made for modifications to the house in order to enable further research. Limitations from the current monitoring setup must be altered to increase the accuracy of prospective work. Given the necessary alterations, there is a large amount of analysis which may be done in the future to gain further understanding of the performance of these two active systems at the house, as well as the house's overall design.

An Evaluation of the Rooftop PV and Solar Water Heating Systems at the NCSU Solar House

by
Nicholas Thomas Llewellyn

A thesis submitted to the Graduate Faculty of
North Carolina State University
in partial fulfillment of the
requirements for the degree of
Master of Science

Mechanical Engineering

Raleigh, North Carolina

2019

APPROVED BY:

_____	_____
Dr. Stephen D. Terry	Dr. Herbert M. Eckerlin
Co-Chair of Advisory Committee	Co-Chair of Advisory Committee

_____
Dr. Joseph F. DeCarolis

DEDICATION

For my loving wife and best friend, Madeline.

BIOGRAPHY

Nicholas Thomas Llewellyn was born in Huntsville, AL to father Peter and mother Terri and raised in nearby Madison. He is the youngest of three brothers - Patrick, Andrew, and himself. As a child, he enjoyed playing sports such as baseball, basketball, and soccer. Throughout middle and high school, Nicholas played trombone in both concert and marching band. Nicholas chose to attend the University of Alabama to pursue his college education.

Unsure of which major to select during freshman orientation, he followed a suggestion from his parents to begin in the mechanical engineering track. The most important event during his time at UA was when Nicholas met his future wife, Madeline Grace Shipley. The two dated for the next six years while Nicholas completed his B.S.M.E. (2015) and Madeline completed both her B.S. (2014) and M.S. (2016) in human development and family science.

Upon graduating, Nicholas accepted a position at Intergraph Corporation in his hometown. During his time there, he gained many skills related to engineering software and general workplace functionality. Nicholas and Madeline were married in November of 2016. In the fall of 2017, the two moved to Raleigh, NC for Nicholas to begin work on his M.S.M.E. at North Carolina State University. The past two years spent in Raleigh have been enjoyable for Nicholas and Madeline, but they are excited to bring this chapter of their lives to a close and look forward to the next one.

ACKNOWLEDGEMENTS

I would like to first thank Dr. Terry for allowing me to study the NCSU Solar House, for his constant advice and input, and for the opportunity to work at the Industrial Assessment Center during my time at NC State. The knowledge I have gained during this time will serve me well in my future career. I would also like to thank my other committee members for agreeing to serve on my advisory committee and for providing useful feedback regarding my work. Specifically, thank you to Dr. Eckerlin for designing and building the NCSU Solar House in 1981. The house is an important resource for anyone interested in passive solar design and I am glad to have had the chance to study and learn from it. Thanks also to Dr. DeCarolis for his part in my education regarding energy use, its effects on our environment, and the complex issues regarding mitigation strategies. I have learned much from you and know that many future students will as well. Thanks also to everyone at the IAC for your encouragement and comradery. I have enjoyed our time spent working together and commiserating over our shared academic difficulties. I know that you will all be successful in the future and wish nothing but the best for each of you.

Finally, unending thanks and love to my family. To Madeline, for the unbelievable patience and love she showed me when I was irrational and overly anxious. I am extremely fortunate to have a spouse as caring and scientifically-literate as you, as it often seems you understand my work better than I do. To the Shipley family, for their constant kindness and support. To Patrick and Andrew, for their invaluable friendship and advice through the years. I am very lucky to call you my brothers and have you to look up to. I lastly thank Mom and Dad, for raising me, unconditionally loving and supporting me, and for providing every opportunity I've had in life. I will never be able to thank you enough for all that you have done and continue to do for me.

TABLE OF CONTENTS

LIST OF TABLES

LIST OF FIGURES

Chapter 1

Background and Introduction

The NCSU Solar House is a model passive solar residential building located at 1201 Gorman Street on the campus of North Carolina State University in Raleigh, NC. The house was designed by NC State University Professor Dr. Herbert Eckerlin and constructed in 1981. The house was built to educate the public on how solar energy can be used in residential settings, and to serve as a platform for research for students and faculty at NC State. The house includes many energy-conserving features while keeping with a regionally conventional appearance. The house was originally fully-furnished and equipped with built-in monitoring devices to collect data used for performance evaluation. Figure 1.1 is a picture taken from the Northwest side of the house showing the front entrance.

Figure 1.1: Northwest view showing front of NCSU Solar House.

Some of the many features which are included in the house are: an active solar domestic water heating system, rooftop solar photovoltaic (PV) panels, earth-bermed north and west first level walls, operational insulating shutters, two single-level Trombe walls, a rock bed thermal storage system, and a two-level sunspace [1]. The Solar House is currently co-operated by the NCSU Department of Mechanical and Aerospace Engineering and the NCSU Engineering Place, a K-12 outreach center which holds summer camps and workshops to promote engineering education.

Over the past 38 years, the house has been the subject of numerous graduate theses at NC State [2]–[5]. However, the majority of the research done concerning the house was completed roughly within the first decade following its construction and has focused on evaluating the passive features of the house (sunspace, Trombe walls, etc.). In order for the house to continue to serve as a topic for new research, its monitoring systems must be reevaluated and updated with useful, modern features. As a first effort towards this goal, this report aims to evaluate the current state of the two main active features in the house (the solar water heating and rooftop PV systems), present useful information that can be gained from their current setup, and propose monitoring setups for these systems which will more readily support research and performance testing.

The report begins with a brief description of the systems considered, their respective operating principles, and details of their use at the NCSU Solar House. This is followed by a review of the relevant literature and results drawn from the data collection currently being done at the house. Finally, ideas and recommendations for future work at the house are presented.

1.1 Solar Photovoltaics Overview

Solar photovoltaic (PV) panels (such as those installed on the roof of the NCSU solar house) make use of a physical phenomenon known as the photovoltaic effect (also known as the

photoelectric effect). Simply put, the photovoltaic effect is the generation of a voltage within a material upon exposure to light. It was first discovered in 1839 by French physicist Edmond Becquerel and later studied by Albert Einstein, who won a Nobel prize for his description of it [6]. An explanation of how the photovoltaic effect is applied to solar cells is presented below.

A solar PV cell is made up of two sections of semiconductor material, which exhibits electrical conductivity properties in-between conductors and insulators. The most common material used for solar cells is silicon, due to its abundance and cost-effectiveness [7]. A silicon atom has four electrons present in its outermost band (known as the valence band) [8]. All of these valence electrons are shared with adjacent atoms in silicon's face-centered cubic crystalline structure, shown below in Figure 1.2 [8].

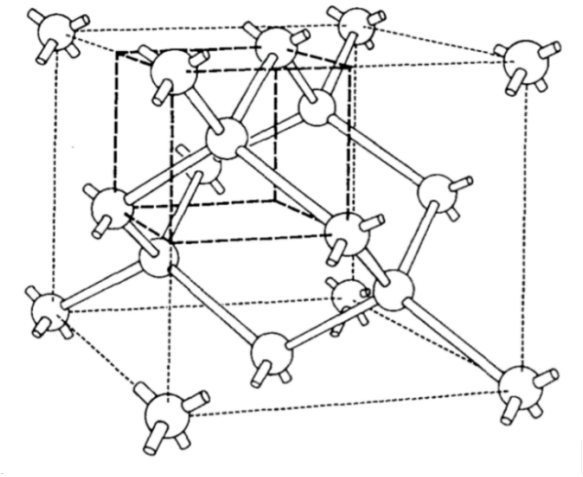

Figure 1.2: Silicon's crystalline structure [8].

When sufficient light energy is absorbed by a silicon atom, an electron in the valence band can be freed from its bond and transition to the conduction band, where it is free to move throughout the crystal structure [8]. The amount of energy needed for this transition to occur in a specific material is known as the band gap energy [8]. The band gap energy for silicon is 1.1 eV [8]. Normally, the freed electron would simply move around for some amount time before

returning to its original state, with the imparted energy dissipated as heat [8]. In a solar PV cell, two layers of silicon are used, and each of the two sections are "doped", or modified with impurities, in order to create an internal electric field [8]. One section of the cell is doped with a material (such as phosphorous) whose atoms have enough electrons to fulfill all of the bonds in a typical silicon crystal with one left unused [8]. This section is referred to as the n-type section, since it has an excess of negative charge carriers (electrons) [8]. The second section of silicon is doped with a material (such as boron) which has only three electrons in its valence band, leaving an "electron hole" where an electron is usually present in a pure silicon structure [8]. This section is known as the p-type section, referring to the presence of excess positive charge carriers (electron holes) [8]. It is important to note that at this point, both sections are independent and remain electrically neutral. When the two sections of silicon are brought into contact with each other, a negative charge builds up on the p-type side of the meeting point while a positive charge builds up on the n-type side, as shown in Figure 1.3 [9]. This local buildup of opposite charges results in a fixed electric field that is vital to the operation of a solar PV panel.

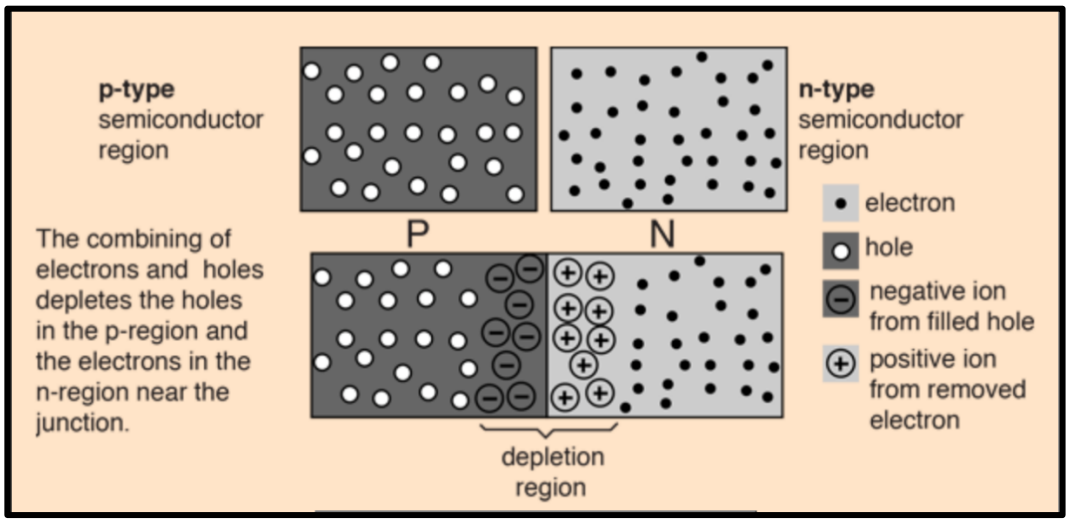

Figure 1.3: Operating principle of a pn-junction [9].

When sunlight strikes the n-type portion of the material, an electron is freed and leaves behind an electron hole. The electron hole "moves" (by way of electrons filling it in) across the junction, as it is attracted by the negative charge presence just across the meeting point on the p-type side [8]. This process repeats and leads to an overall positive charge now building on the p-type side of the cell, while an overall negative charge is established on the n-type side of the cell [8]. If the n- and p-type sections of the cell are electrically connected to form a circuit with a load between them, as seen in Figure 1.4, electrons will flow through the circuit from the n-type side to the p-type side and do useful work on the load along the way [8].

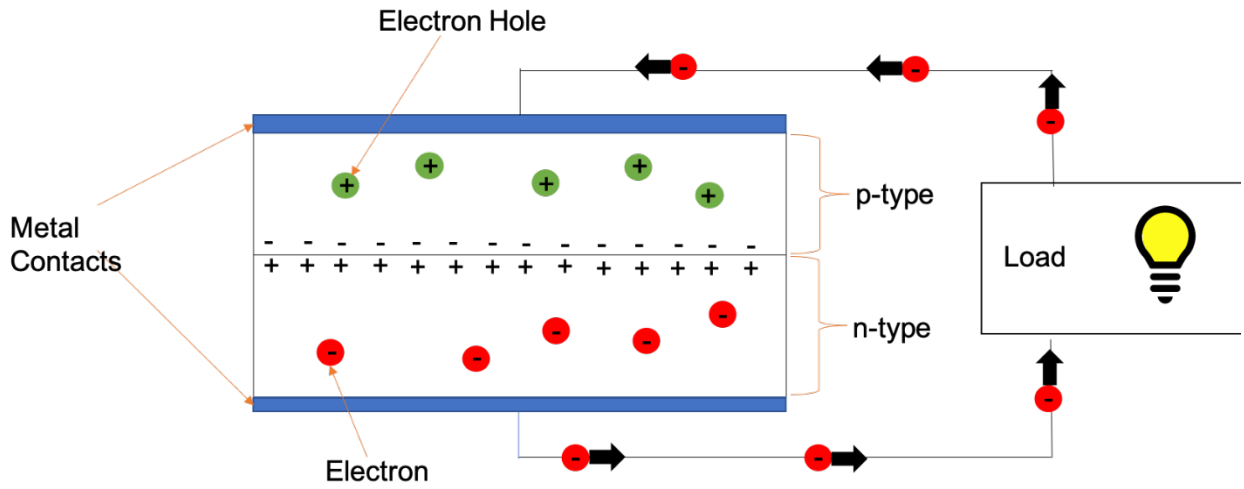

Figure 1.4: Photovoltaic cell with attached load.

The basic operating principle of a solar PV cell has been outlined above, but there are many constraints in the real world which limit the efficiency of converting sunlight directly to electrical energy in a PV system. Some of these factors are: incident light with energy that is too low or high, electron-hole recombination, and operating temperatures that are too low or high [10].

If light absorbed by the solar cell has insufficient energy to free an electron into the conduction band, the energy is dissipated as heat [8]. If the light has energy which is higher than

the band gap energy, the amount needed to free one electron is used, but the rest is dissipated as heat [8]. The goal in solar cell design is therefore to match the band gap energy of the material to the energy of the incoming light [8]. Direct electron-hole recombination occurs when freed electrons encounter electron-holes and recombine, which keeps these charge carriers from contributing to the electrical current flow [10]. Indirect recombination refers to when electrons or electron holes encounter defects in the crystalline structure of the solar cell and combine with other charge carriers present there [10]. Photovoltaic systems are highly dependent on operating temperature of the panels [8]. As temperature rises, physical effects within the material can significantly reduce overall efficiency [8].

While the condition of the PV panels is critical to a solar PV system's performance, there are other essential components. These may include: a combiner box, DC disconnect switch, charge controller, battery bank, inverter, AC disconnect switch, breaker panel, and energy monitoring meters. In the combiner box, the output from multiple sets of panels (wired in series) is combined into one parallel circuit in order to increase the total output current [11]. Sets of PV panels are commonly wired in series prior to entering the combiner box in order to raise the voltage of the system to a value acceptable to the inverter [11]. Figure 1.5 shows an example of typical combiner box wiring.

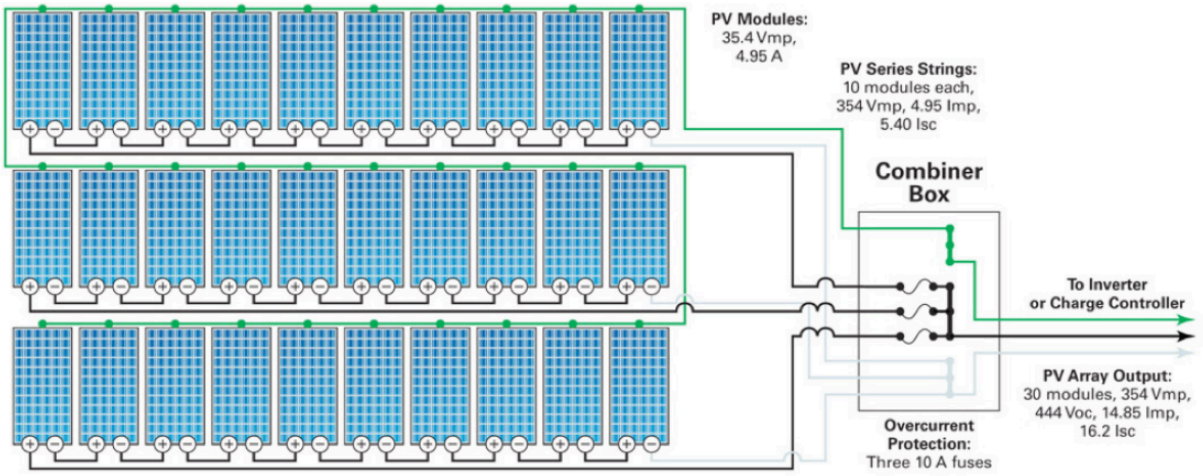

Figure 1.5: Typical combiner box wiring configuration [11].

The DC disconnect switch is a safety feature which allows for the panels to be disconnected from the rest of the system [11]. In systems containing batteries, charge controllers are used to regulate the amount of charge entering the batteries. The inverter is a crucial piece of equipment, as it converts the DC power output from the panels into AC power which can be fed into the electrical grid. The AC disconnect switch is another safety switch which allows the PV system to be easily disconnected from the grid for troubleshooting and maintenance [11]. Breaker panels are common in residential settings and connect the loads of the residence to the utility grid. Energy meters are used by utility providers to determine energy use by customers, while additional meters may be included for the owner's personal use.

1.2 NCSU Solar House PV System

The array of PV panels on the NCSU solar house consists of three horizontal rows of eight SunPower SPR-225 panels which altogether occupy a rectangular area about 21 feet wide by 15 feet tall [12]. Each panel has a peak DC power rating of 225 W, therefore making the total peak DC power for the array 5.4 kW [12]. The panels are rated at 41 V and 5.49 A, and their efficiency is given by the manufacturer as 18.1% [12]. The panels are fixed-mounted (they do not track vertically or horizontally) on the south side of the roof and lie at the same angle as the

roof itself (36° from horizontal). The array was installed in 2008 and replaced a 2.5 kW system which had been in use since 1992 [13], [14]. Figure 1.6 is a picture of the south side of the house, showing the solar PV array on the center roof.

Figure 1.6: Rear (south-facing) side of the NCSU Solar House.

The PV system does not include a charge controller or battery bank - all of the power from the panels is fed directly into the utility grid. The inverter used at the Solar House is a SunPower SPR-6000m model, which carries a peak rated conversion efficiency of 97% [15]. It is rated to operate between 250 and 600 V and has a maximum DC input current of 25 A [15]. The inverter also features a digital readout which displays values pertaining to system operation, including: total energy produced for the day, input DC voltage, output AC power, and total energy produced for the device since installation [15].

Based on the rated voltage and current of the PV panels and the inverter, it is believed that each horizontal row of 8 panels is wired in series, then these three series-wired rows are combined in parallel inside a combiner box. This configuration yields an overall array rated voltage and current of 328 V 16.47 A, respectively, which is acceptable for the inverter [15]. Specification sheets for the SunPower SPR-225 panel and SPR-6000m inverter are included in

Appendix A and B, respectively. Figure 1.7 is a general overview of the PV system layout at the house.

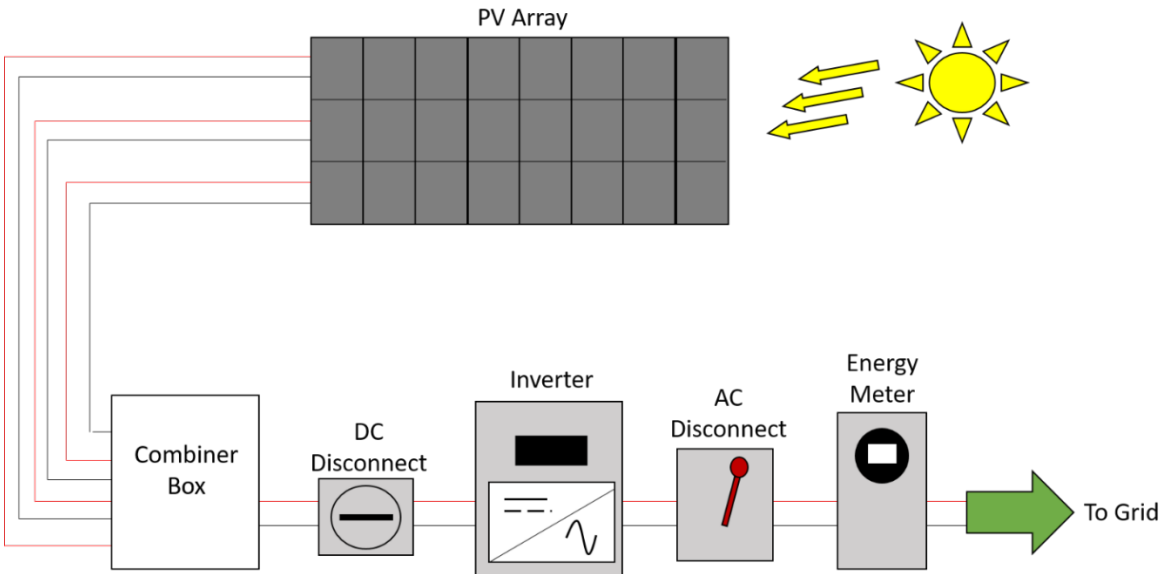

Figure 1.7: PV system components at NCSU Solar House.

1.3 Solar Water Heating Systems Overview

The basic goal of a solar hot water heating system (SWHS) is to capture energy from sunlight, convert it to heat, then transfer that heat to water for domestic use. This is achieved by either: (a) transferring the heat directly to water ("direct" system) or (b) transferring the heat to an intermediate fluid which then exchanges the heat with water ("indirect" system). Direct systems are typically employed in areas where temperatures rarely drop below the freezing point for water [16]. Solar water heating systems may also be categorized as active or passive systems. An active system uses electrically powered pumps and controllers to drive and monitor the flow. A passive system instead makes use of natural convection to move warm water up into a storage tank (installed above the solar collector) [16]. A diagram of an active, indirect solar water heating system is shown below in Figure 1.8.

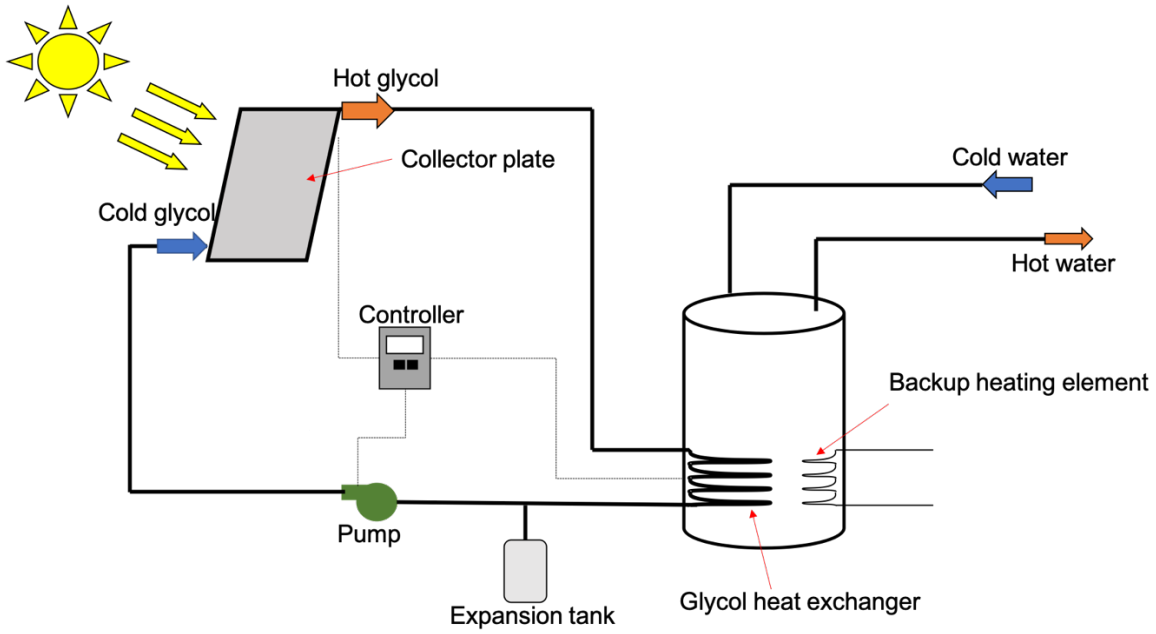

Figure 1.8: Active, indirect solar water heating system.

One of the main components of a solar hot water heating system is the solar collector itself. The most common type used for residential applications is the flat plate collector (FPC), due to its affordability and simple installation [16]. FPCs are insulated, weatherproof boxes which contain internal tubing. The top of the box is covered by a transparent glazing (usually glass) with an antireflective coating, while the inner back panel of the box holds a dark, highly absorptive plate which converts sunlight to heat and transfers it to the tubes [17]. The tubes contain the heat transfer fluid and are typically configured in a header-riser design (shown in Figure 1.9). This tube layout presents issues however, as there may be uneven flow in the riser tubes [17]. To prevent this, an alternative design such as serpentine tubing (also shown in Figure 1.9) may be employed. One drawback to the serpentine design is that it requires a pump to circulate the fluid, and therefore cannot be used with passive systems [17]. Other collectors, such as the evacuated-tube (ETC) type, may be used in applications where higher temperatures are

required. While they are typically more efficient, they also have a higher initial cost than FPCs [17].

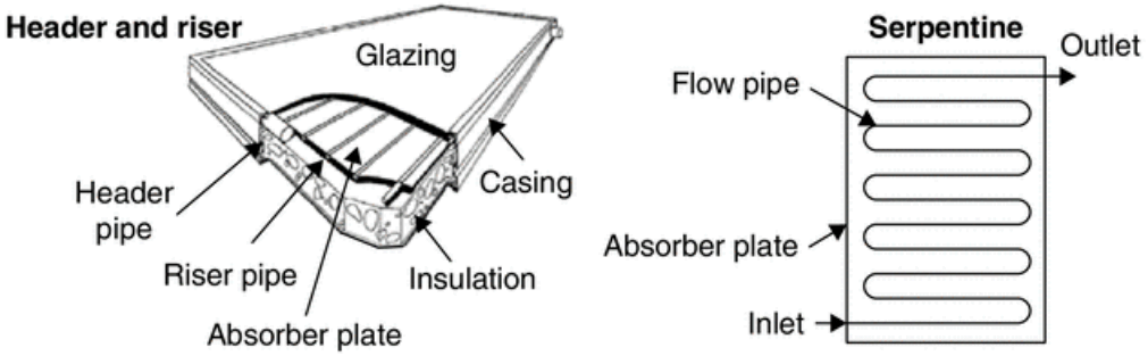

Figure 1.9: Header-riser and serpentine tubing designs for FPCs [17].

After the fluid absorbs heat in the solar collector, it then flows to the storage tank. If a direct system is used, the potable water is deposited into the tank. In an indirect system, the heat transfer fluid is passed through a heat exchanger (HX) where it transfers heat to potable water contained in the storage tank [17]. The HX may be internal to, external to, or wrapped around the storage tank. One common configuration is the single-wall immersed coil type (such as that seen in Figure 1.8). In this design, the coil is submerged in the potable water. These internal HXs offer a simple design but may experience scale deposits on their outer surface, which can diminish performance [18]. While more expensive, external heat exchangers (such as that seen in Figure 1.10) offer greater flexibility of parts and more effectively transfer heat between the two fluids [17], [18]. Double-wall heat exchangers are typically used to decrease the risk that toxic heat transfer fluids (such as ethylene glycol) will leak into potable water [17].

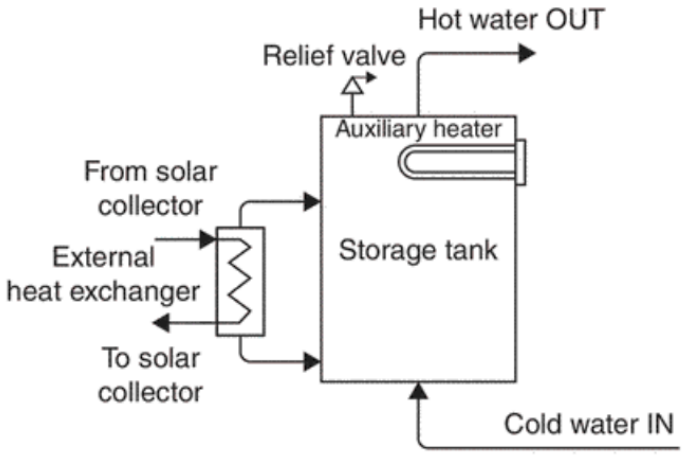

Figure 1.10: External heat exchanger setup for SWHS [17].

1.4 NCSU Solar House Water Heating System

The solar water heating system in use at the NCSU Solar House is an active, indirect system, much like that shown in Figure 1.8. The collector used is a Schüco Slim V Plus FPC. This collector is composed of an aluminum frame, copper absorber plate, 12 mm copper serpentine tubing, and 23 ft^2 of aperture area made of low-iron glass [19]. The collector is visible on the left side of the roof in Figure 1.6. The system also features a Schüco Complete Solar Station (which houses the pump), a Schüco DeltaSol digital controller (now made by RESOL), and an 80-gallon Rheem 81V80HE-1 Solaraide storage tank. Specifications sheets for the Schüco Slim V Plus collector and Rheem 81V80HE-1 water tank are included in Appendix C and D, respectively. The heat transfer fluid used in the collector loop is non-toxic propylene glycol, and the heat exchanger is a wrap-around double-wall type. In this type of heat exchanger, the tubing from the collector loop is spiraled around the storage tank. The tank also features a single 4500 W electric heating element to serve as backup heat supply. The storage tank, pump station, and expansion valve are shown in Figure 1.11 below.

Figure 1.11: Storage tank and pump station at the NCSU Solar House.

The DeltaSol controller used at the house operates by reading the temperature difference between two temperature sensors – one at the top of the solar collector and one at the bottom of the storage tank. A schematic showing temperature sensor placement is shown below in Figure 1.12. Note that sensors S3 and S4/TR are not currently in use at the NCSU Solar House. R1 represents the pump which drives the flow of the propylene glycol solution.

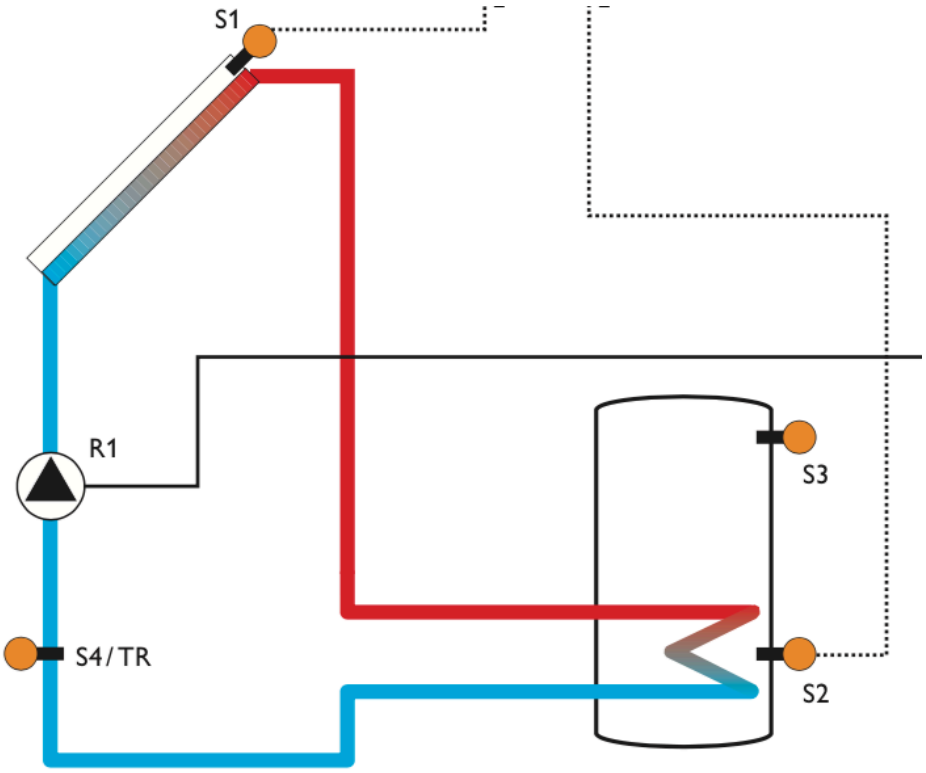

Figure 1.12: Controller schematic with temperature sensor placement [20].

When the temperature difference between S1 and S2 reaches the switch-on temperature difference (12°F or 6.7°C), the controller turns the pump on. The pump remains on for a pre-set length of time or until the switch-off temperature difference is reached. A maximum storage tank temperature may also be set, and the unit comes with a non-adjustable emergency shutdown storage temperature of 200°F (95°C).

Chapter 2

Literature Review

A brief literature review has been conducted in an effort to organize and present relative background information concerning passive solar houses, solar photovoltaic systems, and solar domestic hot water heating systems, as well current practices used to evaluate these systems' performance.

Buildings which incorporate design features to collect, store, and distribute solar energy are known as passive solar buildings [17]. These buildings often contain features such as sunspaces, Trombe walls, large south-facing windows, and roof overhangs to provide space heating during the winter and reduce cooling loads in the summer. In the design of a passive solar home, consideration must be given to ensure the design incorporates the right balance of features such as glazing and thermal mass [17]. Thermal mass is material that is capable of storing a large amount of heat, which can then be distributed later in the day when solar energy is not available [17]. Factors which affect the design of passive solar homes include heating/cooling loads, local climate, and building site [17], [21]. Prior investigation has found that the passive elements of the NCSU Solar House met between 90-100% of the heating load during some months of the house's first and second years of operation, with a heating bill of just $40 during the entire winter of 1981-1982 [22]. It has also been found that the house requires only 3% more energy for cooling during a typical year than a conventional house would in the same area [3].

In addition to being a passive solar home, the NCSU Solar House incorporates some active solar energy systems – specifically a solar PV array mounted on the roof and a solar water heating system. The solar PV array is grid-connected, and its energy production is monitored

using a data logging system to be discussed in detail later. To accurately and usefully evaluate the performance of the array, it is important to determine relevant parameters which are commonly used in the industry. According to Marion et al., there are four key parameters for grid-connected PV systems [23]. These are: final yield, reference yield, performance ratio, and PVUSA rating [23]. The final yield (Y_f) is defined as the AC energy output of the system divided by the array's nameplate DC power rating [23]. This provides a convenient means for comparing systems with various capacities [23]. Reference yield (Y_r) is defined as the total in-plane solar radiation for a given time period divided by the standard test condition (STC) irradiance (1 kW/m^2) [23]. The reference yield quantifies the solar resource available to the system and represents an equivalent amount of hours at the STC irradiance condition [23]. The performance ratio (PR) is defined as the final yield divided by the reference yield. It may also be defined as the overall efficiency of the system divided by the rated efficiency of the PV panels at STC [24]. It is a representation of all inefficiencies in the system when converting from DC power to AC power [24]. The performance ratio is usually reported on a monthly or yearly basis and may be useful for determining either permanent losses in production or temporary component failures [23]. Details on final yield, reference yield, and performance ratio calculations are presented in Chapter 3. Finally, the PVUSA rating has been developed as a means of providing a more realistic estimate of a PV system's performance versus the typically cited standard test conditions (STC) rating [23]. PVUSA test conditions (PTC) are defined as: 1000 W/m^2 of solar irradiance, 1 m/s wind speed measured at 10 m above grade, and an ambient temperature of 20°C [25]. The PTC rating is determined using regression analysis to find four coefficients based on observed performance and meteorological data [25]. The equation used to calculate the PTC rating (P_{PTC}) is shown below in Equation 2.1 [25].

$$P_{PTC} = I_0(a + bI_0 + cW_s + dT_a) \quad (2.1)$$

Where I_0 is solar irradiance (1000 W/m^2), W_s is wind speed (1 m/s), T_a is ambient temperature (20°C), and a, b, c, and d are regression coefficients determined from observed data. By comparison, STC is defined as 1000 W/m^2 solar irradiance, 25°C cell temperature, and 1.5 air mass spectrum [25]. A current list of PTC ratings for many commercially available PV panels is available online from the California Energy Commission and California Public Utilities Commission [26].

The parameters presented above have been used extensively to evaluate and compare PV systems around the world. For example, researchers in Dublin, Ireland calculated the average daily final yield and reference yield, as well as performance ratio of a 1.72 kW peak-rated rooftop grid-connected system on a monthly and yearly basis. This was done in order to assess seasonal performance and for comparison with other systems worldwide [24]. Figure 2.1 shows results from monthly calculations of average daily final, reference, and array yield for this system. The array yield is used to evaluate the performance of the panels alone, and is defined as the DC energy output divided by the array's peak STC rated power [27].

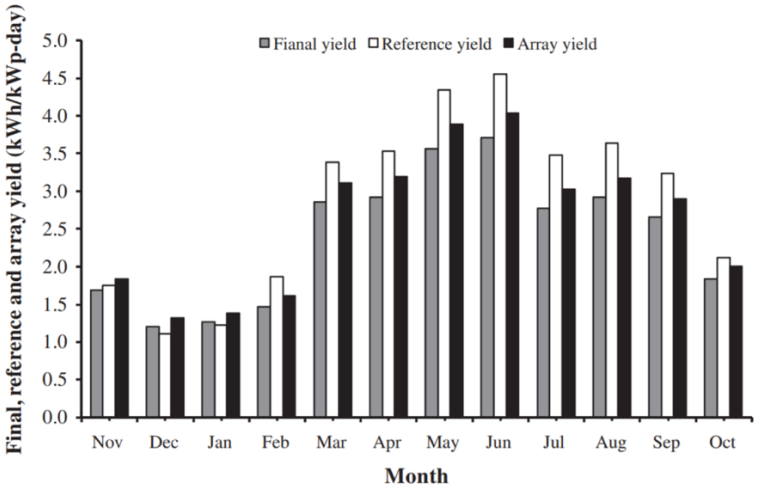

Figure 2.1: Average daily values of final, reference, and array yields for a 1.72 kW system in Dublin, Ireland [24].

Overall results for the system are shown in Table 2.1 alongside 20 other systems from various locations around the world.

Table 2.1: Results for 1.72 kW PV system in Dublin, Ireland and comparisons to other systems worldwide [24].

Location	PV type	Energy output (kW h/kW$_p$)	Final yield (kW h/kW$_p$-day)	PV module efficiency (%)	System efficiency (%)	Inverter efficiency (%)	Performance ratio (%)	Reference
Crete, Greece	PC-Si	1336.4	2.0–5.1	–	–	–	67.4	[8]
Germany		680	1.9	–	–	–	66.5	[13]
Málaga, Spain		1339	3.7	8.8–10.3	6.1–8.0	85–88	64.5	[21]
Jaén, Spain		892.1	2.4	8.9	7.8	88.1	62.7	[22]
Algeria	MC-Si			10.1	9.3	80.7	–	[23]
Calabria, Italy	PC-Si	1230	3.4	7.6	–	84.8	–	[24]
Germany		700–1000	1.9–2.7	–	–	–	–	[15]
Ballymena, Northern Ireland	MC-Si	616.9	1.7	7.5–10.0	6.0–9.0	87	60–62	[10]
Warsaw, Poland	A-Si	830	2.3	4.5–5.5	4.0–5.0	92–93	60–80	[25]
Castile & Leon, Spain	MC-Si	1180	1.4–4.8	13.7	12.2	89.5	69.8	[26]
Umbertide, Italy	PC-Si	–	–	4.0–7.0	6.2–6.7	–	–	[27]
UK		744	–	–	–	–	69	[9]
Liverpool, UK	Tiles	777	–	–	–	–	72	[9]
Dublin, Ireland	**MC-Si**	**885.1**	**2.4**	**14.9**	**12.6**	**89.2**	**81.5**	**Present study**
UK	A-Si	–	–	3.7	3.2	64.5	42.0	[10]
UK	PC-Si	–	–	–	7.5	–	68.0	[10]
UK	–	–	–	–	8.4	90–91	59–61	[10]
Italy	A-Si	–	–	–	–	–	66	[10]
Germany	–	–	–	–	–	–	50–81	[10]
Brazil	A-Si	–	–	–	5	91	–	[10]
Thailand	–	–	2.9–4.0	–	–	92–98	70–90	[28]

PC-Si: poly-crystalline silicon, MC-Si: mono-crystalline silicon, A-Si: amorphous silicon.

The results show that the average daily performance ratio for the year (81.5%) is higher than all other systems considered, except for one in Thailand. Note that this study also includes measures of PV module efficiency, system efficiency, and inverter efficiency. The PV module efficiency is essentially a DC efficiency and is defined as either the instantaneous DC power output from the panels divided by the instantaneous solar irradiance or the average DC energy output over a defined time period divided by the average solar radiation on the panels during the same timeframe [28], [29]. The system efficiency is defined in the same manner with the key difference being that the power and energy values used are the AC values seen after passing through the inverter [28], [29]. Inverter efficiency is defined on an instantaneous basis as the AC power produced by the system divided by the DC power produced by the panels. It may also be evaluated over a specified time period as the AC energy produced by the system divided by the

DC energy produced by the panels [24]. The widespread use of the performance parameters mentioned thus far demonstrates their valuable role in the evaluation and comparison of solar PV systems.

The solar water heater at the NCSU solar house is an active, indirect system which uses a flat-plate Schüco Slim V Plus collector and a Rheem 81V80HE-1 Solaraide tank equipped with a 4500 W backup electric heating element [30]. There are many studies in the literature which assess the performance of various solar collectors used in domestic hot water applications and review the results of these tests [16], [18], [31], [32]. Many of these use tests defined in widely adopted standards such as ASHRAE-93 or EN12975-2 [33], [34]. Although the steady-state test procedures included in these standards are used frequently, Rojas et al. notes that they often call for environmental conditions uncommon in many locations where collectors can be efficiently employed [35]. It is also found that around 75% of the time required for flat-plate collector tests are "pre-data" periods when no useful data is collected and that such lengthy requirements are not likely to contribute to the quality of results [35]. The European EN12975-2 standard includes the option of a transient test method which is found to require a more reasonable time commitment and produce results within 7% of those from steady-state tests [34], [35].

Other studies, such as that by Rodriguez-Hidalgo et al., have aimed to develop models based on real operational data which are more accurate than those obtained from the steady-state standards tests [32]. Ayompe et al. compared the performance and economic feasibility of a flat-plate (FPC) and evacuated tube collector (ETC) for domestic hot water heating using otherwise identical systems installed side-by-side [36]. Their testing showed that FPCs, while typically less efficient than ETCs, compare well considering the small loss in performance and the large economic advantages [36]. Ayompe & Duffy also carried out a detailed analysis of an FPC domestic water heating system in Dublin, Ireland equipped with an automated hot water draw-off

system designed to mimic typical household use [31]. A schematic of the system used in their study in shown in Figure 2.2 below.

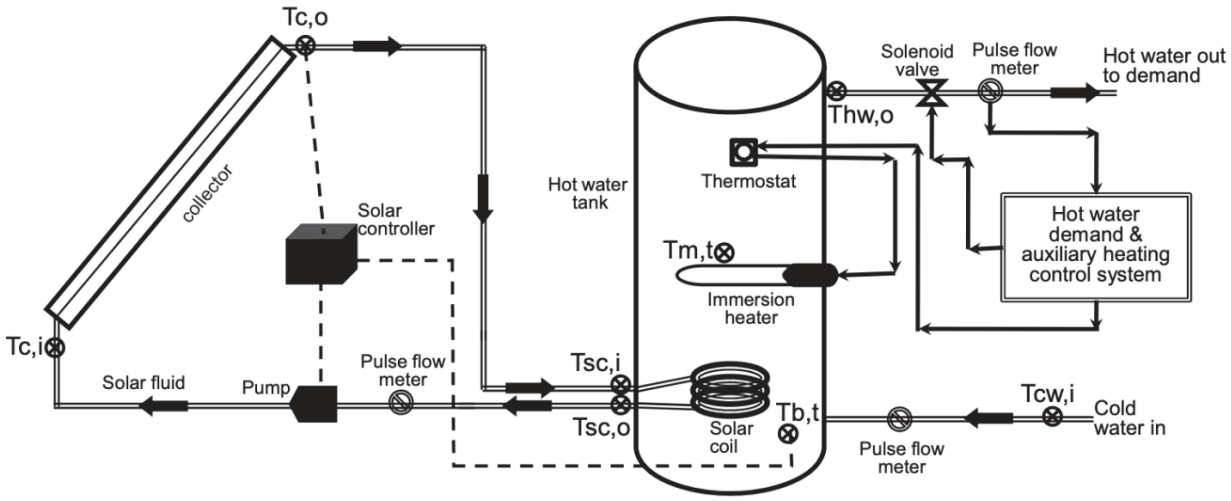

Figure 2.2: Schematic of hot water heating system used by Ayompe & Duffy [31].

The system above is an active (forced circulation) system which is very similar to that installed at the NCSU Solar House. The system includes a 300 L (approximately 80 gallon) tank equipped with an electrical backup heating element and a roof-mounted flat-plate collector tilted at the local latitude [31]. Also shown in the schematic are the temperatures measured and recorded in order to evaluate the performance of the system, including: solar fluid temperature at collector outlet ($T_{c,o}$) and inlet ($T_{c,i}$), water temperature at bottom ($T_{b,t}$) and middle ($T_{m,t}$) of the tank, solar fluid temperature at entrance ($T_{sc,i}$) and exit ($T_{sc,o}$) of the solar coil heat exchanger, cold water inlet temperature ($T_{cw,i}$), and hot water temperature out of the tank ($T_{hw,o}$). The volumetric flow rate of the solar fluid is also measured [31]. These measurements are used to calculate the energy collected by the FPC, delivered to the hot water tank, and lost in the supply pipes [31]. The fraction of total heating energy required that is satisfied by the solar radiation is also considered, as well as collector and system efficiencies [31]. Results of this study show that about 1/3 of the total water heating requirements in this system are satisfied by solar energy [31].

Chapter 3

Present Monitoring Setup and Results

Immediately following its construction, the NCSU Solar House was equipped with over 250 measurement devices used to monitor conditions in the house and evaluate its performance. Figure 3.1 is a picture of a board which once housed connections to many thermocouples in the house and has since been removed.

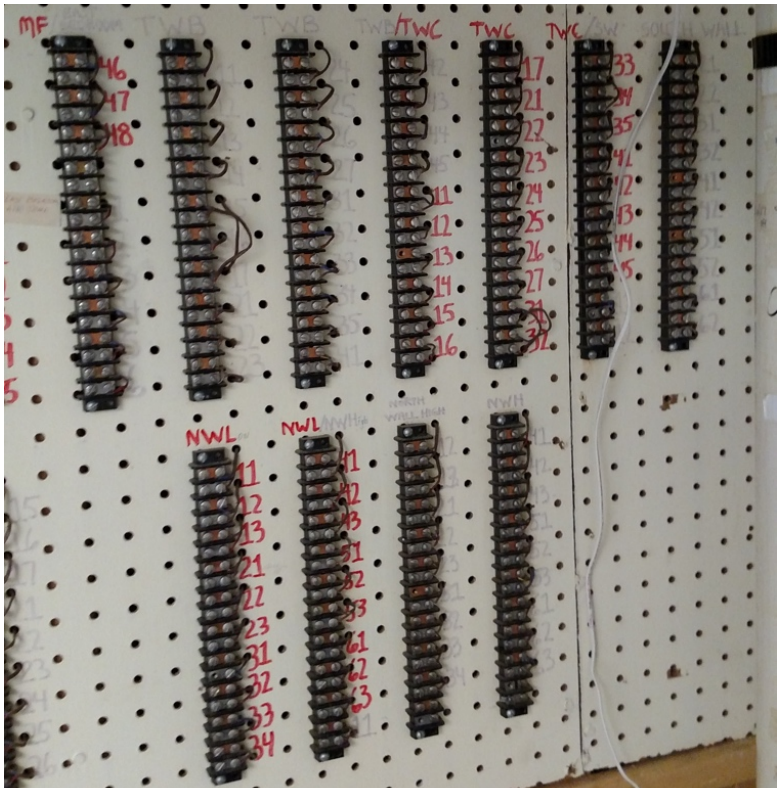

Figure 3.1: Previously used thermocouple monitoring board at NCSU Solar House.

Over time, many of the monitoring devices have been removed or disconnected. Although the large amount of data once available from these devices is now inaccessible, some new monitoring devices have been installed at the house. This chapter provides an overview of the

present equipment used to monitor the house and presents the useful results which may be obtained from them.

There are currently two data loggers (labeled Logger 2 and Logger 3) setup at the NCSU Solar House to monitor various conditions in the house. In addition to these data loggers, there is a weather station (visible in the foreground in Figure 1.6) located just southeast of the house. Logger 2 measures several conditions related to the solar water heating system and the environment inside the house, including: glycol return and supply temperatures, air handling unit power, air-conditioning condenser leaving temperature, supply air temperature, supply air relative humidity, and supply air dew point. Logger 2 also measures downstairs room temperature, relative humidity, and dew point. Logger 3 tracks power usage by various components of the house and the adjacent AFV garage, including: total house, house phase A, house phase B, backup water heating, condensing unit, garage phase A, and garage phase B. Additionally, Logger 3 also tracks power generation from the rooftop solar PV panels. The outdoor weather station captures the following environmental information: solar irradiance, ambient temperature, relative humidity, dew point temperature, wind speed, and wind direction. In addition to these devices, the house uses an ECOBee 4 smart thermostat to control indoor conditions, monitor indoor temperature and relative humidity, control the heating and cooling systems operation, and monitor upstairs occupancy.

3.1 Solar PV Generation and House Demand

As mentioned previously, Logger 3 provides data for power generation from the rooftop solar PV panels and house power demand. This logger retrieves its information using current transformer (CT) clamps placed around the wires coming from each component. CT clamps are essentially a conductive core (the jaws of the clamp itself) wrapped around a wire (the primary winding) with a current passing through it. As the current passes through the wire, an opposing

current is generated in a secondary winding around the core. The opposing current is related to the current flowing in the wire by a proportionality constant which depends on the number of turns present in the secondary winding [37]. For all data taken prior to March 2019, the logger only truly measured AC current from the PV array and an automatic calculation (shown below in Equation 3.1) was carried out by the data logging system to obtain a power value. This calculation assumed a constant voltage of 240 V and a power factor of 1.0.

$$P = I_{AC} * 240 \text{ volts} * \frac{1 \text{ kW}}{1000 \text{ W}} * 1.0 \quad (3.1)$$

The term I_{AC} in Equation 3.1 is the actual AC current (in units of A) measured from Logger 3, while P is the resulting power value in kW. Beginning with March 1st, 2019, voltage leads were installed so that the logger could use the real operating voltage and power factor to calculate the power being produced by the panels. It should be noted however that all prior power measurements are still taken by the assumed voltage and power factor method shown in Equation 3.1.

3.1.1 Solar PV Array Efficiency and Expected Power

The weather station provides solar irradiance data using an attached pyranometer. The irradiance values are reported in W/m^2 and can be downloaded in a .csv file format from an online logger web page. Data was collected from the loggers and the weather station in 5-minute intervals. Solar irradiance values may be used in conjunction with the panels' generated AC power to obtain a rough estimate of panel DC efficiency. To do this, the total incident power on the panels is first found by multiplying the total area of the panels (about 30 m^2) by the solar irradiance in W/m^2. The AC power generated by the panels is next divided by the assumed inverter efficiency of 97% [15]. This yields an assumed value of DC power which correlates to the AC power measurement for the same time. The DC power value is divided by the total incident power on the panels, resulting in the DC efficiency. Results of this calculation are

shown in Figure 3.2 for January 17th, 2019. Weather on this day was partly cloudy with light rain. A small percentage of the values calculated for DC efficiency were impractical (greater than 100%) and have therefore been omitted from the plot below.

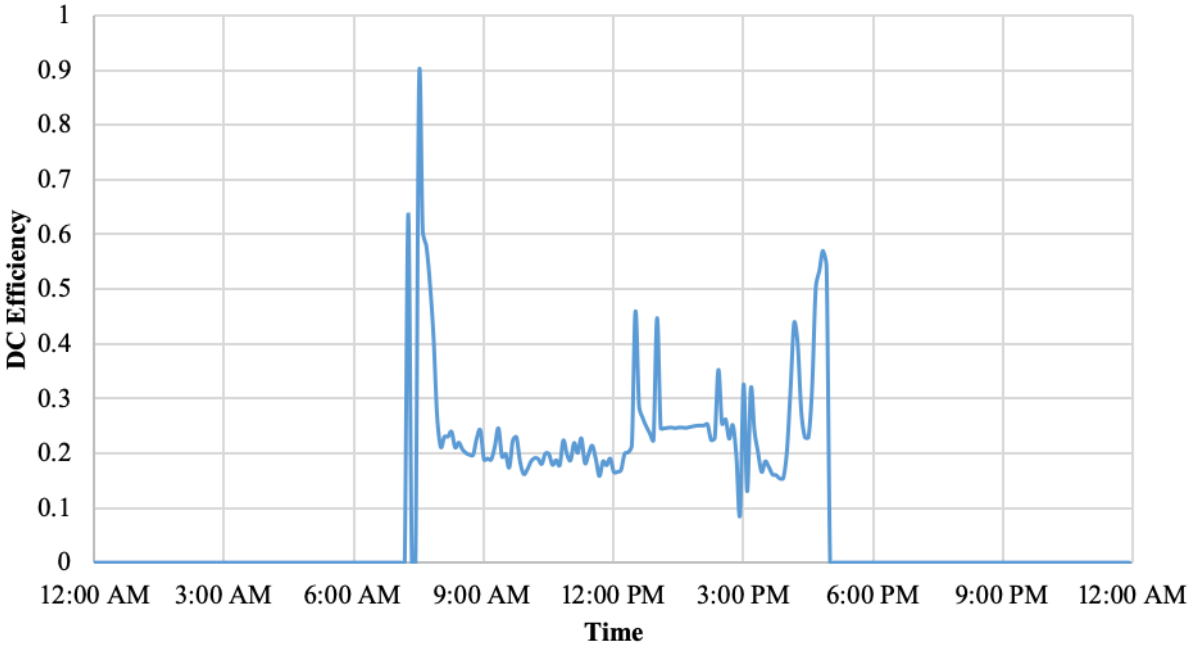

Figure 3.2: DC efficiency of solar array, January 17, 2019.

Assuming ideal performance and therefore using the manufacturer's rated peak DC efficiency at STC for the panels (18.1%), we may also compare the expected AC power generation to the actual recorded AC power generation values [12]. To obtain the expected power value, the incident power on the panels is multiplied by the assumed panel and inverter efficiencies of 18.1% and 97%, respectively [12], [15]. Figure 3.3 shows a comparison between the expected (ideal) power generation vs. the actual recorded power generation, again for January 17th, 2019.

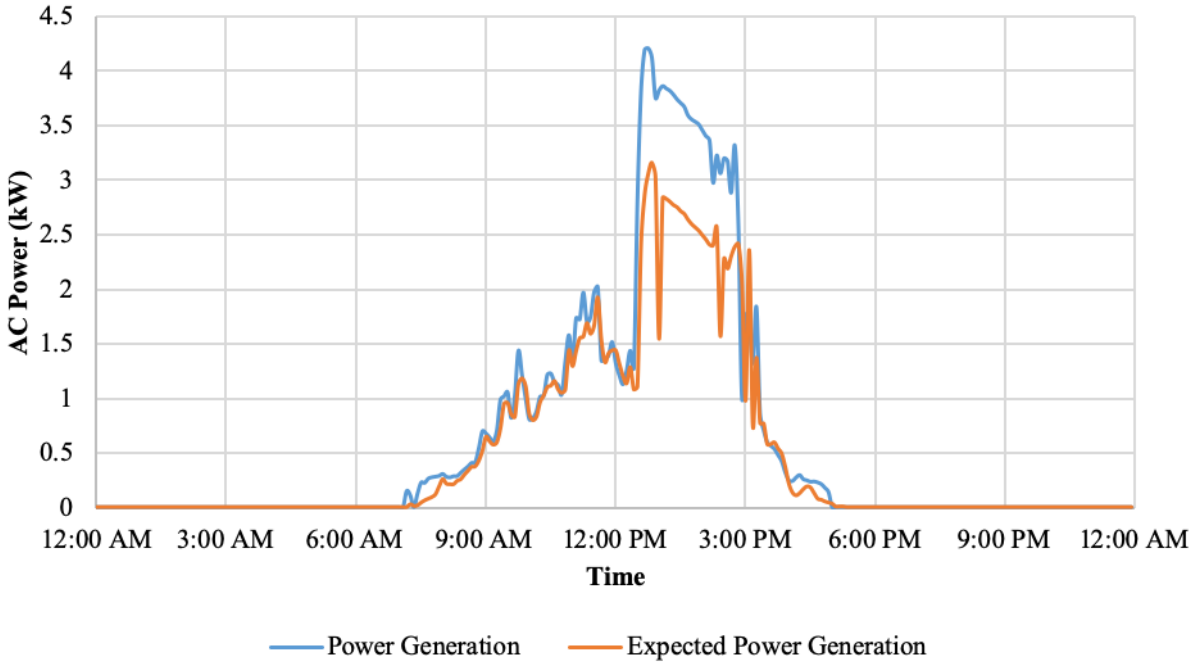

Figure 3.3: Expected and measured AC power generation, January 17, 2019.

The actual power generation tracks relatively well with the expected power generation until around 1:00PM, when a sharp spike occurs. From about 1:00PM to 3:00PM, the actual power generation is around 1 kW higher than expected. These results are clearly unrealistic, since the expected power generation has been calculated using the manufacturer's peak rating for efficiency, which the panels would not likely achieve during the majority of their time in use. The efficiencies shown in Figure 3.2 correspond to an average instantaneous DC efficiency (when the panels are producing some power) of 25.4% - much higher than the peak efficiency rating of 18.1%. Some possible reasons for these unrealistic results are investigated below.

First, the values used for solar irradiance are examined. The solar irradiance is read from an Onset S-LIB-M003 silicon pyranometer mounted on the free-standing weather station located on the rear lawn of the solar house. One immediately obvious source of error here is the fact that the pyranometer is not evaluating solar irradiance at the same location or elevation as where the panels are receiving it, which could cause a misrepresentation of the incident power on the

panels. There are many trees surrounding the house, which may shade the panels at different times than the pyranometer. Aside from the location, the angle at which a surface lies with respect to horizontal will affect the amount of solar irradiance it receives [38]. In fact, if a surface is optimally tilted for its location, the incident radiation may be increased by as much as 20% on average [38]. In order to obtain a more accurate approximation of the increase in solar irradiance due to tilting at the house, the National Renewable Energy Laboratory's (NREL) PVWatts program is used. PVWatts is an online program which allows users to estimate the performance of a solar PV system at a specific location [39]. As noted by Jacobson & Jadhav, the optimal tilting angle for PV panels in Raleigh is about 36° from horizontal - the purposefully chosen angle of the roof at the NCSU Solar House [38]. Using this information, the parameters shown in Table 3.1 are used as inputs for PVWatts to determine the amount of solar radiation incident on a horizontal panel versus one which has been optimally tilted.

Table 3.1: Input parameters for PVWatts program.

	Untilted	Tilted
System Size	5.4 kW	5.4 kW
Module Type	Premium	Premium
Array Type	Fixed (roof mount)	Fixed (roof mount)
System Losses	14.08%	14.08%
Tilt Angle	0°	36°
Azimuth Angle	180°	180°
DC to AC Size Ratio	0.9	0.9

The DC to AC Size Ratio is the DC power rating of the PV array (5.4 kW) divided by the AC power rating of the inverter (6.0 kW) [12], [15]. The System Losses value of 14.08% is the default value used by PVWatts to account for losses due to factors such as shading, soiling, and wiring connections [39]. Using the parameters shown in Table 3.1, the estimated solar radiation for the tilted and untilted cases in January are found to be 4.57 and 2.71 kWh/m^2/day,

respectively. Therefore, the ratio between the tilted and untilted radiation is 1.69. Table 3.2 shows the full twelve-month radiation results from the PVWatts comparison.

Table 3.2: Monthly solar radiation results from PVWatts for tilted and untilted panels.

Month	PVWatts Optimally Tilted ($kWh/m^2/day$)	PVWatts Untilted ($kWh/m^2/day$)	Ratio (tilted/untilted)
January	4.57	2.71	1.69
February	4.96	3.43	1.45
March	5.43	4.49	1.21
April	6.11	5.81	1.05
May	6.04	6.45	0.94
June	5.88	6.62	0.89
July	5.73	6.3	0.91
August	5.76	5.73	1.01
September	5.47	4.76	1.15
October	5.21	3.79	1.37
November	4.72	2.85	1.66
December	4.25	2.39	1.78

The solar irradiance measurements from the weather station pyranometer are now multiplied by this January ratio to yield a more accurate estimation of the irradiance incident on the panels. Results for efficiency and expected power generation using the new solar irradiance values are shown in Figures 3.4 and 3.5 below.

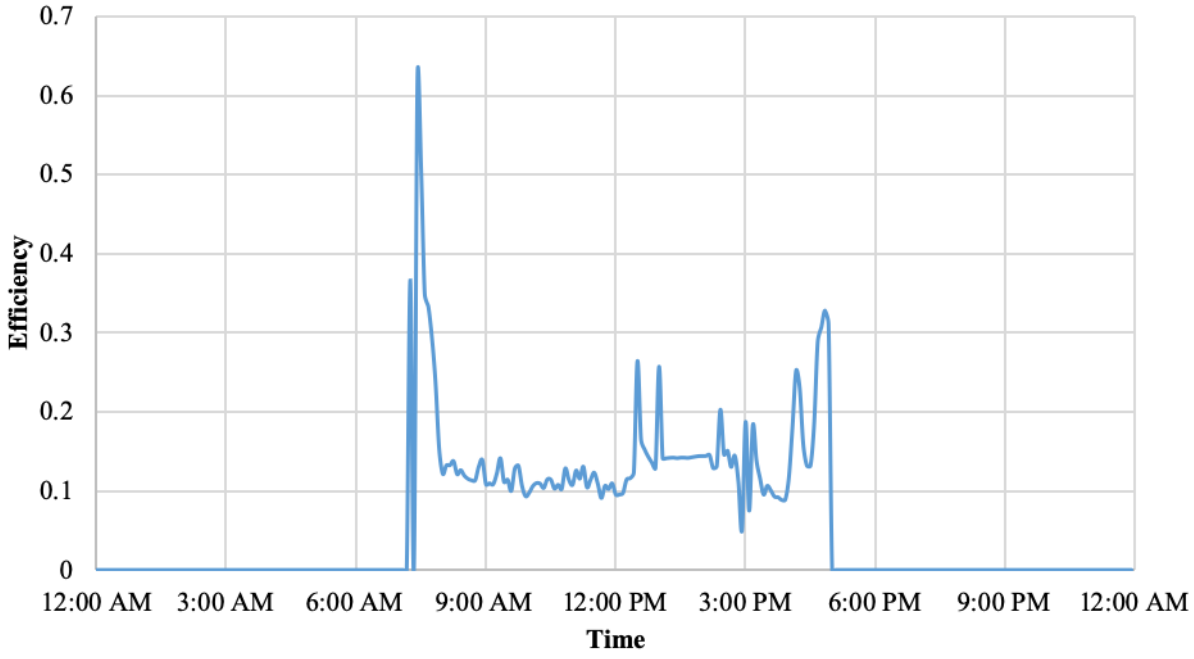

Figure 3.4: Tilt-adjusted DC efficiency of solar array, January 17, 2019.

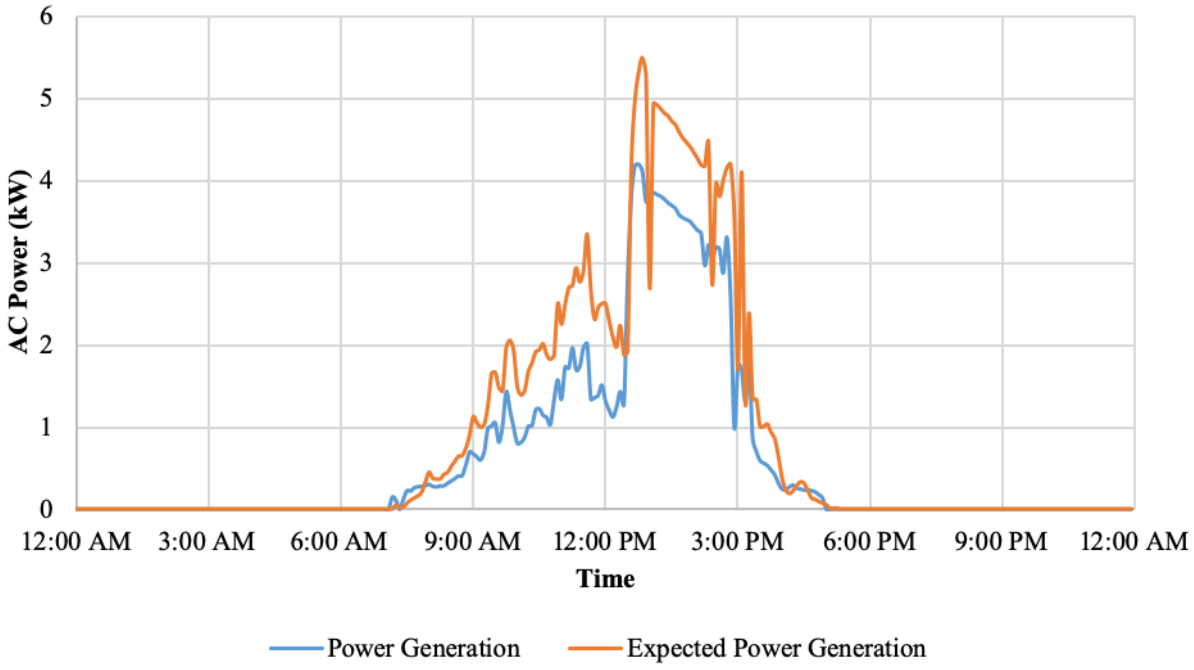

Figure 3.5: Tilt-adjusted expected and measured AC power generation, January 17, 2019.

The new average instantaneous DC efficiency of the panels for this day is 15.1% - a much more reasonable estimation that is well below the peak rating given by the manufacturer. Figure 3.5 presents a more realistic estimation of how AC power generation compares to the expected (or ideal) values. Instead of producing more power than expected, the generation is consistently below the peak generation except for a few data points.

The method used to monitor power generation is subject to at least one additional source of error which has already been addressed in the plots shown above. As stated previously, the CT clamps used are only able to measure current and the data logger performs an automatic calculation to convert this to an "assumed" power measurement (see Equation 3.1). The power factor is the ratio between real power dissipated by the load and the apparent power flowing through the circuit. The power factor is near zero at night when the system is off [40]. The power "measurement" given by the CT clamp is apparent power, which is the vector sum of real and reactive power [41]. When the power factor is zero, the real component is zero and the apparent power is made up entirely of reactive power. Because the clamp cannot distinguish between real and reactive power, readings are inaccurate at night and during low-power generation [42]. Power generation measurements during the night were consistently around 90 W. Because of this, all power generation values under 100 W were set to 0 W in order to give a more accurate representation of the real power being generated by the panels. As noted previously, the data for March 2019 is not subject to these errors, as the real operating voltage and power factor were measured during this month. With these measurements, the values of power generation reported by the logger during the night decreased dramatically to around 3 W. Therefore, power generation values for March have not been filtered in this same manner.

3.1.2 Variations Due to Weather Conditions

Logger 3 monitors the overall current drawn by the house (phase A and phase B) and translates this reading to an estimation of power usage. This information allows a comparison to be made between the house's power demand and production (from the PV array). Figure 3.6 displays the power generation by the solar PV panels alongside the power demand of the house, again for January 17th, 2019.

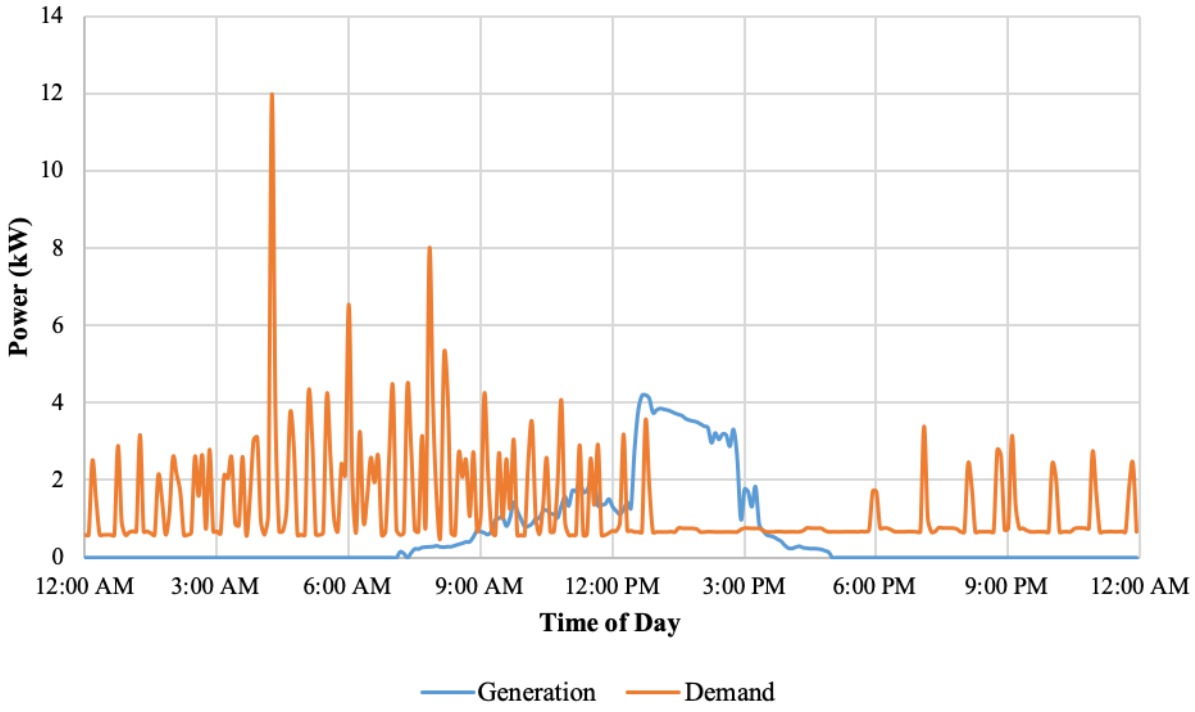

Figure 3.6: Power generation and demand, January 17, 2019.

Observed weather on January 17th was light rain, while the weather station at the house reported a high of 52°F. The plot in Figure 3.6 shows that the PV array on the house began producing a significant amount of power at around 12:30PM. Almost immediately following this increase in production, the demand of the house drops to a near constant value of about 0.8 kW. An increase in power production from the panels suggests that there was a greater amount of incident

sunlight on the house at this time. Due to the passive solar design of the house, this increase in solar radiation translates to a large increase in heat energy supplied to the house. The large usage of power present prior to 12:30PM can therefore most likely be attributed to space heating requirements. The power demand remains steady around 0.8 kW until almost 6:00PM – a full hour after the generation has dropped to zero. This indicates that the passive features of the house are performing well. The reason for the large spike in demand (to around 12 kW) at 4:30am is not known. January 17th, 2019 has been used as an example for the data presented thus far due to its variations in weather conditions and ability to demonstrate the house's performance as these conditions change. In order to further examine these effects, data corresponding to various general observed daily weather conditions is presented below.

Data concerning the house's energy production and usage has been collected for days in June, October, November, and December of 2018, as well as January, February, and March of 2019. One area of interest in the performance of the house is the dependence on weather conditions. Comparisons were therefore made between data collected during several general outdoor weather scenarios. Figures 3.7 through 3.10 illustrate the observed differences in production and demand for various selected weather conditions.

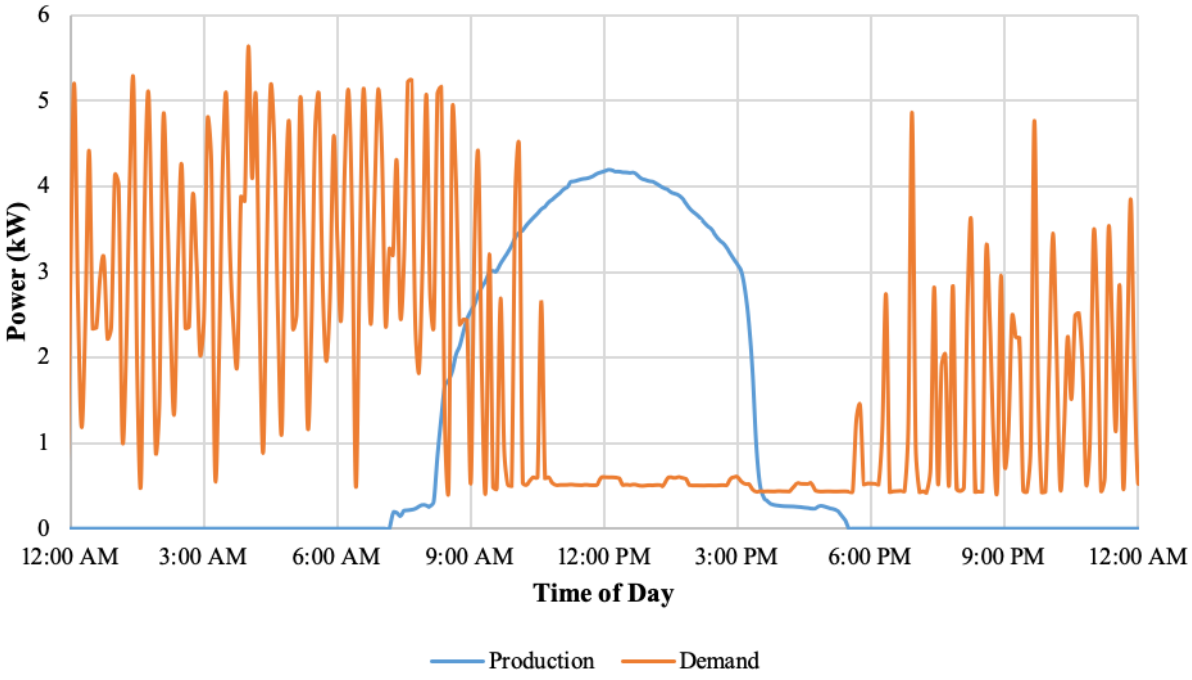

Figure 3.7: Sunny day power generation and demand, January 22, 2019.

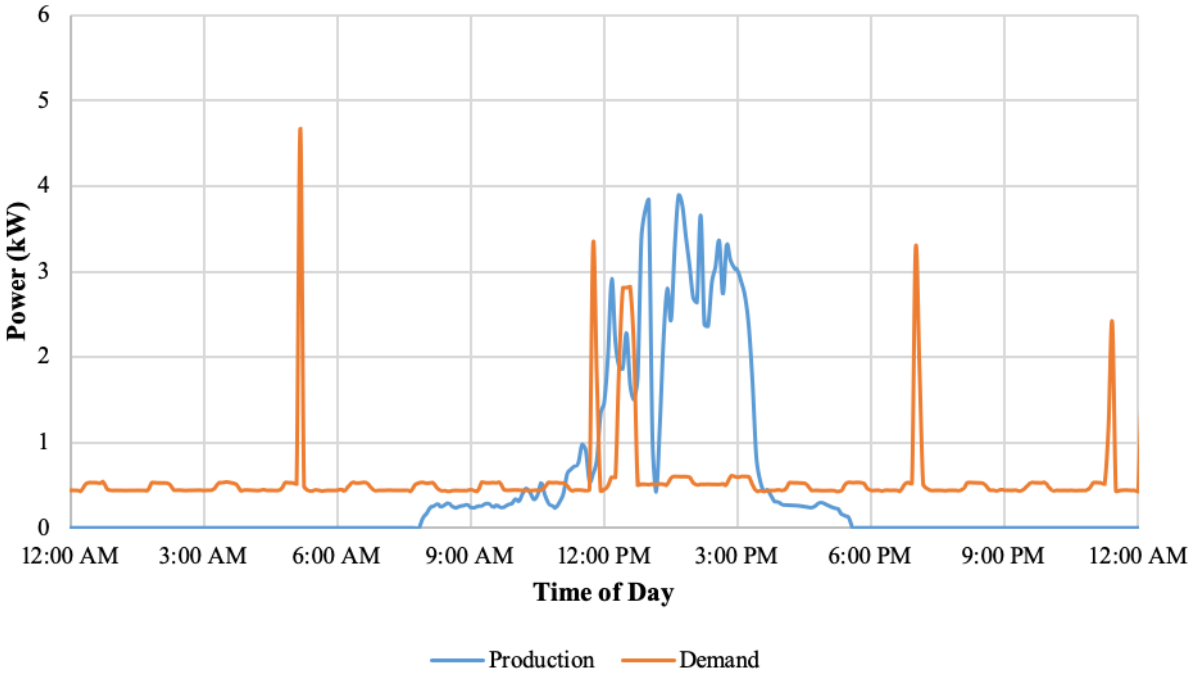

Figure 3.8: Partly cloudy day power production and demand, January 24, 2019.

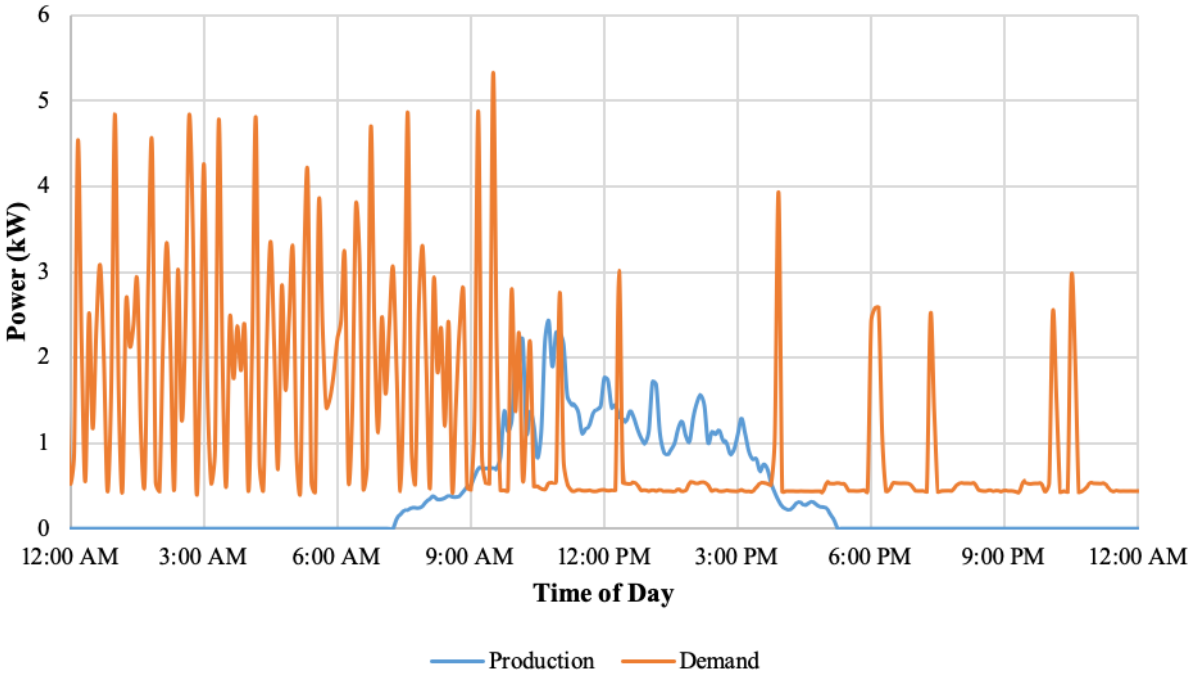

Figure 3.9: Cloudy day power production and demand, January 23, 2019.

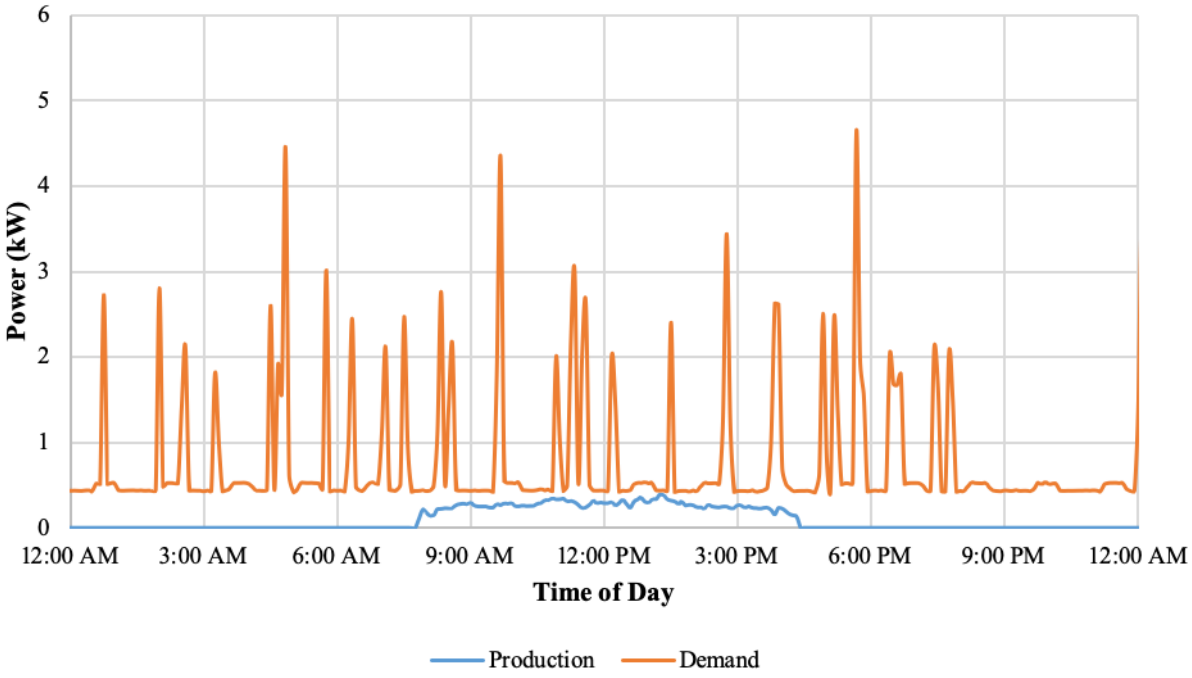

Figure 3.10: Rainy day power production and demand, January 4, 2019.

In Figure 3.7, the power production and demand are shown for a sunny day – January 22nd, 2019. The high and low temperatures for this day were 43°F and 19°F, respectively. The plot displays a relatively high power demand for the house from 12:00AM to around 9:00AM. The day before was sunny also, but the low overnight temperatures likely translated to high power needed for space heating. The power usage drops to a near-constant value of about 0.6 kW at 11:00AM, evidence that the solar irradiance (which follows a similar path as the energy production) is successfully being translated to heat through the passive solar features in the house. Power production reaches a peak of 4.2 kW just after 12:00PM, then declines until returning to zero just before 6:00PM. Power demand begins to increase steadily around 6:00PM as well. The power produced by the PV panels is greater than or equal to the demand of the house for 27% of the data points used for this day. Total energy produced and consumed for this day was 25.5 and 44.7 kWh, respectively.

Figure 3.8 illustrates performance for a partly cloudy day, in this case January 24, 2019. The high and low temperatures for this day were much warmer than January 22nd, at 68°F and 37°F, respectively. In contrast to the sunny day plot, demand begins at a very low level at 12:00AM and remains there until around 5:00AM, when a very short spike occurs. This is most likely due to the fact that the previous day's high was 65°F, while the overnight low reached just 58°F. The three spikes with the shortest time durations in Figure 3.8 are due to auxiliary water heating, while the other (occurring just after 12:00PM) is likely due to space heating. Production does not increase significantly until around 11:00AM, and changes sporadically throughout the day, until falling to zero just before 6:00PM. The peak production for this day is 3.9 kW. Production is greater than demand for 17% of the data points used in the figure. Total energy produced and consumed for this day were 11.1 and 13.6 kWh, respectively.

An example of cloudy day performance is shown next in Figure 3.9. The high and low temperatures for this day were 65°F and 30°F, respectively. Similar to Figure 3.7, the power demand begins high, as the low was 29°F for the previous night. Demand does not decrease significantly until around 11:00AM, after which only short intermittent spikes occur for the rest of the day. Peak production for this day was just 2.4 kW, which was greater than or equal to demand for 25% of the time. Although the power production is higher than demand for a greater portion of time than for the partly cloudy example, the total energy produced and consumed for this day was 9.3 and 29.2 kWh, respectively. This means that energy production for January 23 was 16% lower than January 24, and 19.9 kWh short of the need compared to just 2.5 kWh short on January 24.

Finally, the last example shown in Figure 3.10 is January 4, 2019 – a day with consistent rain. Immediately evident in this plot is the fact that the power production rate is never above or equal to the demand. Also, the energy produced on this day is lower than for the rest of the days shown, at just 2.3 kWh. This is 23.2 kWh lower than the sunny day example. Recorded high and low temperatures for this day are 60°F and 49°F, respectively. The maximum power production rate reached was just 0.4 kW, also the lowest of any conditions shown, as expected.

The results discussed above reveal the impact that current weather conditions have on the PV array's ability to effectively produce power. The theoretical maximum achievable AC power production rate (based on panel rating and assumed inverter efficiency) of 5.2 kW was not achieved during any of the days shown. Key characteristics of the weather conditions comparison are summarized in Table 3.3 below.

Table 3.3: Results of weather conditions comparison.

Date	Weather Condition	High (°F)	Low (°F)	Maximum Power Production (kW)	Maximum Power Demand (kW)	Production > Demand	Energy Produced (kWh)	Energy Consumed (kWh)
1/22/19	Sunny	43	19	4.2	5.6	27%	25.5	44.7
1/24/19	Partly Cloudy	68	37	3.9	4.7	17%	11.1	13.6
1/23/19	Cloudy	65	30	2.4	5.3	25%	9.3	29.3
1/4/19	Rainy	60	49	0.4	4.6	0%	2.3	18.3

3.1.3 Variations with Time of Year

Variations in power production and consumption are expected to vary throughout the year due to changes in the sun's path and the available solar radiation. One way to graphically display the sun's path throughout the year is a sun chart. The sun charts shown in Figures 3.11 and 3.12 below have been generated for Raleigh, NC using an online program from the University of Oregon's Solar Radiation Monitoring Laboratory [43].

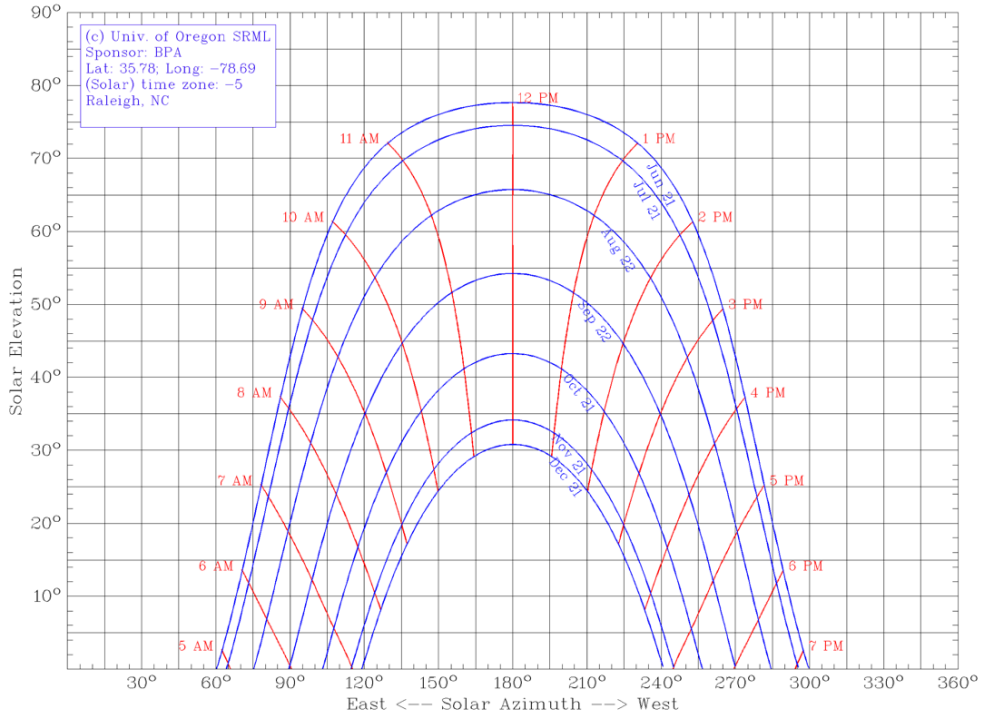

Figure 3.11: Sun chart for June through December in Raleigh, NC [43].

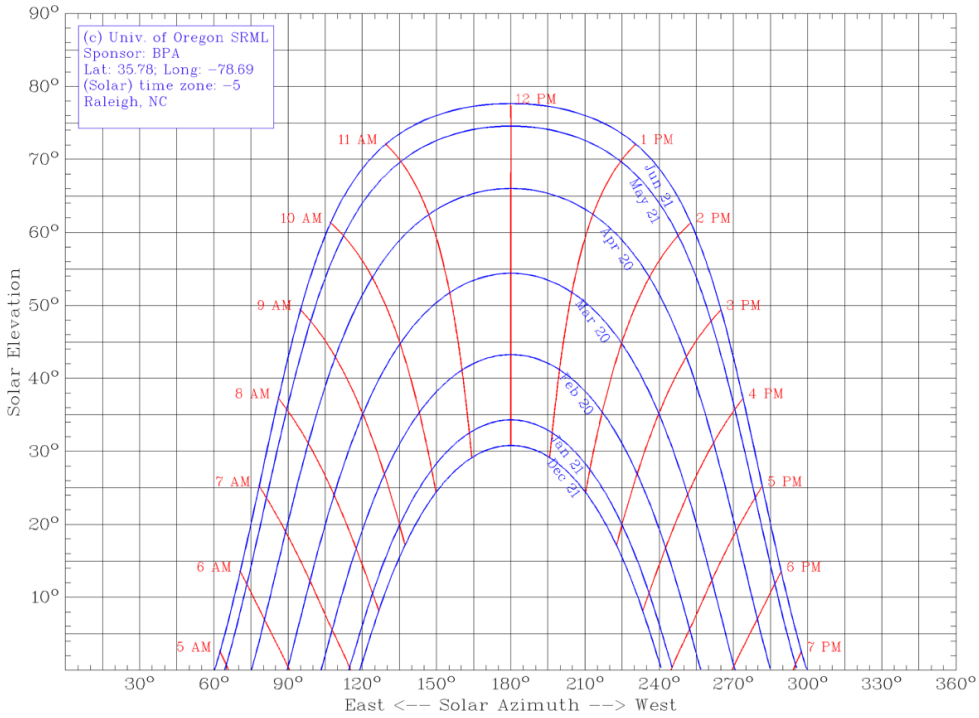

Figure 3.12: Sun chart for December through June in Raleigh, NC [43].

The horizontal lines and the degree measurements shown on the vertical axis represent the sun's altitude angle. This is the angle made between horizontal and a straight line drawn from the sun's position to the observer [44]. The vertical lines and degree measurements on the horizontal axis represent the azimuth angle of the sun's position measured clockwise from true north, making 180° equal to true south [44]. A graphical definition of these angles is shown in Figure 3.13 below, with the key difference of the azimuth angle being measured from true south instead of true north.

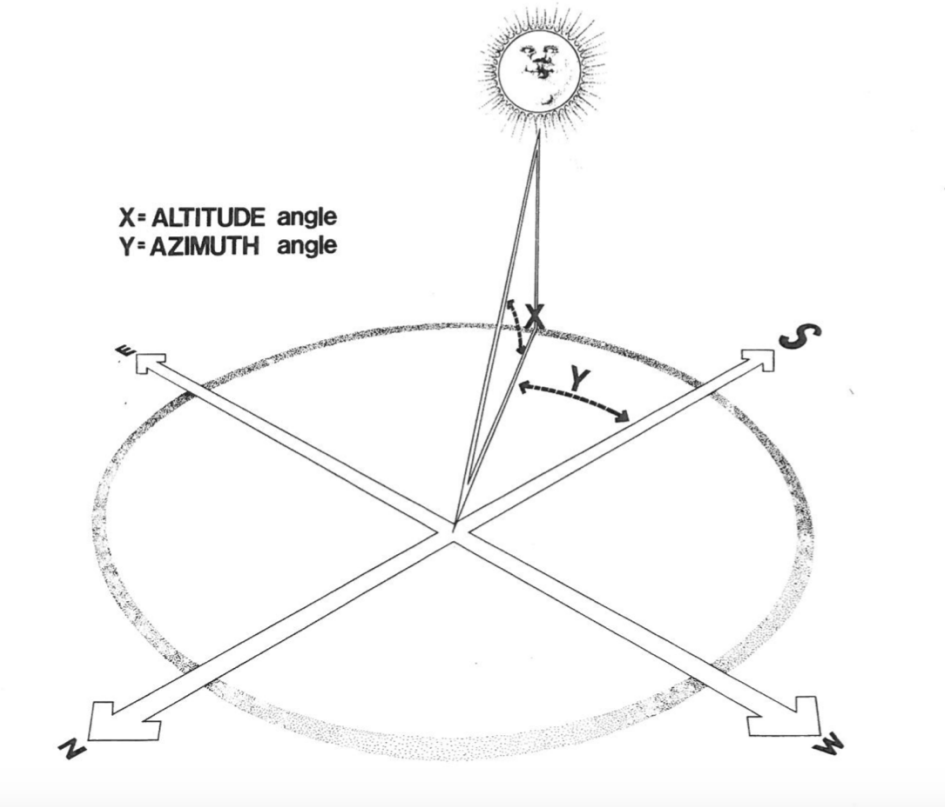

Figure 3.13: Solar altitude and azimuth angles [44].

It is also worth noting that the times plotted in Figures 3.11 and 3.12 represent solar time and not the local time in Raleigh. Given the large difference in the sun's path throughout the year, it is easy to understand why variations in solar PV output are expected. During months when the sun spends more time in the sky, a greater output is expected, and vice versa.

Data have been collected for the following time periods: June 16-24 of 2018, October 15-31 of 2018, November 4-30 of 2018, December 1-31 of 2018 and January 1-31, February 1-28, and March 1-31 of 2019. For these time periods, representative measures of performance have been calculated, including: average and maximum instantaneous power generation (kW), average and maximum instantaneous power demand (kW), average instantaneous solar irradiance (W/m^2), total and average daily energy production (kWh and kWh/day), and total and average daily energy consumption (kWh and kWh/day). Average instantaneous power

generation/demand and solar irradiance were calculated as simple arithmetic mean values over the datasets, including when values were equal to zero. To calculate energy production and consumption, the assumption was made that the power values (in kW) remained constant from the time when they were measured until the next measurement was taken 5 minutes later. Equation 3.2 details the manner in which this was done.

$$E = P * (5 \text{ minutes}) * \frac{1 \text{ hr}}{60 \text{ minutes}} \tag{3.2}$$

Here, E is the energy value for production or consumption in units of kWh and P is the power reading in units of kW. Once energy values were obtained for all 5-minute intervals, the results were summed over each day and month. The daily average values given for each month represent the monthly energy sum divided by the amount of days for which data is available.

Figure 3.14 shows the results for average instantaneous power generation and demand for each month plotted alongside the average instantaneous solar irradiance for each month.

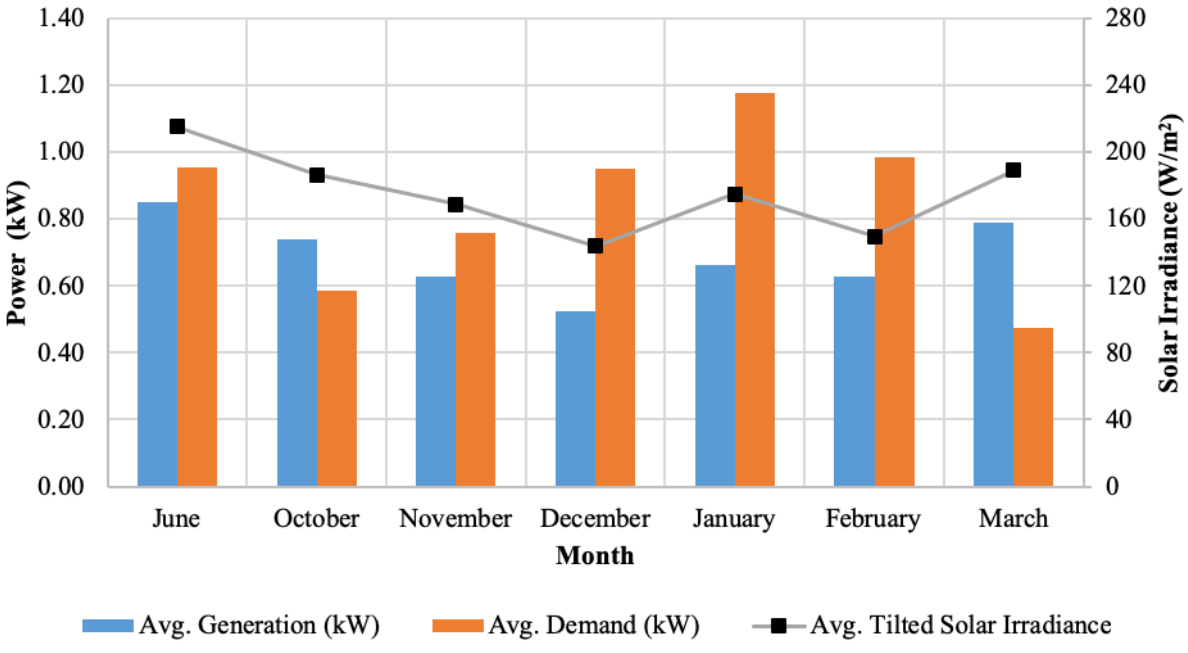

Figure 3.14: Average instantaneous power generation, demand, and tilted solar irradiance.

The average generation follows a trend similar to that seen for solar irradiance. The peak for both of these quantities occurs in June, which is followed by a decline through December. Both values then rise slightly in January, fall in February, and rise again in March. This trend corresponds well with the sun charts seen in Figures 3.10 and 3.11, except for the decline from January to February. In June, the highest value for power generation is expected since the sun spends more time visible in the sky. December is also expected to produce the least amount of power on average since during this time the sun spends the least amount of time in the sky. The cause for the decline in average generation from January to February is unknown but could be due to more favorable weather conditions in January. Average demand does not follow the same trend as the other two quantities in the chart. Beginning at a value of 0.96 kW in June, the demand falls significantly from June to October, then rises steadily until January, where its peak value of 1.18 kW is reached. The average demand then falls steadily through March, where its minimum value of 0.47 kW occurs. The cause of this trend is likely the temperatures during these months. Average daily highs and lows for the months considered are shown below in Table 3.4.

Table 3.4: Average daily temperature conditions for each month.

Month	Average High (°F)	Average Low (°F)
June	95	74
October	69	48
November	61	42
December	58	39
January	55	34
February	61	39
March	64	41

With an average daily high of 95°F in June, there is clearly a large cooling load present. Temperatures are much more moderate in October, where the average high is only 69°F and the average low is just below 50°F. In November, average temperatures begin to dip well below

typically comfortable levels for inhabitants, and heating needs rise accordingly. Temperatures continue to fall through January and demand rises as expected. Although one would expect the increase in solar irradiance from December to January to reduce heating loads through the house's passive solar features, the accompanying decrease in average temperatures seems to overshadow this effect.

Maximum power generation and demand are shown for each month in Figure 3.15, again plotted alongside the average instantaneous solar irradiance.

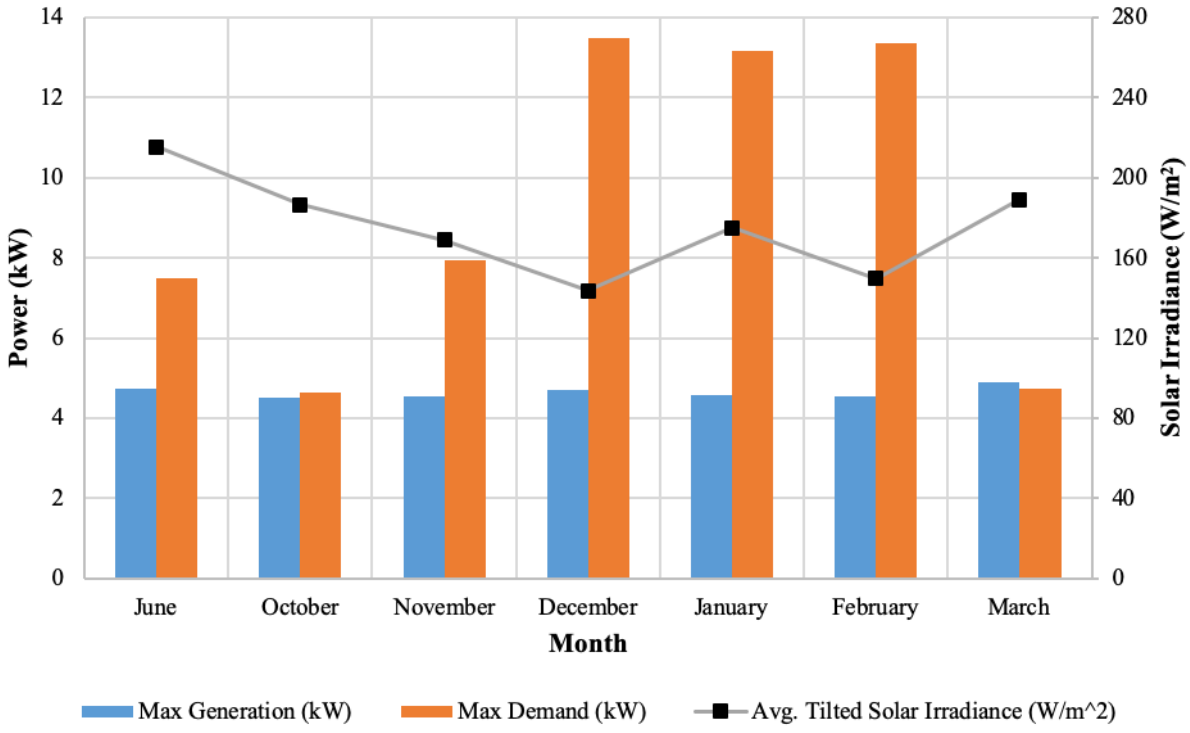

Figure 3.15: Maximum power generation, maximum power demand, and average instantaneous tilted solar irradiance.

The maximum values for generation and demand do not follow the same pattern as their instantaneously averaged representations. Maximum power generation remains at a near-constant value for all months considered, with the largest difference being just 7% between February and March, indicating that near peak power is reached in optimal weather conditions, regardless of

the time of year. Maximum demand is lowest in October with a value of just 4.64 kW, and highest in December at 13.5 kW. This may again be attributed to the large heating and cooling loads present in cooler and warmer months, respectively. Shoulder months such as October and March show more comfortable temperature conditions, and therefore require less energy for indoor conditioning.

Figure 3.16 is a presentation of the average daily energy production plotted alongside the average tilted solar irradiance values for each month. As expected, these two values follow very similar trends. For example, from June to October the average daily energy produced falls by 12.8%, while the average irradiance falls 13.4%. The two parameters continue to decrease in similar amounts until rising from December to January, falling from January to February, and finally rising from February to March.

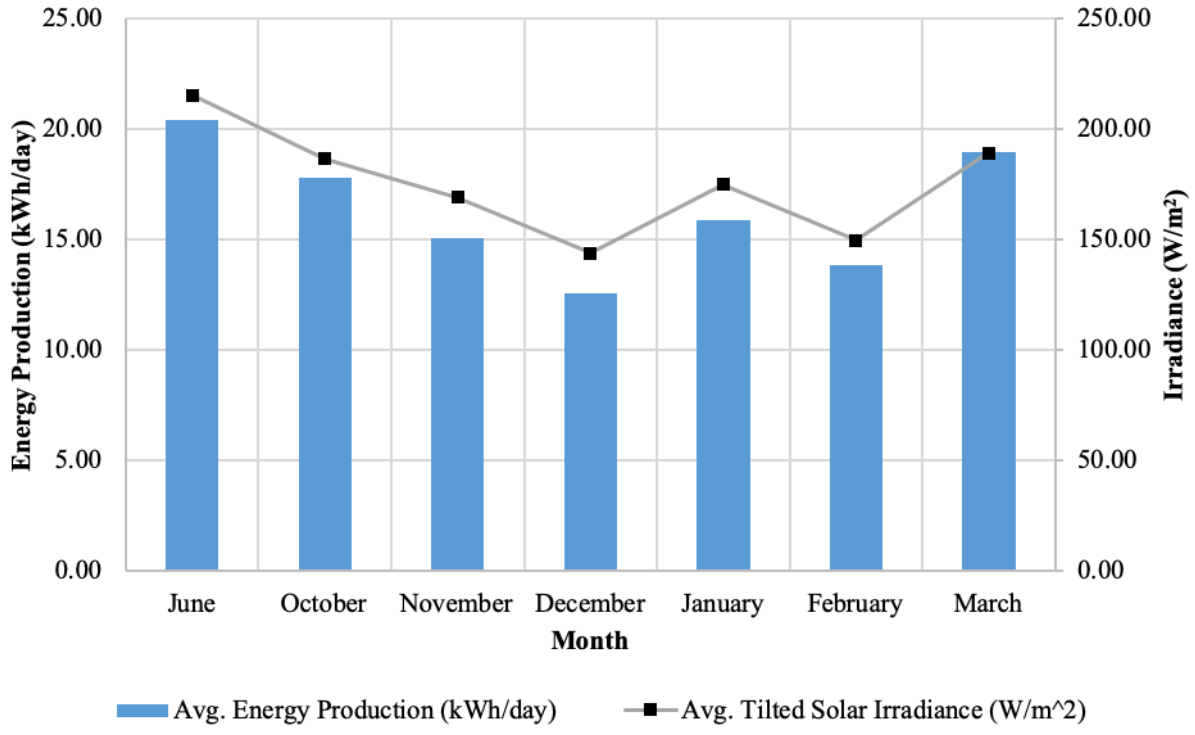

Figure 3.16: Average daily energy production and average instantaneous tilted solar irradiance for each month.

To provide a means of comparison to other PV systems, several performance parameters have been calculated using the collected data. These include array, final and reference yields, as well as performance ratio, capacity factor, system efficiency, and module efficiency. Explanations of their meaning, the processes used to calculate them, and their results are presented below.

The array yield serves as a measure of the performance of the PV panels alone and is defined on a daily basis in Equation 3.3 below [27].

$$Y_{A,d} = \frac{E_{\mathrm{DC,d}}}{P_{\mathrm{PV,rated,}}} \tag{3.3}$$

Here, $Y_{\mathrm{A,d}}$ is the daily array yield in units of kWh/kW$_{\mathrm{p}}$, E_{DC} is the DC energy produced by the panels for the day in kWh, and $P_{\mathrm{PV,\,rated}}$ is the nominal power rating of the array in kW. The unit of kW$_{\mathrm{p}}$ denotes the peak kilowatt rating of the array. The average daily array yield for each month has been found using Equation 3.4 [45],

$$Y_{\mathrm{A,m}} = \frac{1}{N}\sum_{\mathrm{d}=1}^{N} Y_{\mathrm{A,d}} \tag{3.4}$$

Where N is the number of days in the month. The DC energy from the panels is not currently measured and was therefore estimated by assuming an inverter efficiency of 97%, as shown in Equation 3.5 [15].

$$E_{\mathrm{DC}} = \frac{E_{\mathrm{AC}}}{97\%} \tag{3.5}$$

The reference yield represents the equivalent number of peak sun-hours for the array and is therefore a measure of available energy [27]. The daily reference yield and average daily reference yield values are found using Equations 3.6 and 3.7, respectively.

$$Y_{\mathrm{R,d}} = \frac{H_{\mathrm{d}}}{G_{\mathrm{STC}}} \tag{3.6}$$

$$Y_{\mathrm{R,m}} = \frac{1}{N}\sum_{\mathrm{d}=1}^{N} Y_{\mathrm{R,d}} \tag{3.7}$$

$Y_{R,d}$ and $Y_{R,m}$ are the daily and average daily reference yields in units of kWh/kW$_{STC}$ and kWh/kW$_{STC}$/day, respectively. H_d is the total solar radiation for the day in kWh/m^2, G_{STC} is the solar irradiance at standard test conditions (1 kW/m^2), and N is the number of days in the month.

The final yield is defined as the AC energy output from the PV system for a set time period divided by the rated power for the array [45]. Equations used to calculate the daily and average daily final yield are presented in Equations 3.8 and 3.9 below.

$$Y_{F,d} = \frac{E_{AC,d}}{P_{PV,rated}} \tag{3.8}$$

$$Y_{F,m} = \frac{1}{N}\sum_{d=1}^{N} Y_{F,d} \tag{3.9}$$

$Y_{F,d}$ and $Y_{F,m}$ are the daily and average daily final yields in units of kWh/kW$_p$ and kWh/kW$_p$/day, respectively. $E_{AC,d}$ is the AC energy output from the PV system for the day in kWh. As it does not account for the energy available to the array, the final yield may only be used to compare systems with a similar orientation and tilt in a shared geographic region with similar orientation [45].

Average daily array, reference, and final yield values for each month are presented in Figure 3.17.

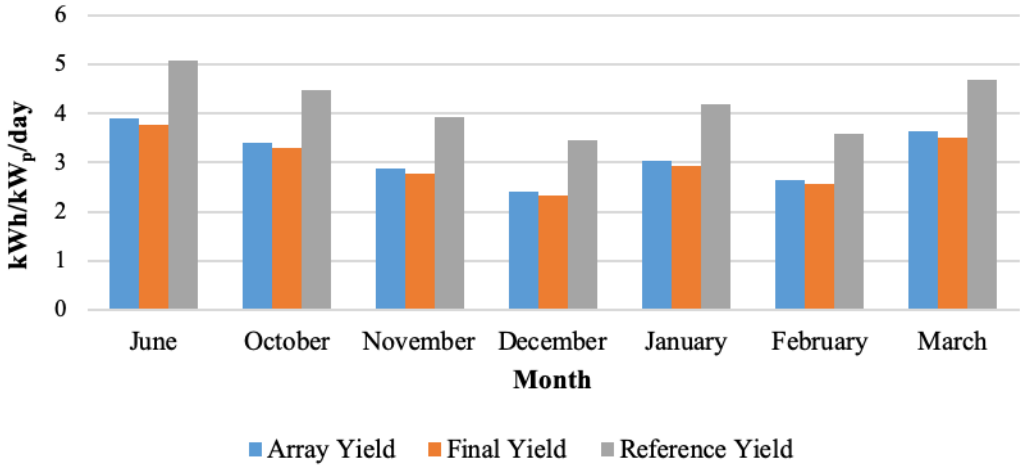

Figure 3.17: Average daily array, reference, and final yields for each month.

The average daily array, reference, and final yield values vary between 2.40 and 3.89, 3.45 and 5.09, and 2.32 and 3.78 kWh/kW_p/day for December and June, respectively. A comparison between the array and final yields in a given month is not useful due to the assumed inverter efficiency used to obtain E_{DC} values. The final and reference yields may be compared however, as they are both derived from measured values. The greater the difference between the reference yield (gray bars) and final yield (orange bars), the smaller the amount of available energy which has been successfully converted into AC energy. It is worth noting again that the solar irradiance measurements from the pyranometer have been adjusted to account for tilting by using output from PVWatts.

The complete month-by-month PVWatts AC energy prediction, the total monthly AC energy output for the NCSU Solar House, as well as the amount of days for which data from the NCSU Solar House is omitted for each month is shown in Table 3.5.

Table 3.5: Monthly PVWatts AC energy prediction, solar house output, and days omitted.

Month	PVWatts AC Energy (kWh)	NCSU Solar House AC Energy (kWh)	Amount of Days Omitted
January	596	492	0%
February	588	388	0%
March	684	587	0%
April	723	-	-
May	735	-	-
June	681	183	70%
July	686	-	-
August	686	-	-
September	645	-	-
October	635	302	45%
November	582	406	10%
December	553	389	0%

In order to compare the monthly output values, the PVWatts results have been reduced by the percentage shown in the last column of Table 3.5. Figure 3.18 displays the resulting comparison.

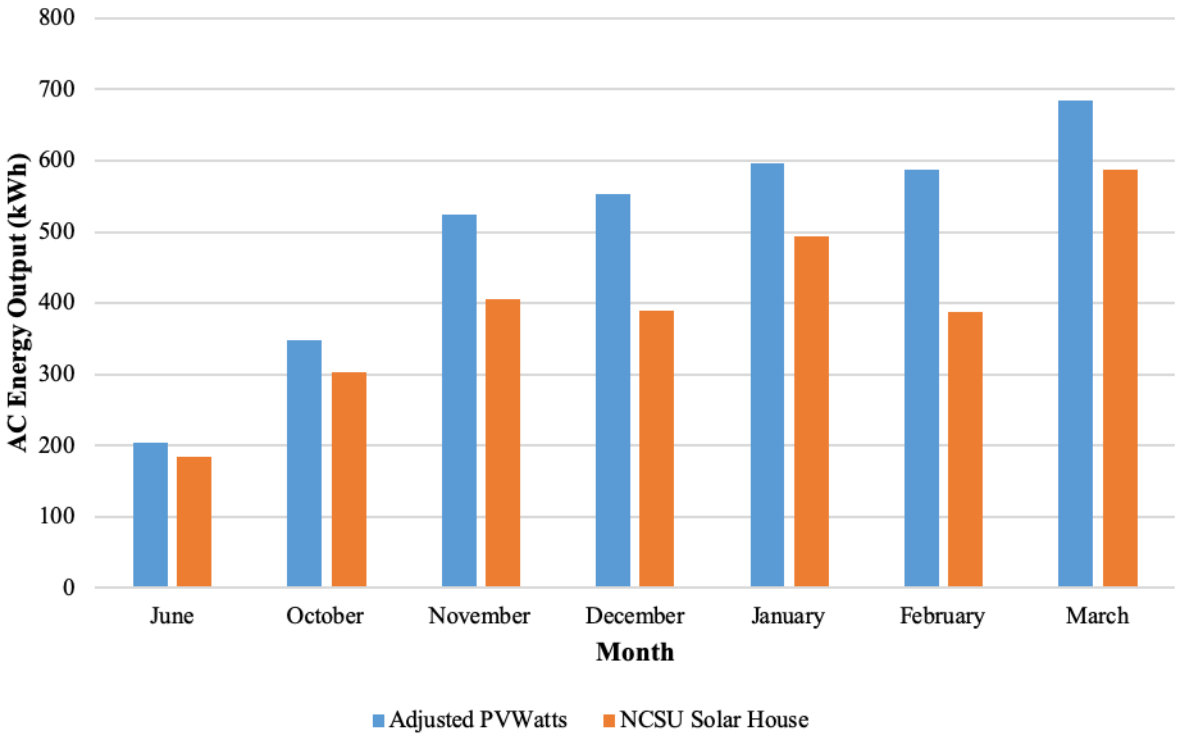

Figure 3.18: Adjusted PVWatts output compared to NCSU Solar House output.

The energy output measured from the house is consistently lower than the predicted output from PVWatts even after the prediction has been adjusted to account for omitted days. This suggests that there are components in the system at the house which are not performing as well as assumed by PVWatts or that the incident solar energy available is not as abundant as PVWatts expects. Further investigation is needed to determine the exact cause of this discrepancy.

A widely used parameter for evaluating PV system performance is the performance ratio (PR). The PR serves as a measure of how closely system performance mimics its ideal rated performance [24]. Because the performance ratio is normalized by the amount of solar radiation incident on a system as well as its rated efficiency, it may be used to compare systems with

varying locations, tilt angles, efficiency ratings, and orientation [24], [46]. Performance ratio is calculated using Equation 3.10 [24], [45].

$$\mathrm{PR} = \frac{\eta_{sys}}{\eta_{\mathrm{STC}}} = \frac{Y_{\mathrm{F}}}{Y_{\mathrm{R}}} \tag{3.10}$$

Y_{F}, Y_{R}, and η_{sys} are the final yield, reference yield, and system efficiency calculated over a defined time period. η_{STC} is the panel rated efficiency at STC. System efficiency is defined later in this chapter.

Capacity factor is a parameter which quantifies the fraction of full-load capacity that the system achieves within a given time period [27]. In other words, it represents how much energy the system produces compared to if it constantly produced energy at its peak power rating. The capacity factor has been calculated on a monthly basis as defined in Equation 3.11 below.

$$\mathrm{CF} = \frac{E_{\mathrm{AC,m}}}{(24\ \mathrm{hours/day})(N\ \mathrm{days})(P_{\mathrm{PV,rated}})} \tag{3.11}$$

Monthly values for performance ratio and capacity factor are presented in Figure 3.19.

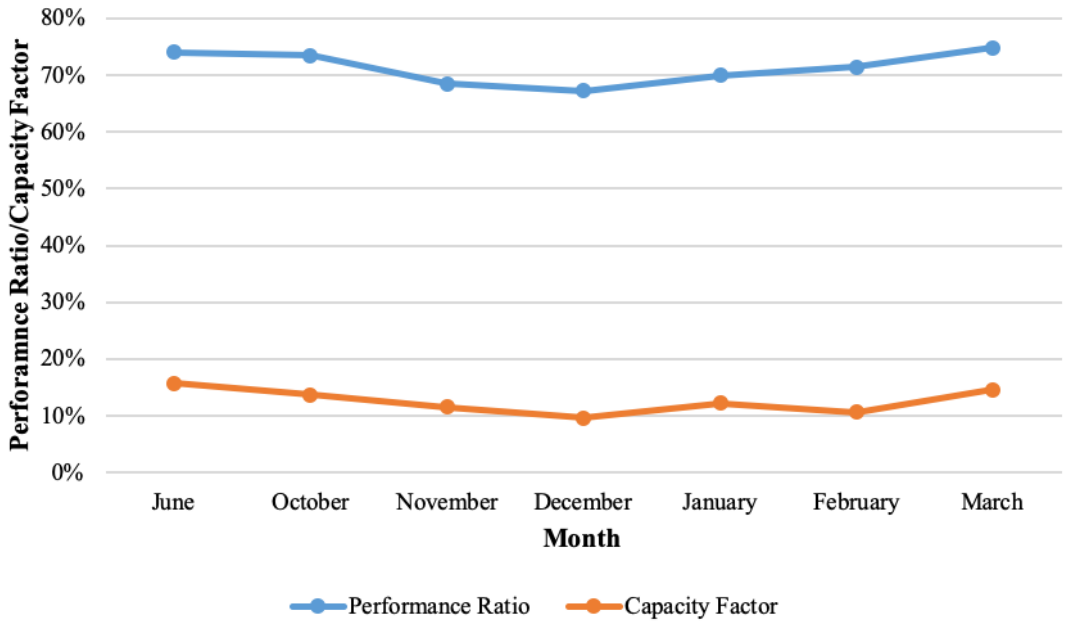

Figure 3.19: Monthly performance ratios and capacity factors.

The performance ratio varies between 67% and 75% in December and March, respectively. This suggests that the solar array performed closest to its ideal performance in March, perhaps due to clear weather and low temperatures. Note again that power data was measured directly in March, which may also have an effect on this result. The capacity factor varies between 10% and 16% in December and June, respectively. June is expected to have the highest value for capacity factor, since the sun spends the longest amount of time in the sky during this month (see the sun charts in Figures 3.10 and 3.11). For the same reason, it is expected that December would have the lowest capacity factor. Following the pattern seen in previous plots, there is a decrease seen for capacity factor for February.

Module and system efficiencies are calculated as follows [28], [29]:

$$\eta_{\mathrm{m}} = \frac{\bar{E}_{\mathrm{DC,d}}}{\bar{H}_{\mathrm{d}} A_{\mathrm{m}}} \tag{3.12}$$

$$\eta_{\mathrm{sys}} = \frac{\bar{E}_{\mathrm{AC,d}}}{\bar{H}_{\mathrm{d}} A_{\mathrm{m}}} \tag{3.13}$$

where $\bar{E}_{\mathrm{DC,d}}$, $\bar{H}_{\mathrm{d}}$, A_{m}, and $\bar{E}_{\mathrm{AC,d}}$ are the average daily DC energy produced, average daily solar radiation, solar PV module (array) area, and average daily AC energy produced, respectively. The average daily DC energy and solar radiation are evaluated over the same time period. Results of these calculations for each month are shown in Figure 3.20.

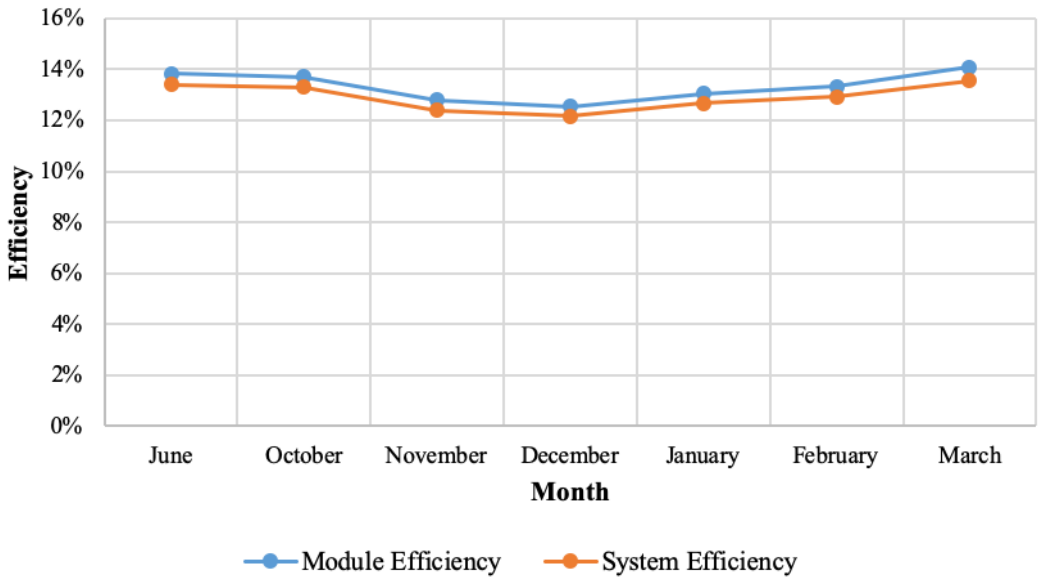

Figure 3.20: Monthly module and system efficiencies.

The module efficiencies and system efficiencies range from 12.6% to 14.1% and 12.2% to 13.6% in December and March, respectively. Again, these results suggest that the panels and system performed best during March and worst in December. These two efficiency values follow the same pattern due to the fact that the DC energy term used in the calculation of module efficiency is simply the measured AC energy divided by the assumed inverter efficiency of 97% [15].

Next, a sunny day was selected using past recorded weather forecasts for each considered month. Power generation for each day was plotted on the same figure, seen below in Figure 3.21. Dates used for the plots in figure are June 19th, October 24th, November 21st, December 22nd, January 22nd, February 25th, and March 28th.

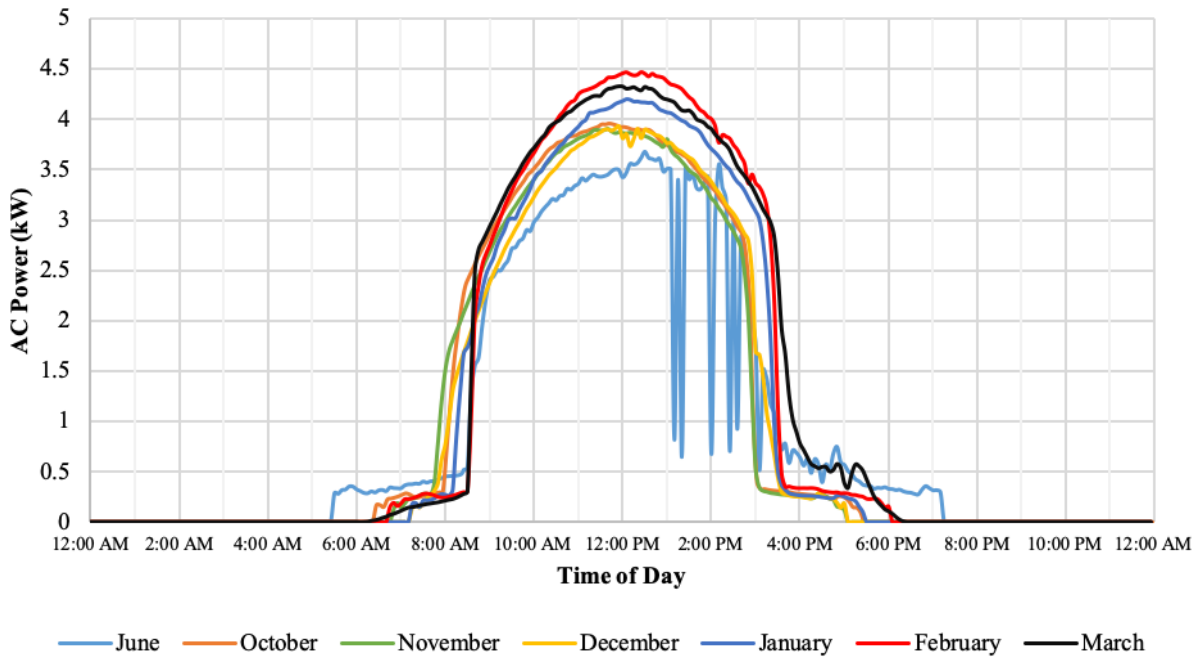

Figure 3.21: Power generation during a sunny day in each month.

The plots for June, October, and March in Figure 3.21 have been shifted 1 hour earlier than reported by the data logger to account for daylight savings time. Power generation begins earliest for June, followed by October/March, February, November, and December/January. A somewhat unexpected detail seen in the plot is the relatively low power achieved during the sunny day in June. One may at first expect June to have one of the highest peak power production rates, since the sun is in the sky longest during this month and also most directly overhead. Of the days for which June data is available (June 16 – June 24), this day had one of the sunniest forecasts. Despite the clear weather, the maximum power generation was 18% lower than that for February 25th. One possible explanation for this difference is the fact that the sun is most directly overhead in June, but the panels are not horizontal (facing directly overhead). As noted earlier, the panels are angled at 36° from horizontal, so that they will produce the maximum amount of energy annually. However, since they are angled, radiation from the sun during the summer will be less direct.

Another potential reason for the power decrease in June is panel operating temperature. As noted previously, elevated panel temperatures have adverse effects on performance [23]. The temperature coefficient for the SPR-225 panels is given as -0.38%/K [12]. The temperature coefficient is multiplied by the difference between actual elevated panel operating temperature and STC panel operating temperature (25°C) in order to find the reduction in power production. During periods of high incident irradiance, PV panels typically operate around 25°C higher than the surrounding ambient air temperature [47]. The high for June 19th was 99°F, which is equal to about 37°C. Therefore, the panels likely were at a temperature around 62°C during this time (37°C higher than the STC condition of 25°C that has been used to rate the panels). Multiplying the temperature coefficient by the difference of 37°C yields a power reduction factor of 14%. Multiplication of the maximum power output for June 19th (3.67 kW) by 1.14 gives a power output of 4.18 kW, which is the assumed value of output power that would have been achieved without any effects from temperature. This value is higher than all of the maximum values shown in Figure 3.21, except for January, February, and March. The highest recorded temperatures for the rest of the days considered in Figure 3.21 are 69°F (20°C), 60°F (15°C), 56°F (13°C), 43°F (6°C), 63°F (17°C), and 70°F (21°C) for October 24th, November 21st, December 22nd, January 22nd, February 25th, and March 28th, respectively. The maximum power achieved over the entire monitoring period is in June, however this value occurred on a partly cloudy day when the recorded high was 94°F. That the maximum power generation shown in Figure 3.21 is in February is also somewhat unexpected, given the fact that February exhibits one of the lowest values for both average energy production and incident solar irradiance. However, it is important to remember that the sunny day plots shown represent only one day out of each month.

To evaluate their correlation, each instantaneous AC power generation data point has been plotted against its corresponding solar irradiance value on a monthly basis in Figures 3.22 through 3.28.

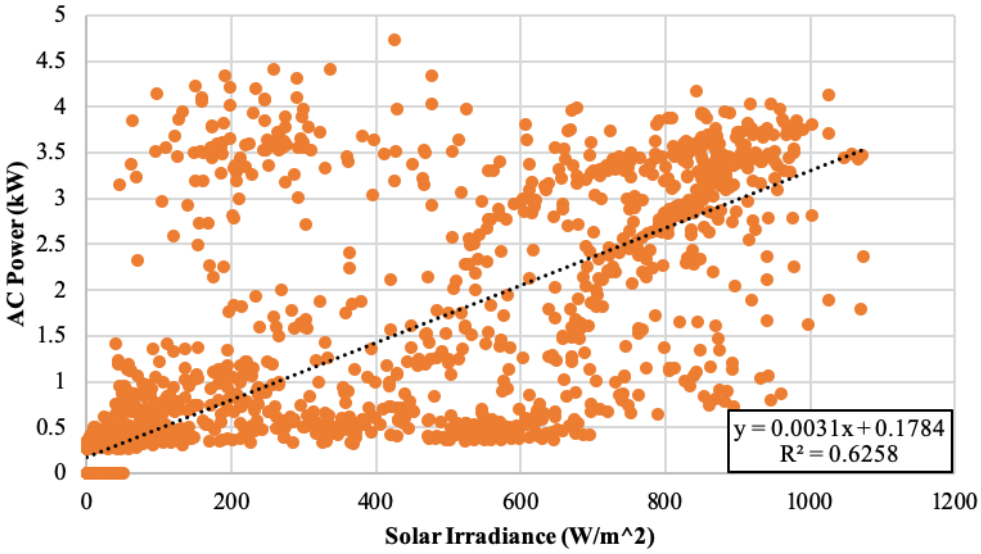

Figure 3.22: AC power production vs. solar irradiance, June 2018.

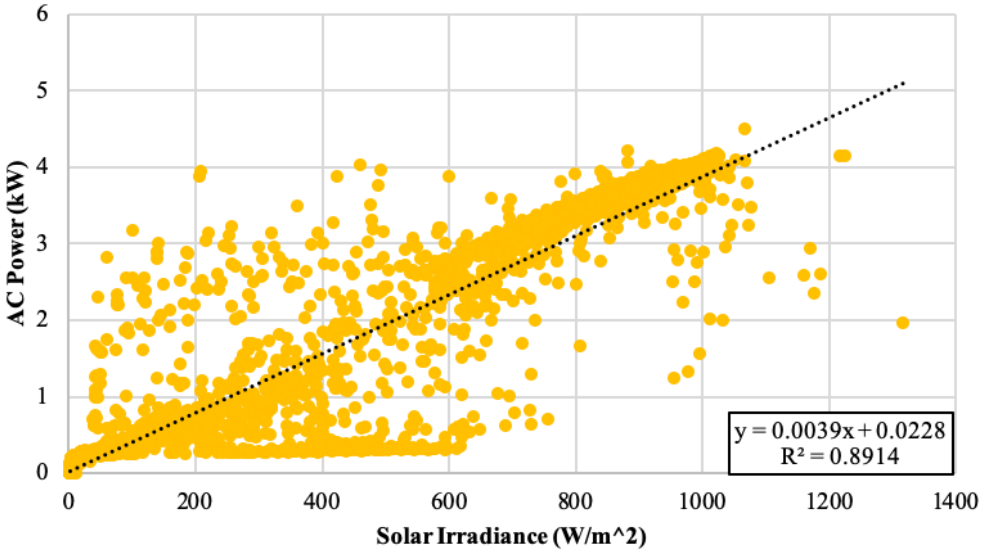

Figure 3.23: AC power production vs. solar irradiance, October 2018.

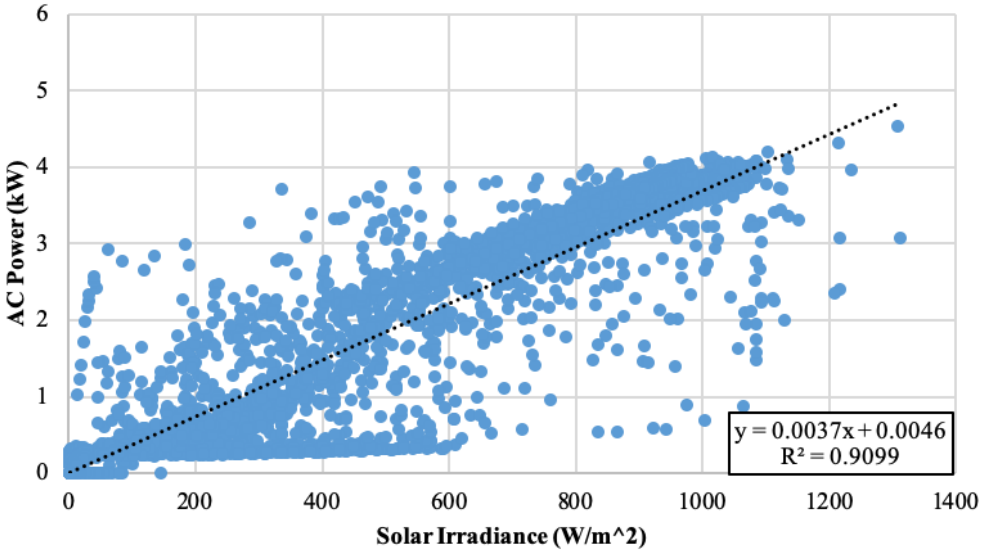

Figure 3.24: AC power production vs. solar irradiance, November 2018.

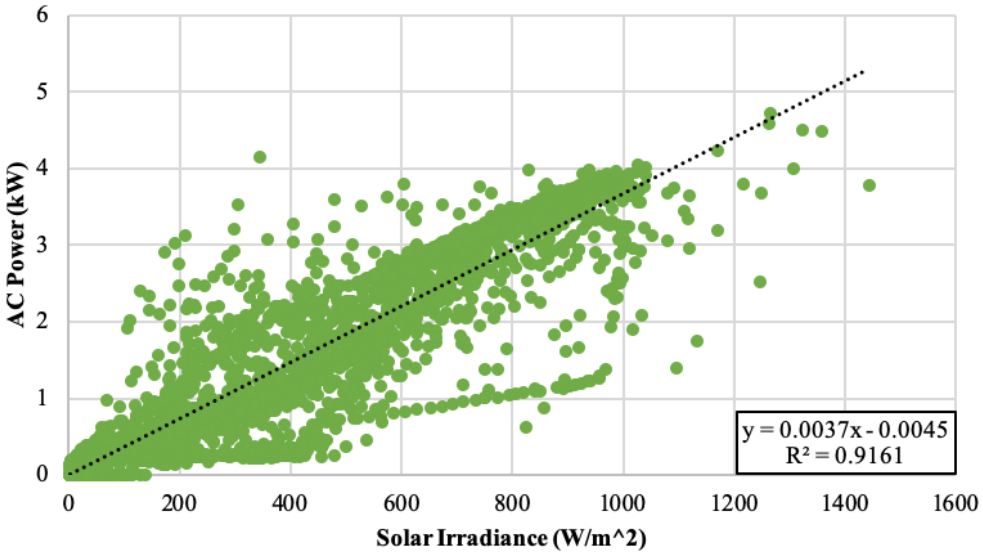

Figure 3.25: AC power production vs. solar irradiance, December 2018.

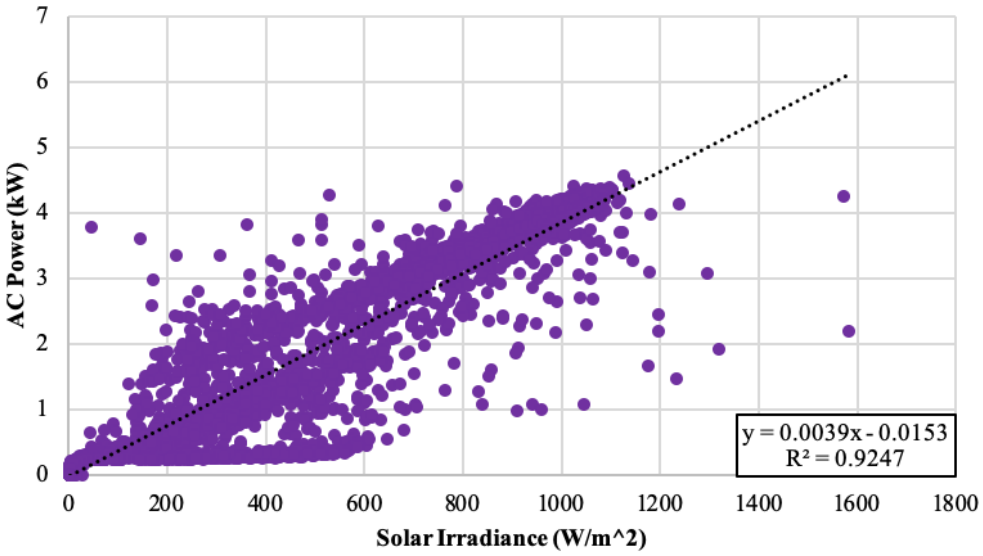

Figure 3.26: AC power production vs. solar irradiance, January 2019.

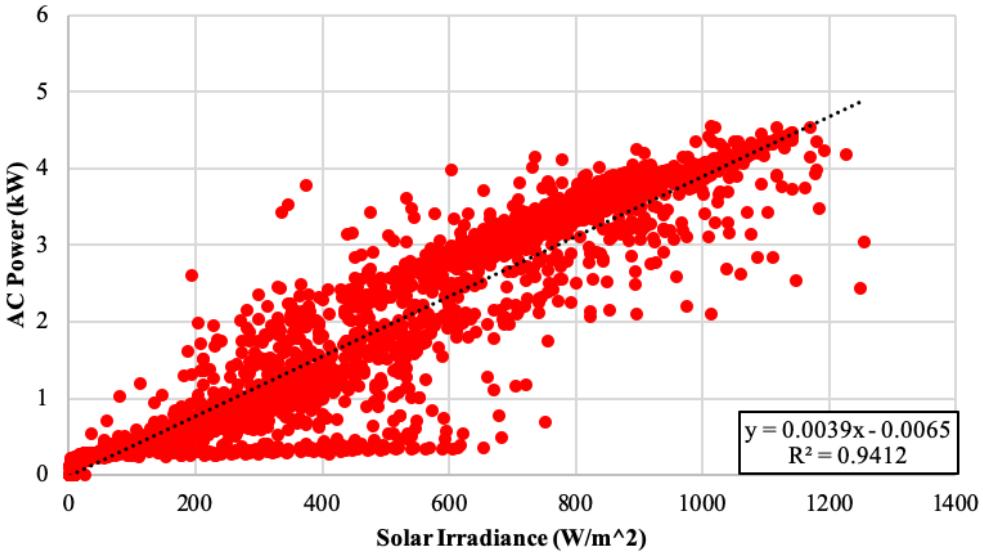

Figure 3.27: AC power production vs. solar irradiance, February 2019.

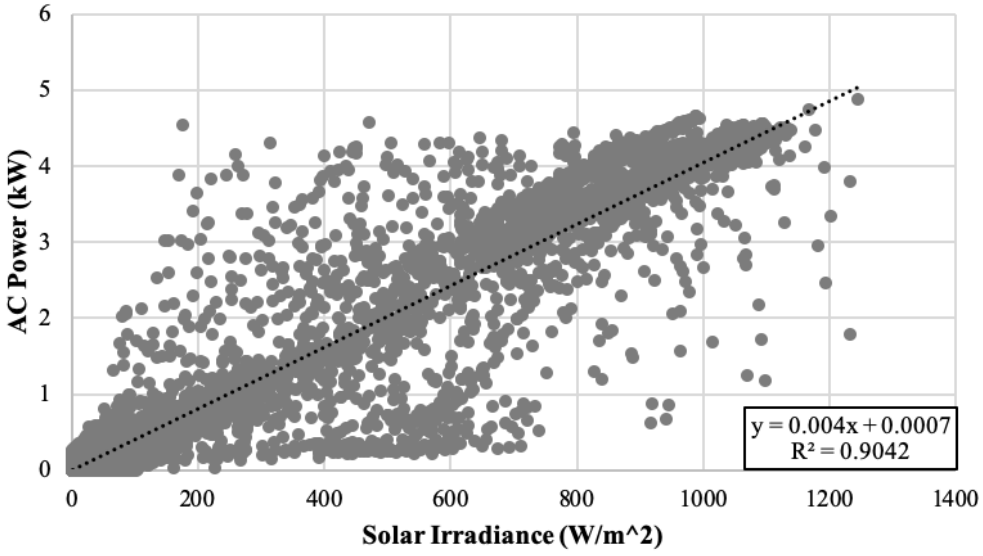

Figure 3.28: AC power production vs. solar irradiance, March 2019.

The relationship between AC power output and solar irradiance is strongest in February and weakest in June, as evidenced by the R^2 correlation coefficient value for each plot. For June, the R^2 value is 0.6258 – which is 34% lower than the maximum value of 0.9412 in February. The large scatter of data in June may be due to very high ambient temperatures or a large mismatch between irradiance measured by the pyranometer and the actual amount incident on the panels. Further investigation is needed to definitively determine the cause of this scatter. The slope of the trendline for each plot remains relatively similar throughout all months, with a maximum of 0.004 occurring in March and a low of 0.0031 in June. A large slope value is desirable, as this translates to a high power output for a small amount of solar irradiance.

Lastly, the percentage of data points where the instantaneous power production from the solar PV array was greater than or equal to the house's demand was calculated. The total amount of energy produced and consumed during each month was also compared. The results of these calculations are shown in Figure 3.29 below.

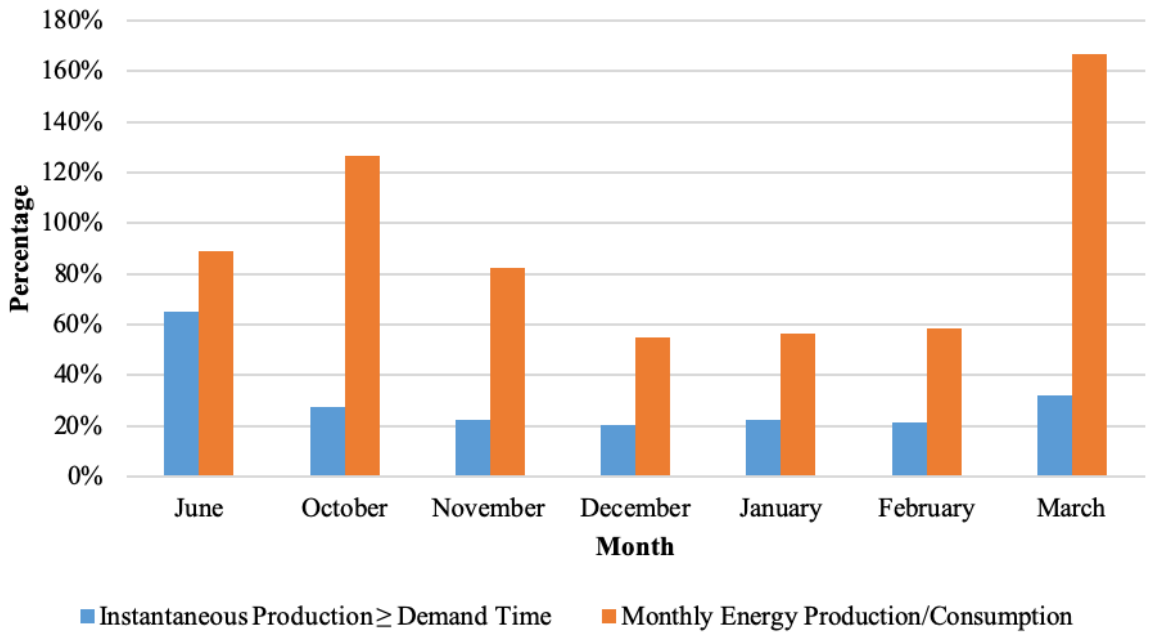

Figure 3.29: Instantaneous power generation vs. demand and monthly energy production vs. consumption.

Immediately evident from the figure is that the amount of time when instantaneous power production is greater than or equal to demand is much higher during June than the rest of the months. This is due to the much lower baseline power demand from the house (the cause of which is unknown) and the increased amount of time the sun spends in the sky during June. The minimum value for the instantaneous production/demand comparison is 21% in December and February. During these months, the sun spends relatively little time in the visible sky and the heating demand is high. Instantaneous values are essentially the same for November through February, while they increase significantly for October and March.

The monthly total comparison shows that October and March were by far the best months, as they are the only two months with a higher total production than consumption. Total energy production was 67% and 27% higher than total energy consumption for March and October, respectively. This is again due to the relatively low heating and air conditioning requirements for these months coupled with clear weather conditions. The worst month is again

shown by this metric to be December, when energy produced was just 55% of the energy consumed.

3.1.4 Overall Monitoring Period Performance

To quantify the overall performance of the solar PV system, each of the performance parameters presented above has been calculated based on the entire monitoring period. Results are presented in Table 3.6.

Table 3.6: Overall results for 2018-2019 monitoring period.

Parameter	Value	Units
Array Yield	3.02	$kWh/kW_p/day$
Final Yield	2.93	$kWh/kW_p/day$
Reference Yield	4.08	$kWh/kW_{STC}/day$
PR	72%	-
CF	12%	-
Module Efficiency	13.3%	-
System Efficiency	12.9%	-
Total AC Energy Produced	2750.01	kWh
Average AC Energy Produced	15.8	kWh/day
Total Energy Consumed	3534.5	kWh
Average Energy Consumed	20.3	kWh/day
Production > Demand Time	26%	-
Energy Production/Consumption	78%	-

These results may be compared to results from PVWatts and other similar studies. It is important to keep in mind that this is not an “apples-to-apples” comparison however, since the other studies considered here use data from a full year. The total AC energy produced by the PV array at the NCSU Solar House is 2750 kWh, which is 36% lower than the PVWatts predicted total for the same months of 4319 kWh. Some deficiency is expected, as the monitoring period does not include all days for each month. A total of 38 days is not included in the monitoring period – just an 18% decrease compared to if all days had been included. Therefore, the decrease in AC

energy output may not be solely due to the days omitted from the study, suggesting that the array is underperforming compared to the PVWatts model. Most of the days omitted occurred in June however, which is the fourth highest energy producing month according to PVWatts.

The average daily array, final, and reference yields are 15%, 21%, and 43% higher than those given for the system tested by Ayompe et al., respectively [24]. However, the comparison of these yield values is not a good indicator of performance, since Dublin has a very different climate from Raleigh and also lies at a much higher latitude (about 53° N). Although the climates may still be very different, Crete and Málaga lie at latitudes much closer to Raleigh (about 35° N and 37° N, respectively). The final yields reported for the systems in Crete and Málaga in Table 2.1 are 2.0 – 5.1 and 3.7, respectively. While none of these comparisons are particularly useful, the yield values calculated for the NCSU Solar House will allow its performance in the future to be compared to its present performance. Also, if studies are done in the future for PV systems near Raleigh, comparisons between these systems would be meaningful.

The overall performance ratio is 10% lower than for the "Present Study" system shown in Table 2.1 but is higher than most of the rest. Since the performance ratio allows comparison between systems of varying location, climate, and orientation, this is significant. The high performance ratio of the NCSU Solar House system suggests that it is performing well overall. The capacity factor, module efficiency, and system efficiency compare relatively well with the system evaluated by Ayompe et al. (2011), differing by +2%, -1.6%, and +0.3%, respectively [24]. The capacity factor is also 4.5% lower than the estimate from PVWatts. The "Energy output" term shown in Table 2.1 is calculated as the AC energy produced divided by the array's peak kW rating. The corresponding value for the house's array is therefore 509.3 kWh/kW_p, which is 55% lower than the "Present Study" value of 885.1 given in Table 2.1. Note again that the value shown in Table 2.1 was found using a full year's worth of data. The amount of data

points where the solar PV array production was recorded as greater than or equal to the house's total power demand is 26%. The total energy production from the PV panels divided by the total energy consumption of the house is 78%. The correlation between AC power output and incident solar irradiance for the entire monitoring period is shown in Figure 3.30.

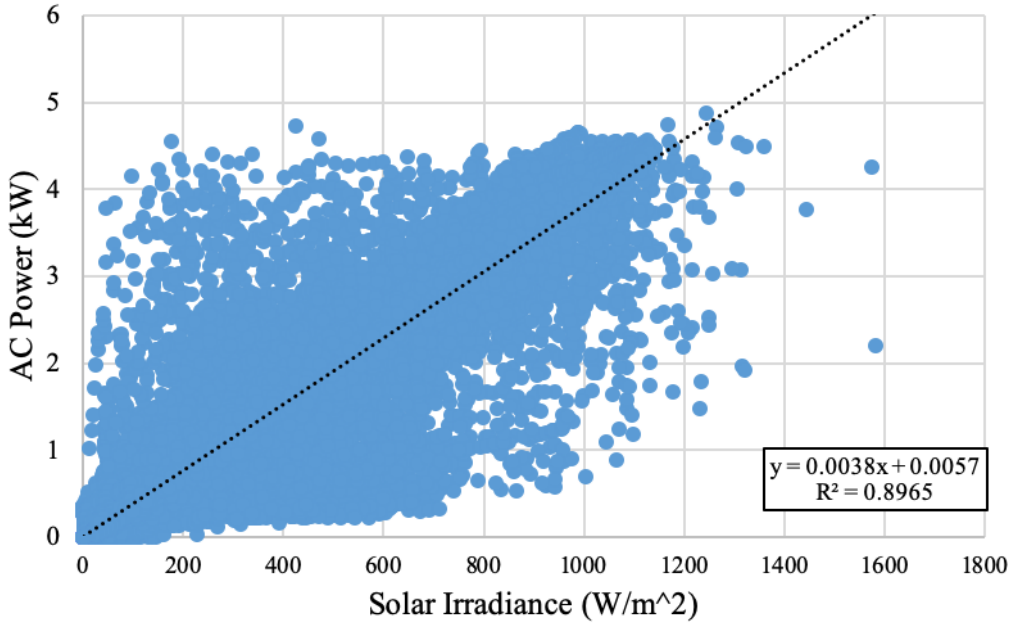

Figure 3.30: AC power production vs. solar irradiance, entire monitoring period.

The R^2 value of 0.8965 shows that AC power production may not be easily predicted by solar irradiance.

The economics of a system such as the one installed at the solar house have been briefly investigated to give a financial estimate of the PV array's performance. It is estimated that the total, out-of-pocket cost of a 5 kW residential PV system in Raleigh, NC is in the range of $11,900 - $16,099 [48]. However, the typical homeowner would be able to the deduct 30% of the cost of their PV system from their federal taxes through the Residential Renewable Energy Tax Credit [49]. The new total cost of a 5 kW system would be in the range of $8,330 - $11,269. For

the incomplete months, the fraction of days considered over total days in the month was found. A projected total energy production value for each incomplete month was then found by dividing the actual measured energy production by the fraction of days considered. Results from these calculations are shown in Table 3.7.

Table 3.7: NCSU Solar House monthly energy production projections.

Month	Days Considered	Total Days	Fraction of Total Days Considered	Projected Total Production (kWh)
June	9	30	0.30	612.00
October	17	31	0.55	551.35
November	27	30	0.90	451.15
December	31	31	1	389.19
January	31	31	1	492.83
February	28	28	1	388.14
March	31	31	1	587.85
Total	174	212	0.82	3472.52

According to PVWatts, the energy produced during the months in Table 3.7 accounts for 55% of total annual production. To obtain an estimate for the annual production, the total projected energy production for the monitoring period (3472.52 kWh) was therefore divided by 55%. This yields an estimate of 6314 kWh produced annually. Based on the residential rate schedule RES-53 from Duke Energy Progress, the electrical rates for single-phase service from July to October and November to June are $0.10868/kWh and $0.10395, respectively [50]. Total savings for each month based on these rate schedules and the actual energy saved each month (not the projected totals) are shown in Figure 3.31.

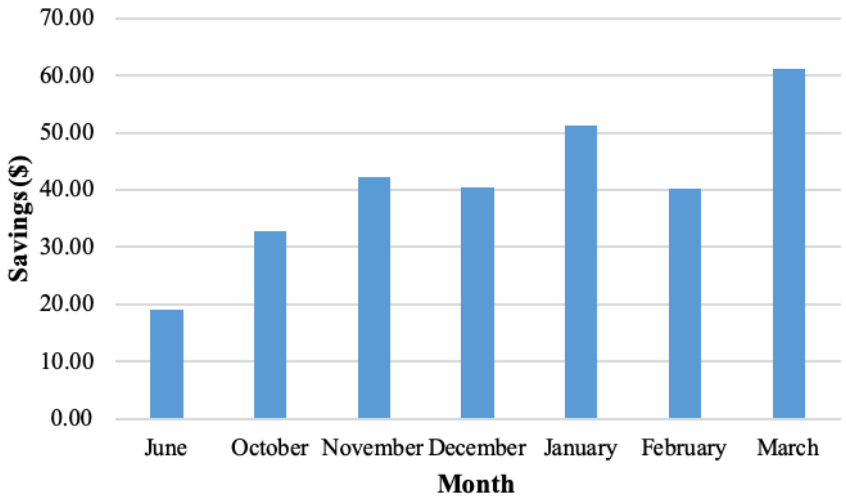

Figure 3.31: Monthly electricity savings at NCSU Solar House based on Duke Energy Progress RES-53 rate schedule.

A representative annual electric rate of $0.10553/kWh has been found using the weighted average of the seasonal rates given above. Using this rate and the estimated 6314 kWh annual production, the electricity savings for the NCSU Solar House are expected to be around $666/year. Assuming the total installed cost of the system to be in the range of $8,330 - $11,269, the simple payback period for the system would be between 13 and 17 years. SunPower currently offers a 25 year warranty on their new products similar to those on the house [51].

3.2 Solar Water Heating System

As mentioned previously, the primary data available regarding the solar water heating system is the glycol return temperature (to the collector), glycol supply temperature (to the tank), and the water heater electrical usage. The water heater electrical usage is the electrical consumption of the backup water heating element inside the storage tank. With the available data, trends may be observed between the temperatures of the glycol and the local weather conditions. One such plot is shown for January 17, 2019 in Figure 3.32 below.

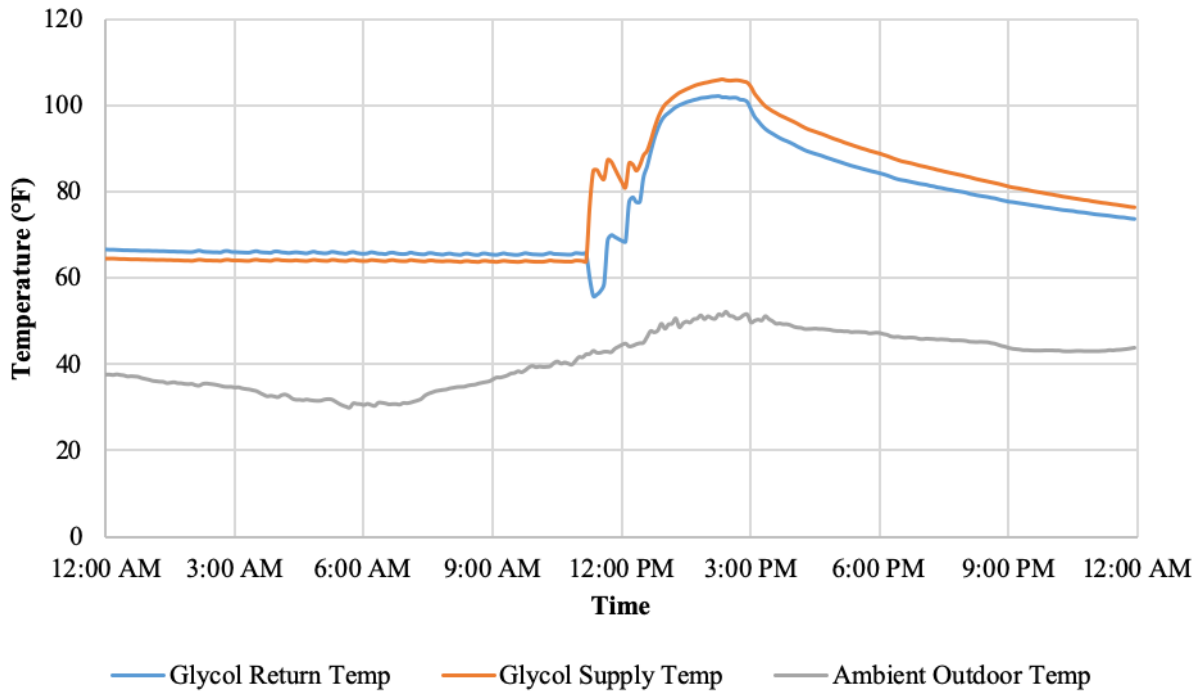

Figure 3.32: Ambient outdoor, glycol return, and glycol supply temperatures, January 17, 2019.

The plot shows an expected positive correlation between the ambient outdoor temperature and the glycol supply temperature (from the collector into the tank) from about 12:00PM January 17th to 12:00AM January 18th. From 12:00AM to 12:00PM January 17th, the glycol return and supply temperatures remain flat and nearly equal. This is during a time when the pump is not running, since the temperature at the roof-mounted collector is not high enough. It appears that around 11:30AM, some hot water was used (hence the drop in the glycol return temperature) and the pump was turned on automatically. The supply and return temperatures then steadily decline throughout the evening, following a trajectory similar to the ambient outdoor air temperature. Although these trends are interesting to observe, more information is needed to properly monitor the performance of the system.

Data is also available concerning the power used by the backup water heating element in the tank. Plotted below in Figure 3.33 is the backup water heating power usage for January 17, 2019.

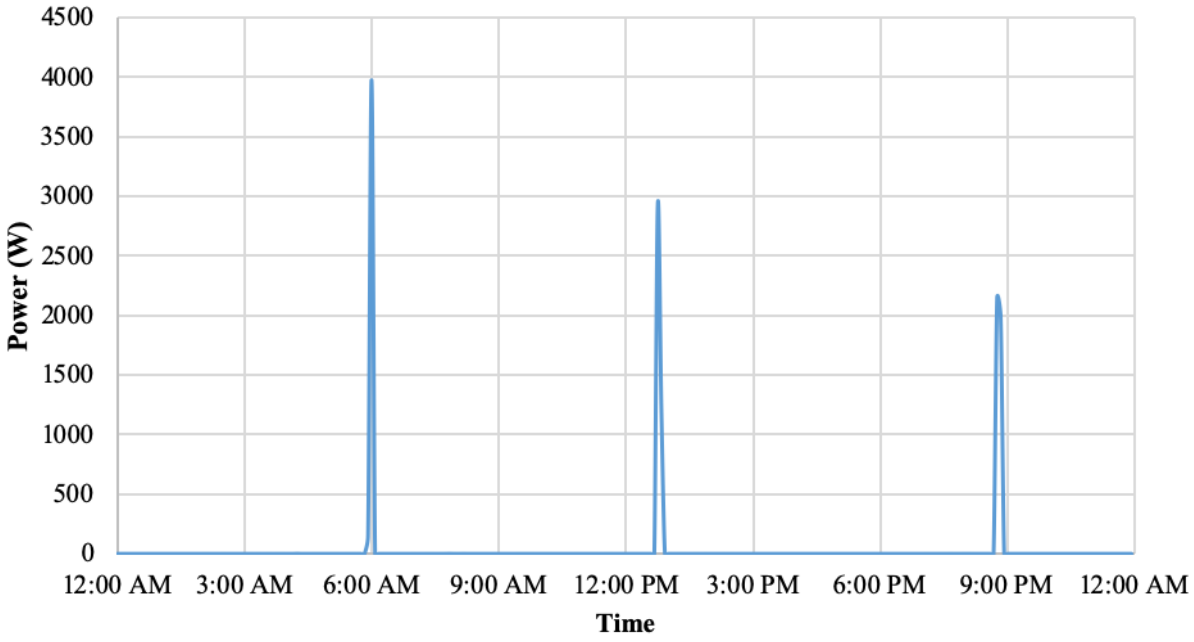

Figure 3.33: Backup water heater power usage, January 17, 2019.

The plot above shows that the water heater uses a significant amount of power (between 2 and 4 kW), but only for a very brief periods of time. The peak power demand achieved by each "spike" shown in Figure 3.33 demonstrates the decline in heating energy needed as the day goes on due to the solar energy supplied by the glycol loop. The peak temperature for glycol supply is not reached until around 2:30PM. The total energy used by the backup water heater on this day was about 1.1 kWh.

3.2.1 Variations Due to Weather Conditions

The same days which have been used to compare performance of the PV array in different weather conditions have been examined again for the solar water heater. Plots

displaying the water heater power and glycol return/supply temperatures are shown in Figures 3.34 through 3.37 below.

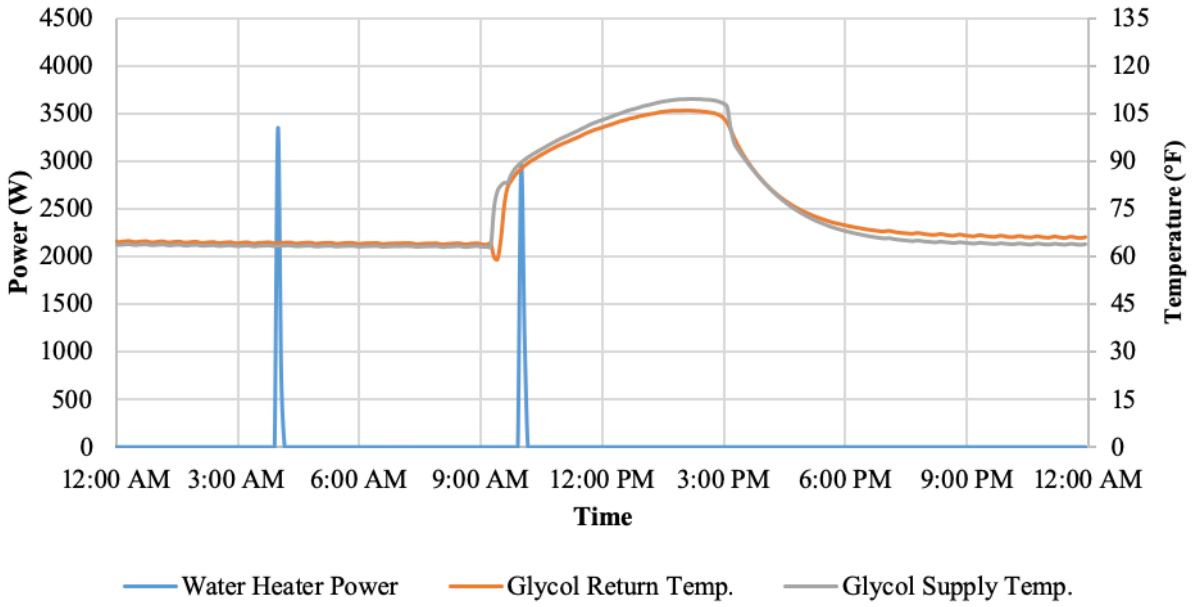

Figure 3.34: Sunny day backup water heater power and glycol temperatures, January 22, 2019.

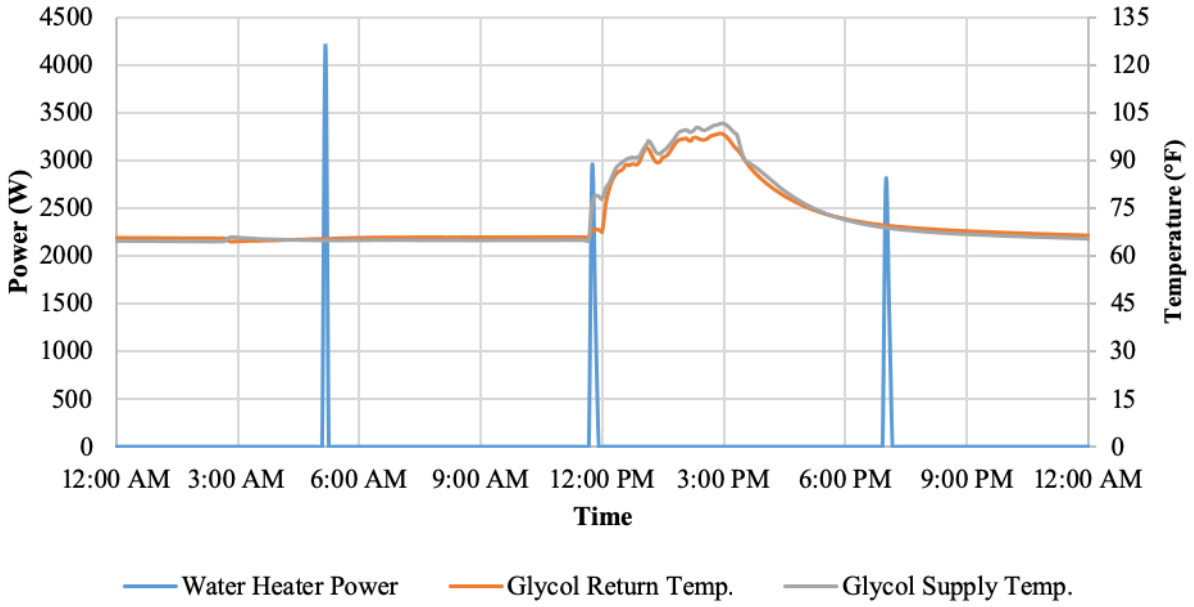

Figure 3.35: Partly cloudy day backup water heater power and glycol temperatures, January 24, 2019.

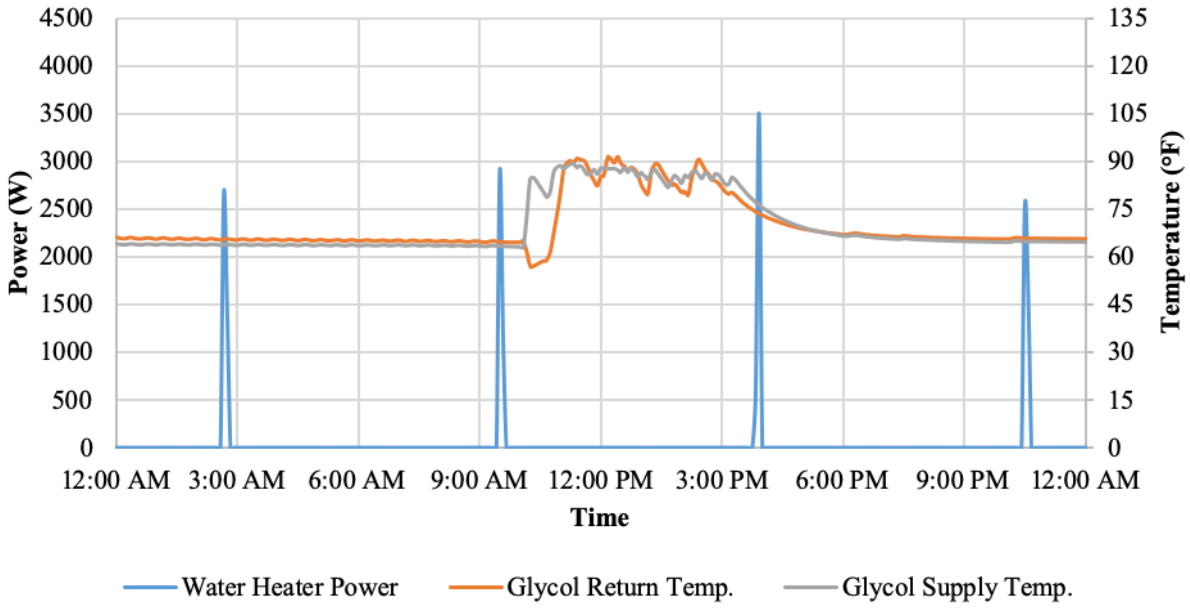

Figure 3.36: Cloudy day backup water heater power and glycol temperatures, January 23, 2019.

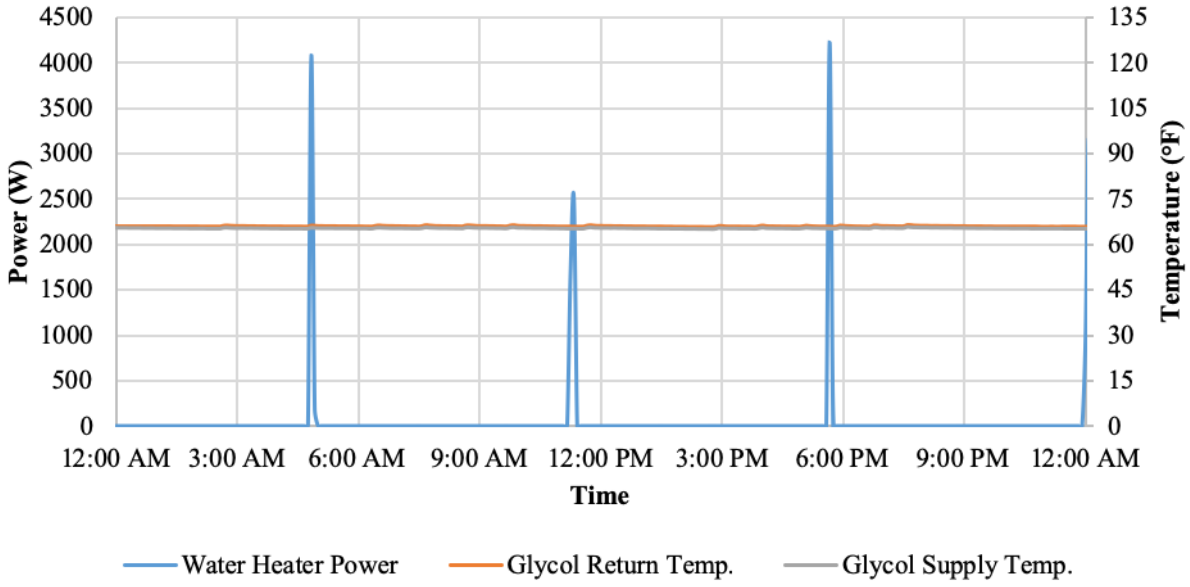

Figure 3.37: Rainy day backup water heater power and glycol temperatures, January 4, 2019.

A clear correlation is seen between the weather conditions and the power used by the hot water heater. For example, on January 22nd there are only two power spikes, whereas for the rest of the days shown there are either three or four. The two instances of power usage on January 22nd also

stay below 3500 W, whereas on January 24th and 4th the power spikes reach nearly 4500 W (the maximum power for the heating element). Total energy used by the water heater varied between 0.77 kWh on January 22nd and 1.48 kWh on January 4th.

It is also interesting to observe the patterns for glycol supply (to the tank) and return (to the solar collector) temperatures. On January 22nd (the sunny day condition) both temperatures begin to rise rapidly beginning just after 9:00AM, reaching a maximum around 2:30PM and then falling steadily to near their beginning temperatures around 8:00PM. For January 24th (partly cloudy conditions) the temperatures do not rise significantly until just before 12:00PM, reaching a peak just before 3:00PM and falling through about 8:00PM. In the cloudy condition on January 23rd the temperatures increase around 10:00AM and reach their (much lower) maximum much earlier at around 11:00AM. From 11:00AM to 2:30PM the temperatures exhibit a very irregular pattern which is indicative of the effect of sporadic cloud cover on the system. Finally, on January 4th the consistently rainy conditions yield essentially constant glycol temperatures around 65°F. This shows that no useful heating energy was extracted from solar radiation on this day. The maximum glycol supply temperature of the days shown was 109°F, which occurred on January 22nd.

3.2.2 Variations with Time of Year

In a similar manner to the monthly comparisons made for the PV system, monthly data has been gathered for the solar water heater. Data is not available for the solar hot water heater in June 2018, but the rest of the monitoring periods are the same as discussed previously. Figure 3.38 shows the average energy use per day and the average glycol supply temperature (to the storage tank) for each month. Average glycol return temperatures are not shown due to their similarity to supply temperatures.

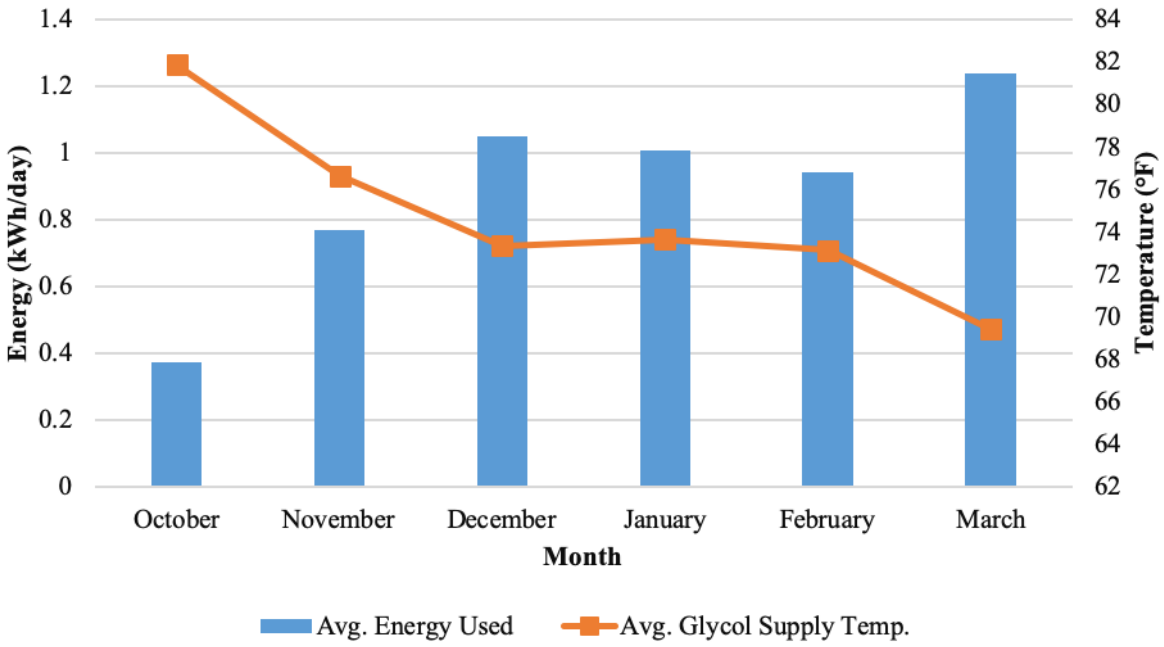

Figure 3.38: Average daily energy use and glycol supply temperature for each month.

It appears that average daily energy use is mostly inversely correlated to the glycol supply temperature. This serves as evidence that the glycol loop is successfully reducing the amount of electrical energy needed to sufficiently heat the water by supplying heat from solar energy.

Chapter 4

Future Work

The NCSU Solar House is currently equipped with a data logging system which allows limited performance assessments of its subsystems. The results and evaluations provided in Chapter 3 provide an overview of its capabilities. In order to more accurately and completely evaluate the performance of the solar PV array and solar hot water heating system, additional measurement devices are required. This chapter aims to lay a framework for potential equipment and data measurement additions which will provide more useful insights into the performance of these systems. Suggestions are also made for possible research avenues in the future.

4.1 Overview of Existing Measurements

To assist with future work, a brief summary of the current measurements being taken at the house is presented in this section. Tables 4.1 through 4.3 show the measurements being taken by Logger 3, Logger 2, and the outdoor weather station, respectively.

Table 4.1: Summary of measurements currently taken by Logger 3.

Port	Measurement Description	CT Size (A)
1	AFV Garage Main Power - Phase A	75
2	AFV Garage Main Power - Phase B	75
3	Solar House Water Heater Auxiliary power	20
4	Solar House Main Power - A	100
5	Solar House Main Power - B	100
6	Solar House HVAC Compressor / Condensing Unit	20
7	Solar House PV Panel AC Power Output	50
8	Computer Server / IT Closet	10

Table 4.2: Summary of measurements currently taken by Logger 2.

Measurement Description	Units
Air Handling Unit Fan Power	A
Water Heater Glycol Supply (into tank)	°F
Water Heater Glycol Return (out of tank)	°F
Downstairs Temperature	°F
Downstairs Relative Humidity	%
Computed Downstairs Dewpoint Temperature	°F
House HVAC Supply Air Temperature	°F
House HVAC Supply Air Relative Humidity	%
Computer House Supply Air Dewpoint Temperature	°F
House HVAC Unit Compressor Suction Temperature	°F
House HVAC Unit Leaving Condenser Temperature	°F

Table 4.3: Summary of measurements currently taken by outdoor weather station.

Measurement Description	Units
Solar Irradiance	W/m^2
Outdoor Air Temperature	°F
Outdoor Air Relative Humidity	%
Computed Outdoor Air Dewpoint Temperature	°F
Outdoor Wind Speed	mph
Outdoor Wind Direction	Degrees bearing

Logger 3 is housed in a metal, wall-mounted box in the utility closet on the bottom level of the house, while Logger 2 rests on top of a wooden box next to the water storage tank in the main bottom level room. The weather station resides in the back lawn of the house and can be seen in the foreground of Figure 1.6. Figures 4.1 and 4.2 are pictures of the front and bottom of Logger 3, respectively. The bottom of the logger shows ports where the connections noted in Table 4.1 are made. Figure 4.3 is a picture of Logger 2.

Figure 4.1: Logger 3 in the utility closet of the NCSU Solar House.

Figure 4.2: Bottom of Logger 3, showing details of port connections.

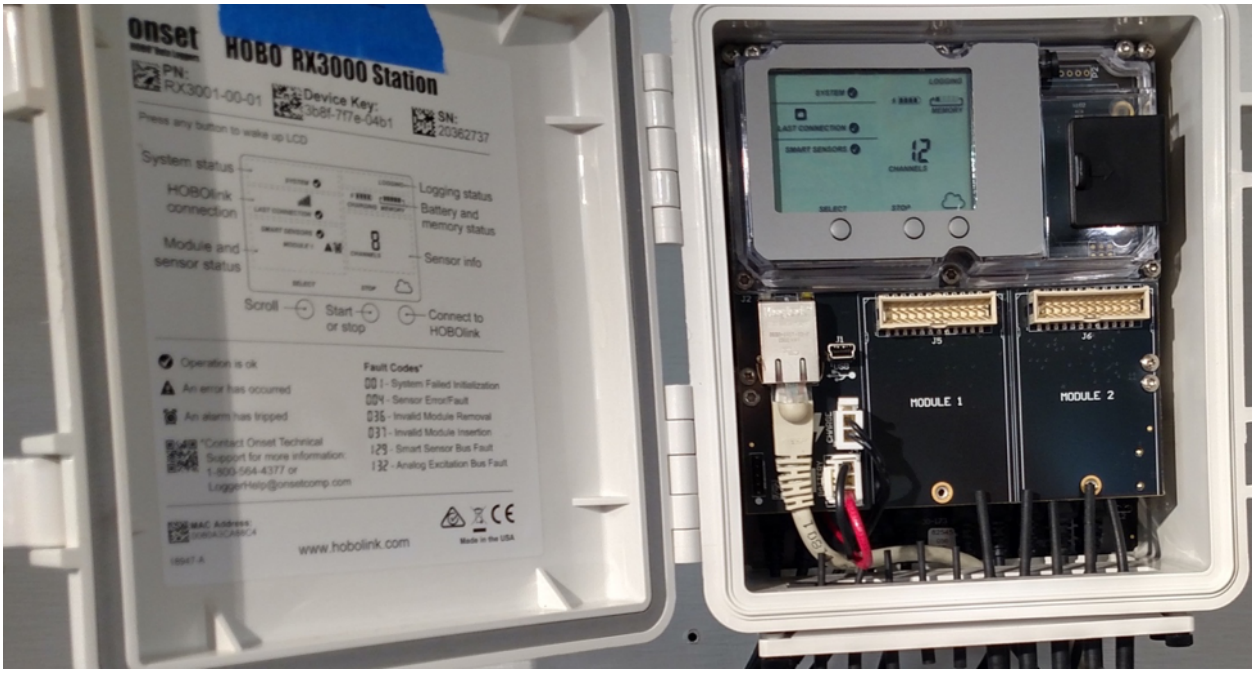

Figure 4.3: Logger 2 and its housing.

Note that many of the measurements in the tables above have not been used in this study. Suggestions for modifications to systems at the house which may allow more of these measurements to be used are presented in the following sections.

4.2 Solar PV System

There are several measurements which could be added or modified to improve the accuracy of results regarding the solar PV system. Firstly, as has already been noted in Chapter 3, the pyranometer used to measure incident solar irradiance should be moved to be closer to the PV array and tilted at the same angle as the panels (36° from horizontal). An example of how this could be done is shown in Figure 4.4 [52]. The example shown is taken from work previously done to evaluate the performance of panels on the roof of the AFV garage adjacent to the house.

Figure 4.4: Pyranometers placed next to solar panels on the AFV garage [52].

This would eliminate the need for a modification of the solar irradiance measurements to account for tilting (as was done in this study using the results from PVWatts) and ensure that the readings provide an accurate representation of the energy available to the solar panels. A more accurate solar irradiance measurement would likely also display a stronger linear correlation between solar irradiance and AC power output, similar to that seen in Figure 4.5 (also taken from the AFV garage study) [52].

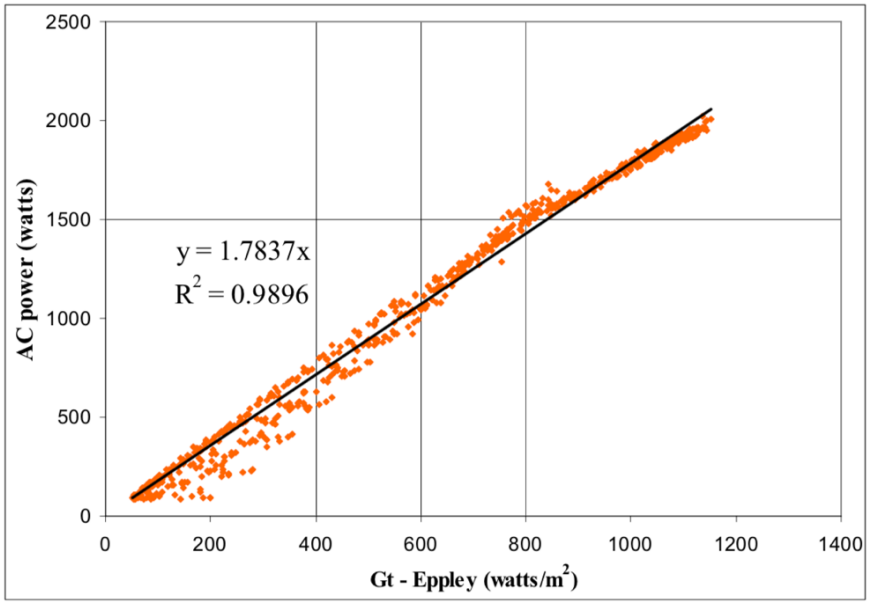

Figure 4.5: Solar irradiance and AC power correlation for the panels on the AFV garage [52].

It would also be desirable to measure the DC current from the array and its operating DC voltage (upstream from the inverter). With this measurement in hand, it would be possible to calculate the DC power produced by the array without assuming an efficiency for the inverter to "back out" a value from the AC power measurement (as was done in this study). With AC and DC power measurements, the inverter efficiency may be determined to evaluate how closely it performs to the manufacturer's rating. Performance parameters which depend upon DC power and energy measurements (such as array yield and module efficiency) may also be calculated more accurately in this case. This would greatly assist in assessing the operational performance of the array itself, without effects from the rest of the system.

Although ambient temperature is currently recorded at the house's weather station, it would be advantageous to monitor the temperature of the panels directly. This may be achieved by placing a thermocouple on the back of one or more of the panels. This would allow for an assessment of the AC power production's dependence on panel temperature, which may then be compared to the manufacturer's given temperature coefficient (-0.38% / K) [53]. As noted in

Chapter 3, wind speed is also currently being measured by the weather station at the house, but at a location which does not represent the conditions experienced by the array. Like the pyranometer, the anemometer should be placed as close to the array as possible. Examination of the relationship between panel temperature, wind speed, ambient temperature, and solar irradiance levels would provide useful insight. An example plot from Ayompe et al. is shown below in Figure 4.6 [24].

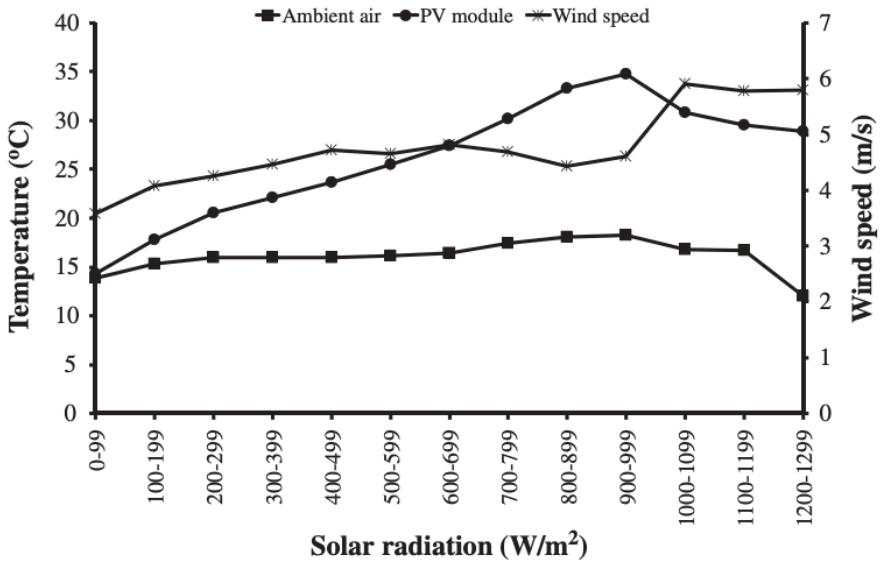

Figure 4.6: Example plot of the interdependence of solar radiation, wind speed, and ambient air temperature on PV array temperature [24].

There is a significant amount of work which may be done to assess the performance of the individual panels in the array. In order for this work to be done however, further knowledge regarding the system's layout and interconnections must be obtained. For example, the exact circuit wiring of the panels (i.e. how many are in series or parallel with each other) is not currently known. With this information, additional performance testing will be possible. A current monitoring box (such as the one shown in Figure 4.7) may be set up in order to monitor the output from subsets of panels. In the setup shown below, 24 panels were connected in series

pairs (termed “circuits”) [52]. The current from each circuit was sent through a resistor with a known resistance value. By measuring the voltage drop across each resistor, the current output was then found using Ohm’s law.

Figure 4.7: Monitoring box used in a previous study to monitor current from panels on roof of the AFV garage [52].

This comparison of current output would be helpful in determining if some panels at the house are underperforming compared to others. DC voltage and current measurements of individual panels would also allow for the generation of current-voltage (I-V) curves. I-V curves are obtained by connecting the array/panel to a variable resistor at some constant condition of solar irradiance and cell temperature, then recording voltage measurements as the resistance is varied [10]. The rated I-V curve provided by for the SunPower SPR-225 panels is shown in Figure 4.8 [12].

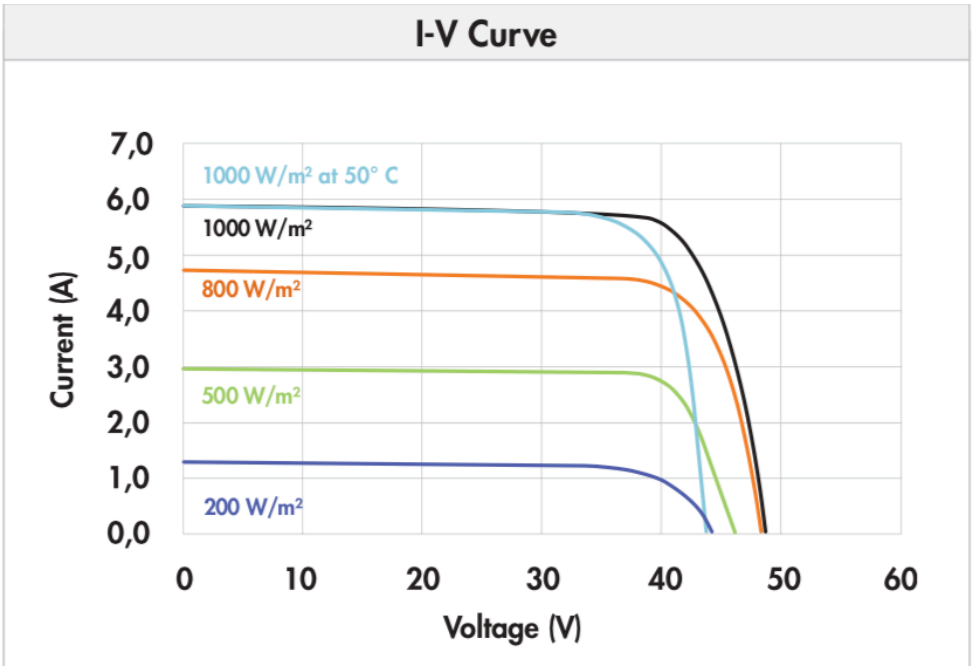

Figure 4.8: Current-voltage curve for SPR-225 panels [12].

The effect of controlled shading may be investigated also. Tests similar to those performed in [52] would provide an understanding of how different levels of shading effect the output of the array. The tests in this previous study involved shading different amounts of a solar panel contained in an array (from 0 to 6.8%) and observing the effect on panel current and voltage [52]. These previous tests were done on the amorphous silicon panels located on the AFV garage. Testing on the monocrystalline SPR-225 panels would therefore provide new information which would allow for comparison between two types of PV panels.

Additionally, a small battery bank could be added to the PV system to investigate its impact on the house's demand. As rebates for grid-fed electricity generation and PV system installations decline worldwide, usage of energy storage for local use has become more prevalent [54]. For example, the Tesla Powerwall 2 is a compact residential battery storage system that is installed with an accompanying Tesla Backup Gateway unit which uses automated control strategies to manage charging and discharging [55]. As shown in Figures 4.9 and 4.10, the

Powerwall contains an integrated inverter and is connected to the main electrical panel of a home [55], [56]. The inverter converts the incoming AC power to DC power for storage, then reconverts it back to AC power to provide energy to the home. These conversions translate to a roundtrip efficiency of 90% for the Powerwall 2 [55].

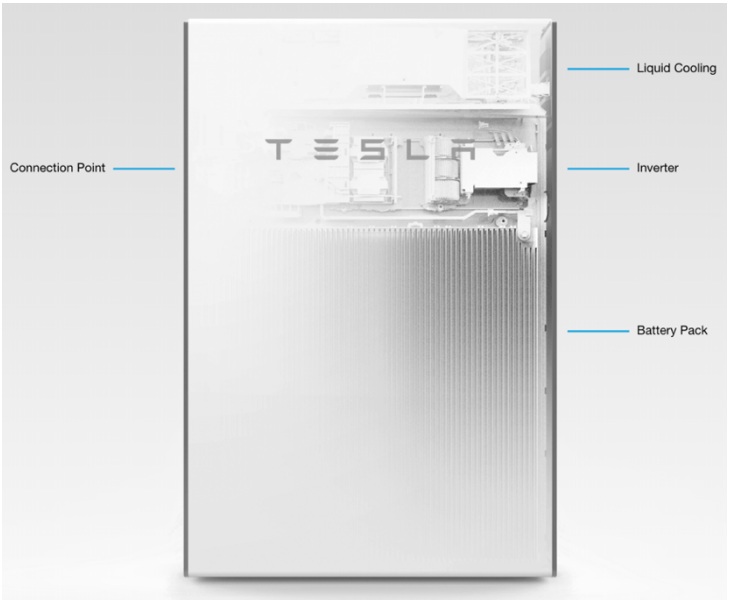

Figure 4.9: Schematic of the Tesla Powerwall 2 battery pack [55].

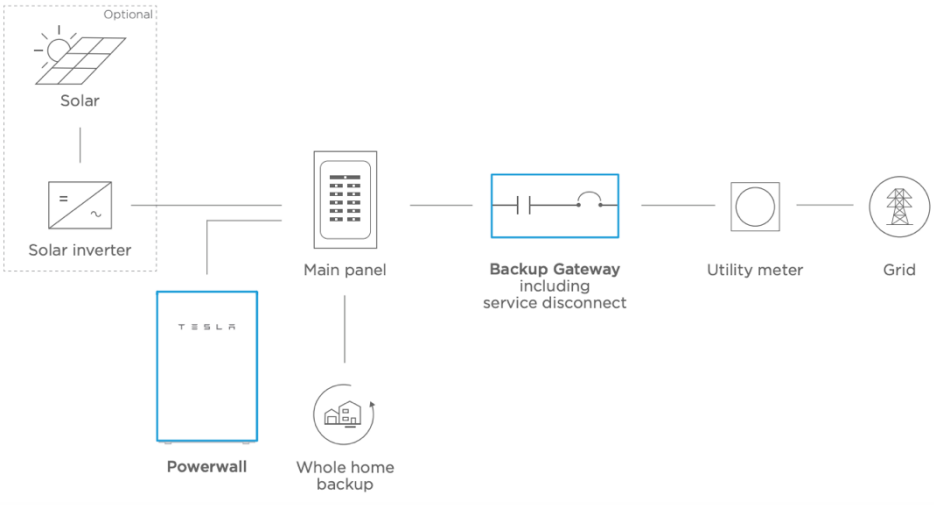

Figure 4.10: "Whole home backup" system layout for Tesla Powerwall 2 [56].

Powerwall control strategies include: “Backup Only”, “Self-Powered”, and two “advanced time-based methods” termed “Balanced” and “Cost-Saving” [57]. Backup Only mode will charge the battery and only discharge during outages, while Self-Powered mode stores excess energy generated by the PV array during the day then discharges it when the sun goes down [57]. For a residential rate schedule such as Duke Energy Progress RES-53, Self-Powered mode would be the preferable operating mode. However, if a time-of-use schedule is used, the time-based control methods would be optimal. With a time-of-use schedule, the customer is charged more for electricity provided by the utility if it is provided during “on-peak” times. The time-based control methods allow the user to input their specific on- and off-peak times and adjusts the charging and discharging of the battery accordingly [57]. The Balanced strategy prioritizes charging the battery when excess solar energy is being generated, then uses this excess energy to power the home when either: (a) electricity is “on-peak” or (b) when the sun goes down [57]. Alternatively, the Cost-Saving strategy will charge the battery with either solar or grid-provided “off-peak” energy, then discharge during “on-peak” times [57]. Note that all PV-generated electricity at the NCSU Solar House is currently fed directly to the grid (i.e. it does not power anything at the house directly). In order to install the Tesla Powerwall system, the system would need to be rewired so that the power from the PV panels feeds into the main electrical panel of the house. North Carolina did not allow net-metering at the time when the initial PV system was installed at the house. Therefore, the house was (and still is) set up with two separate meters. One meter measures the energy being sent to the grid from the panels, while the other measures incoming energy from the grid to the house. Figure 4.11 is a picture of the current metering setup at the house, with the red and green lines depicting the incoming electricity from the grid to the house and the electricity produced by the PV array, respectively.

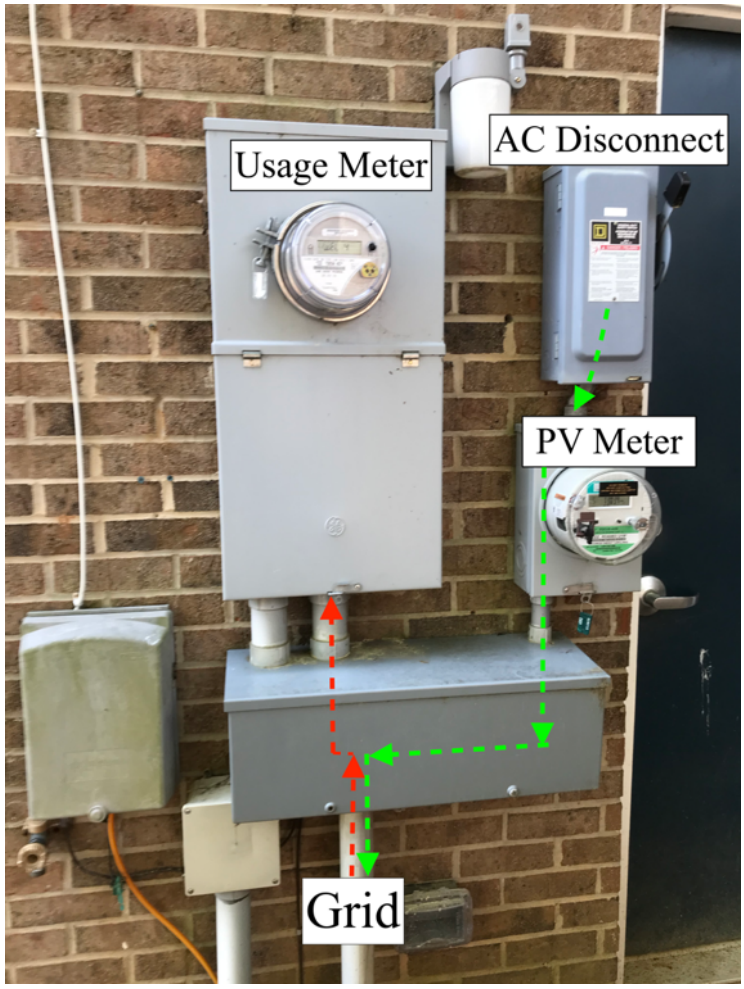

Figure 4.11: Energy metering setup at the house.

In North Carolina, customers may participate in net metering, which allows them to offset monthly electricity bills by the amount of generated energy provided to the grid [58]. In the absence of a time-of-use rate schedule, net metering does not provide an incentive for residential energy storage [59]. Customers in North Carolina may reduce their kWh usage bill by the amount of kWh they produce during the billing cycle. If excess energy is produced, credits for this energy may be carried over to future months until May 31st, when all excess energy is reset to zero [60]. These net metering practices apply whether or not a time-of-use rate schedule is used [60]. If a time-of-use rate schedule is used, implementation of energy storage may still be

beneficial, as the customer may be able to shift their usage away from “on-peak” times and also shift their exportation of energy to the grid to “on-peak” times (when energy is more valuable).

Net metering is currently available in forty-four out of fifty states in the U.S. [61]. Of these forty-four states, twenty-five of them currently have some type of restriction on their net metering practices [61]. These restrictions include peak demand and total installed capacity caps [61]. Additionally, three states have “trigger policies” which allow the legislature to review current net metering regulations and make changes if deemed necessary [61]. North Carolina currently has no restrictions or trigger policies related to net metering, but this may not always be the case. Duke Energy customers in South Carolina recently reached a 2% total generation capacity cap last year [62]. Due to concerns from energy utilities regarding lost revenue from net metering, many more states may see restrictions implemented in the near future. Residential energy storage which limits interactions with the grid could benefit utility providers by reducing the required capacity of transmission equipment and also reducing the need for the addition of new generating capacity to meet peak demand loads [59].

For the reasons mentioned above, the installation of a battery pack system at the NCSU Solar House could lead to interesting and beneficial research. It is important to note that adding energy storage under the current time-independent rate schedule used at the NCSU Solar House would most likely increase utility bills. The house operates on net-metering - each kWh of energy is sent to the grid and holds the same value as the energy consumed from it. If energy storage is added, some of the energy generated by the panels will be lost due to battery system inefficiencies. Because this lost energy could have been sent to the grid for a fixed credit amount, overall cost will increase. Additionally, it has been found that implementation of Lithium-ion storage increases grid energy consumption by homes due to the inherent energy usage by the battery system each time it charges and discharges [59]. Fares and Webber found that for 99

homes studied in Texas, the addition of Lithium-ion battery storage with rated power capacity of 3.3 kW, rated energy capacity of 7 kWh, and a roundtrip efficiency of 85% to pre-existing solar PV systems would yield an annual energy consumption increase between 8-14%, depending on the control method used [59]. The same model also found an increase in emissions of CO_2, SO_2, and NO_x due to this increased energy consumption and also the fact that energy storage shifts times of electricity demand, which changes the generators (coal, natural gas, etc.) used to meet this demand [59]. Multiple simulations have been performed regarding implementation of residential battery storage systems for locations around the world, including Germany, Portugal, and several U.S. states [54], [63]. A specific study on an installed system would provide valuable real-world results that would aid in informing the local public on benefits and drawbacks of similar systems.

Another option for storing energy produced by the PV array is chilled water. This would involve using the excess electricity produced during peak sunlight or off-peak electricity rate times to run a vapor-compression chiller, then storing that chilled water to be used later in the day for cooling. One example of this is the system proposed by Serag-Eldin for cooling a middle-eastern residence [64]. This design is an efficient and environmentally-friendly multi-tank system which is buried underneath the basement floor in order to reduce heat infiltration from the environment [64]. The system presented may also be used with an absorption chiller which is directly run by solar thermal energy [64]. For the PV system case, it is predicted that the proposed chilled water storage system would be much more efficient and cost-effective than traditional battery storage, as the theoretical efficiency is given as 98% [64]. Although the cost to implement a similar system at the NCSU Solar House would most likely be high, there would be a unique opportunity to study the effectiveness of chilled water storage vs. the battery storage mentioned previously.

4.3 Solar Water Heating System

Similar to the solar PV system, there is great potential for further understanding of the solar water heating system's performance with the addition of a few key parameter measurements. Perhaps the most critical of these is the volumetric flow rate of the propylene glycol in the collector loop. This will require the installation of a flow meter somewhere on the piping which contains the propylene glycol solution. To evaluate the amount of solar radiation collected by the FPC on the rooftop, temperature measurements should be taken of the glycol just prior to entering the collector and just after exiting, as shown below in Equation 4.1 [17].

$$\dot{Q}_c = \dot{m}_g C_p (T_{\mathrm{c,o}} - T_{\mathrm{c,i}}) \tag{4.1}$$

Where: $\dot{m}_g$, C_p, $T_{c,o}$ and $T_{c,i}$ are the mass flow rate, constant-pressure specific heat, collector exit temperature, and collector inlet temperature of the glycol solution, respectively. The $\dot{Q}_c$ term is the instantaneous power collected by the solar collector. The total energy collected may be found by evaluating Equation 4.1 over a defined time period. The power delivered to the hot water storage tank may also be calculated using Equation 4.2 [31].

$$\dot{Q}_d = \dot{m}_g C_p (T_{\mathrm{hx,o}} - T_{\mathrm{hx,i}}) \tag{4.2}$$

Where: $T_{hx,o}$ and $T_{hx,i}$ are the temperatures exiting and entering the heat exchanger surrounding the hot water storage tank, respectively. Note that these two temperatures are already being monitored as glycol supply (into tank) and return (to the collector) temperatures. Finally, the addition of the flow rate and collector inlet/outlet temperature measurements will allow for calculation of supply line losses from the collector outlet to the tank inlet, as shown below in Equation 4.3 [31].

$$\dot{Q}_L = \dot{m}_g C_p (T_{\mathrm{hx,i}} - T_{\mathrm{c,o}}) \tag{4.3}$$

Results from the calculations shown above may be used with measures of the auxiliary energy consumed by the backup electrical heating element in the storage tank to determine the

solar fraction of the system for a given time period. The solar fraction (as shown in Equation 4.4) is the portion of the total heating energy requirements that is fulfilled by the delivered energy from the glycol loop [65].

$$SF = \frac{Q_d}{Q_d + Q_{\text{aux}}} \tag{4.4}$$

In the equation above, Q_{aux} is the energy used by the backup heating element and Q_d is the energy supplied by the glycol loop.

In addition to the parameters above, the efficiency of the solar collector and the overall system may be calculated using solar insolation data (provided that the pyranometer location is adjusted as noted in section 4.1). Collector efficiency is found using Equation 4.5 [28], [66].

$$\eta_c = \frac{\dot{Q}_c}{A_c G} \tag{4.5}$$

The terms A_c and G are the area of the collector and solar irradiance, respectively. System efficiency is calculated as [28], [66]:

$$\eta_s = \frac{\dot{Q}_d}{A_c G} \tag{4.6}$$

In order for the calculations above to be useful, the operation of the house would need to be changed in order to more accurately reflect typical domestic hot water use. To do this, one solution is to implement an automatic draw-off system. An example of one such system is that used in [31], which uses a programmable logic controller (PLC), solenoid valves, and impulse flow meters to regulate draw-offs which follow a specified demand profile. Refer to Figure 2.2 for the overall schematic used in that study. Figures 4.12 and 4.13 show the PLC operational flow chart and hot water demand profile used in the study, respectively [31], [34].

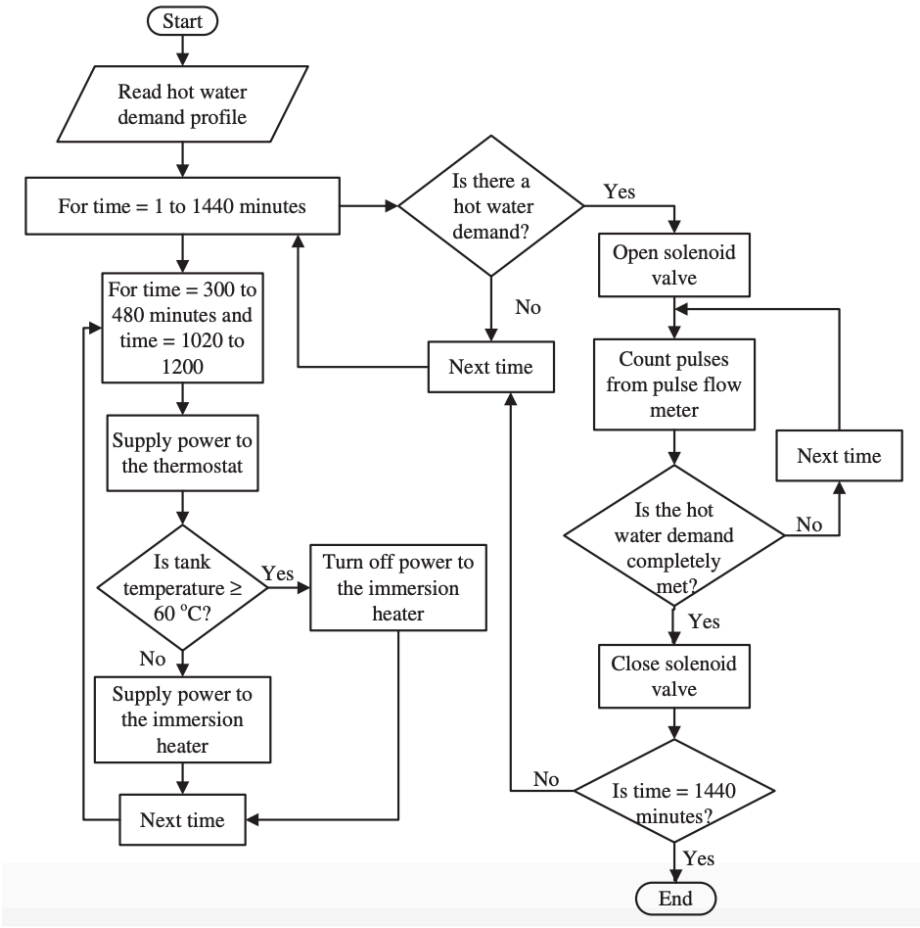

Figure 4.12: PLC operational flow chart for automatic draw-off system [31].

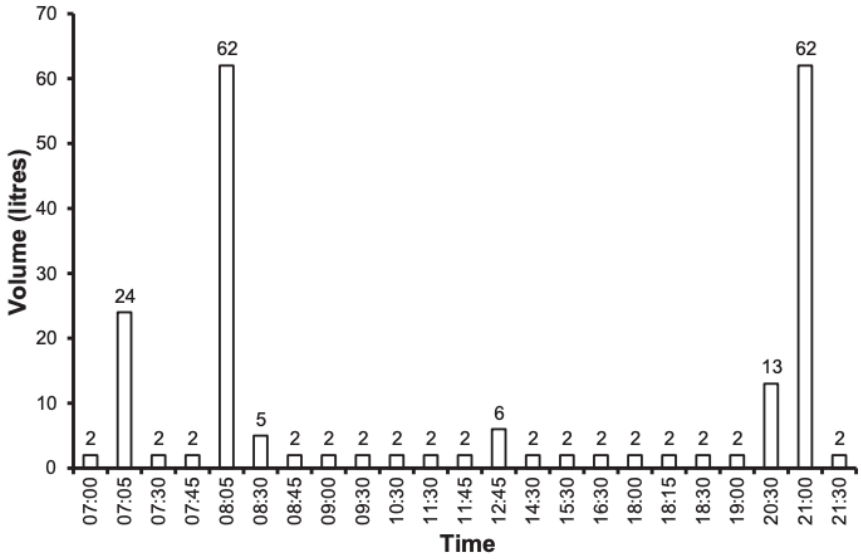

Figure 4.13: EU reference tapping cycle number 3 [31], [34].

The demand profile shown is for a typical household consumption in Europe. For the NCSU Solar House system, it is important to use a demand profile representative of the area. A comparison of hot water demand profiles commonly employed for testing purposes in the United States has been carried out in [67]. They recommend either the demand profile given by ASHRAE Standard 90.2 or Becker be used to analyze performance of hot water heating systems [68]. A comparison of these two profiles against another commonly used profile is seen below in Figure 4.14.

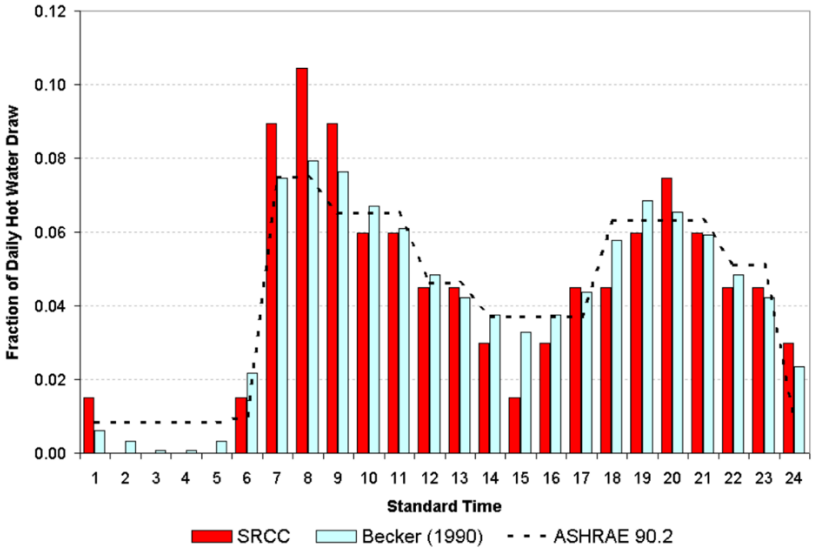

Figure 4.14: Comparison of commonly used hot water demand profiles [67].

The values seen in Figure 4.14 above show the fraction of daily hot water consumption that occurs at each hour during the day. To use these values in an automated draw off system, they must be multiplied by the average daily hot water usage for the area where the system is installed. The Becker (1990) profile is derived partially from data obtained by Merrigan from 24 domestic solar water heating systems installed in North Carolina homes during 1985 [69]. One result from this study was that the average daily hot water consumption for these homes was 56.9 gallons (215 L) [69].

4.4 Overall House Recommendations

The suggestions presented above which relate directly to the solar PV and solar water heating systems provide ample opportunities for investigation in the future. Still, there are other avenues of research which focus on the overall performance of the house. This section presents some of those ideas.

One area of study which remains interesting is determining the overall effective thermal mass of the house. The NCSU Solar House sunspace contains a large amount of heavy materials (masonry, tiles, etc.) which were included for their ability to store heat and re-release it over time. The effective thermal mass of the house could be evaluated by estimating the amount of energy entering the house over a certain time period and noting the observed temperature difference. The effects of the internal thermal mass have been somewhat indirectly explored previously [2], [4]. However, a study directed solely at monitoring the house's indoor temperature response to varying outdoor conditions would be useful to anyone interested in its design. A study of this nature may include observations of the maximum indoor temperature reached on days during the summer or the amount of energy required to maintain a certain preset thermostat temperature. Correlations could then be found between these data and the temperature swing from the night before. Also, the amount of ventilation used at night to remove heat from the thermal mass may be varied by opening windows or running the fan in the air conditioning system. Simulation models for these situations may also be developed, as was done by Shaviv, Yezioro, and Capeluto for apartment buildings located in different areas of Israel [70]. Additional moveable thermal mass could also be brought in as needed to examine its effect on energy usage. Much of the previous work regarding the house's performance thus far has focused on heating season performance, with further analysis in the cooling season still needed.

Additionally, varying cooling strategies may be tested at the house and compared to predicted results from programs such as EnergyPlus. These strategies may include setting the thermostat at a constant temperature throughout the day or pre-cooling the house during certain chosen periods of the day and measuring the cooling energy used by the house for each scenario [71]. A model of the house may then be built in EnergyPlus based on observed indoor and outdoor parameters from the testing days such as ambient temperature, solar irradiance, relative humidity, and wind speed. Simulation predictions can then be compared to experimental results. If high enough accuracy is achieved by the model, the simulations could be carried out further to predict energy use for an entire cooling season [71].

Finally, the solar PV system on the nearby AFV garage (now being used as a classroom space) may be evaluated. The most recent study concerning the performance of this system was conducted in 2007 [52]. Unfortunately, much of the equipment (shown below in Figure 4.15) required for this system to operate has since been removed. If the necessary equipment were reinstalled, tests similar to those completed before could be done, and the results compared. This would allow assessment of the degradation of the panels over a long period of time.

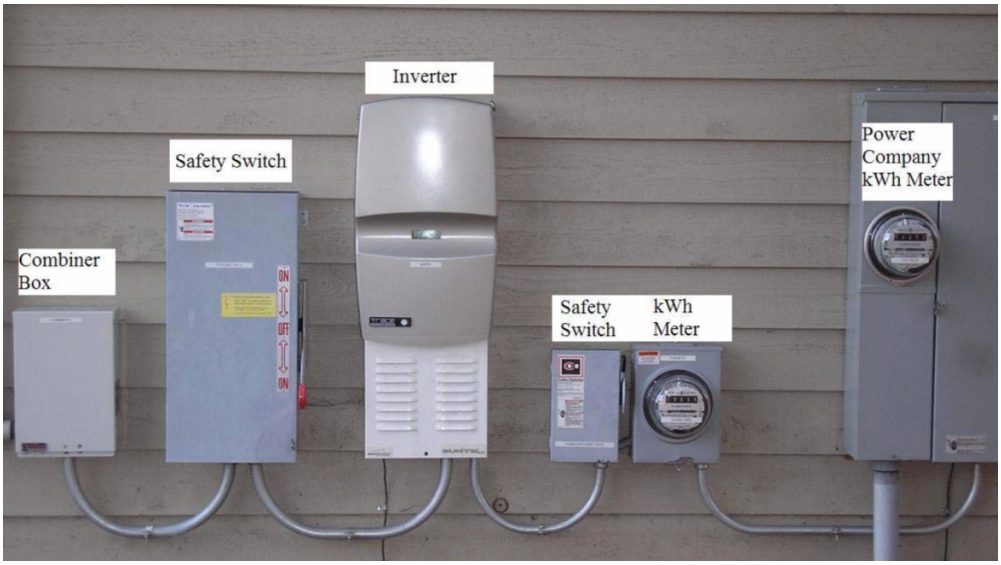

Figure 4.15: Power conditioning equipment at AFV garage which has been removed [52].

Storage systems similar to those mentioned earlier in this chapter could be adopted for the garage, as well as energy modeling techniques. Due to their close vicinity to each other, comparisons made between some aspects of the garage and house performance may be appropriate.

The recommendations made in this chapter provide an overview of the possibilities for future research surrounding the NCSU Solar House. There is clearly a myriad of opportunity for future students to investigate the performance of the house (provided the needed equipment additions). It is hoped that the house will continue to serve as an experimental resource and provide results useful to those interested in solar energy.

REFERENCES

[1] H. M. Eckerlin and A. S. Boyers, “The NCSU Solar House: A Guide to Passive Solar Design in the Southeast,” in *Progress in Solar Energy, AS/ISES Annual Conference*, 1982, pp. 121–126.

[2] J. M. DeCicco, “Thermal performance evaluation of the NCSU Solar House : heating season results and data analysis,” North Carolina State University, 1983.

[3] J. F. Simon, “Performance of the passive solar elements of the NCSU Solar House,” North Carolina State University, 1984.

[4] W. F. Brooks, “An experimental determination of the building loss coefficient and overall heating season performance for the NCSU solar house,” North Carolina State University, 1992.

[5] D. H. Nielsen, “An experimental performance analysis of southern exposure frame walls, trombe walls, and sunspace interface walls at the North Carolina State University solar house,” North Carolina State University, 1988.

[6] DOE, “The History of Solar Energy.” [Online]. Available: https://www1.eere.energy.gov/solar/pdfs/solar_timeline.pdf.

[7] DOE, “Solar Photovoltaic Cell Basics,” 2013. [Online]. Available: https://www.energy.gov/eere/solar/articles/solar-photovoltaic-cell-basics.

[8] P. Hersch and K. Zweibel, “Basic photovoltaic principles and methods,” Golden, CO, Feb. 1982.

[9] C. R. Nave, “The P-N Junction.” [Online]. Available: http://hyperphysics.phy-astr.gsu.edu/hbase/Solids/pnjun.html.

[10] DOE, “Solar Performance and Efficiency,” 2013. [Online]. Available: https://www.energy.gov/eere/solar/articles/solar-performance-and-efficiency.

[11] E. Franklin, “Solar Photovoltaic (PV) System Components,” 2018. [Online]. Available: https://extension.arizona.edu/sites/extension.arizona.edu/files/pubs/az1742-2018.pdf.

[12] SunPower Corporation, “225 Solar Panel,” 2009. [Online]. Available: http://static1.squarespace.com/static/550788b1e4b0985f434d4037/551aefb0e4b0f1d203c9ee82/551aefb0e4b0f1d203c9ee93/1266328680000/Datasheet-SPR-225-BLK-U.pdf?format=original.

[13] North Carolina Solar Center, “NCSU Solar House Information.” Raleigh, NC.

[14] North Carolina Solar Center, “The N.C. State University Solar House, 1981-2006.” Raleigh, NC, 2006.

[15] SunPower Corporation, “5000m, 6000m & 7000m Inverters,” 2007. [Online]. Available: http://www.sunlightsolar.com/img/sunpower-inverter.pdf.

[16] N. V. Ogueke, E. E. Anyanwu, and O. V. Ekechukwu, “A review of solar water heating systems,” *J. Renew. Sustain. Energy*, vol. 1, no. 4, Jul. 2009.

[17] S. A. Kalogirou, *Solar Energy Engineering - Processes and Systems*, 2nd ed. Elsevier, 2014.

[18] J. Gong and K. Sumathy, “Active solar water heating systems,” *Adv. Sol. Heat. Cool.*, pp. 203–224, Jan. 2016.

[19] Schüco USA L.P., “Schüco Slim V Plus,” 2008. [Online]. Available: http://sunlightsolar.com/cms/wp-content/uploads/schucco-slim-v.pdf.

[20] RESOL – Elektronische Regelungen GmbH, “DeltaSol BS/2.” [Online]. Available: https://www.resol.de/Produktdokumente/48005952_DeltaSol_BS2_V2.monen.pdf.

[21] DOE, “Passive Solar Home Design.” [Online]. Available: https://www.energy.gov/energysaver/energy-efficient-home-design/passive-solar-home-design.

[22] J. M. DeCicco, H. M. Eckerlin, and A. S. Boyers, “Heating Season Performance and Thermal Characteristics of the NCSU Solar House,” in *Progress in Passive Solar Energy Systems*, 1983, pp. 327–332.

[23] B. Marion *et al.*, “Performance parameters for grid-connected PV systems,” in *Conference Record of the Thirty-first IEEE Photovoltaic Specialists Conference, 2005.*, 2005, pp. 1601–1606.

[24] L. M. Ayompe, A. Duffy, S. J. McCormack, and M. Conlon, “Measured performance of a 1.72 kW rooftop grid connected photovoltaic system in Ireland,” *Energy Convers. Manag.*, vol. 52, no. 2, pp. 816–825, Feb. 2011.

[25] R. N. Dows and E. J. Gough, “PVUSA procurement, acceptance, and rating practices for photovoltaic power plants,” Albuquerque, NM, Sep. 1995.

[26] California Energy Commission, “PV Modules,” 2019. [Online]. Available: https://www.gosolarcalifornia.org/equipment/pv_modules.php.

[27] E. Kymakis, S. Kalykakis, and T. M. Papazoglou, “Performance analysis of a grid connected photovoltaic park on the island of Crete,” *Energy Convers. Manag.*, vol. 50, no. 3, pp. 433–438, Mar. 2009.

[28] J. A. Duffie and W. A. Beckman, *Solar Engineering of Thermal Processes*, 3rd ed. New York, NY: Wiley, 2006.

[29] J. D. Mondol, Y. G. Yohanis, and B. Norton, “The effect of low insolation conditions and inverter oversizing on the long-term performance of a grid-connected photovoltaic system,” *Prog. Photovoltaics Res. Appl.*, vol. 15, no. 4, pp. 353–368, Jun. 2007.

[30] Rheem Water Heating, “Solaraide HE,” 2008. [Online]. Available: https://www.discountsolarwaterheaters.com/wp-content/uploads/Rheem-HX.pdf.

[31] L. M. Ayompe and A. Duffy, “Analysis of the thermal performance of a solar water heating system with flat plate collectors in a temperate climate,” *Appl. Therm. Eng.*, vol. 58, no. 1–2, pp. 447–454, Sep. 2013.

[32] M. C. Rodríguez-Hidalgo, P. A. Rodríguez-Aumente, A. Lecuona, and J. Nogueira, “Instantaneous performance of solar collectors for domestic hot water, heating and cooling applications,” *Energy Build.*, vol. 45, pp. 152–160, Feb. 2012.

[33] ASHRAE, “ANSI/ASHRAE Standard 93-2003, Methods Of Testing To Determine The Thermal Performance Of Solar Collectors.” Atlanta, GA, 2003.

[34] CEN, “European Standard EN12975-2:2001, Thermal Solar Systems and Components – Solar Collectors – Part 2: Test Methods.” Brussels, Belgium, 2001.

[35] D. Rojas, J. Beermann, S. A. Klein, and D. T. Reindl, “Thermal performance testing of flat-plate collectors,” *Sol. Energy*, vol. 82, no. 8, pp. 746–757, Aug. 2008.

[36] L. M. Ayompe, A. Duffy, M. McKeever, M. Conlon, and S. J. McCormack, “Comparative field performance study of flat plate and heat pipe evacuated tube collectors (ETCs) for domestic water heating systems in a temperate climate,” *Energy*, vol. 36, no. 5, pp. 3370–3378, May 2011.

[37] A. Hargrave, M. J. Thompson, and B. Heilman, “Beyond the knee point: A practical guide to CT saturation,” in *2018 71st Annual Conference for Protective Relay Engineers (CPRE)*, 2018, pp. 1–23.

[38] M. Z. Jacobson and V. Jadhav, “World estimates of PV optimal tilt angles and ratios of sunlight incident upon tilted and tracked PV panels relative to horizontal panels,” *Sol. Energy*, vol. 169, pp. 55–66, Jul. 2018.

[39] NREL, “PVWatts.” Golden, CO, 2016.

[40] Continential Control Systems LLC, “Inverter Power Factor.” [Online]. Available: https://ctlsys.com/support/inverter-power-factor/.

[41] DOE, “Reducing Power Factor Cost.” [Online]. Available: https://www.energy.gov/sites/prod/files/2014/04/f15/mc60405.pdf.

[42] The OWL, “PV generation readings / data inaccurate,” 2018. [Online]. Available: https://theowl.zendesk.com/hc/en-gb/articles/201284733-PV-generation-readings-data-inaccurate.

[43] University of Oregon Solar Radiation Monitoring Laboratory, “Sun path chart program,” 2007. [Online]. Available: http://solardat.uoregon.edu/SunChartProgram.html.

[44] E. Mazria, *The Passive Solar Energy Book*. Emmaus, PA: Rodale Press, 1979.

[45] Photovoltaic Power Systems Programme, “Cost and Performance Trends in Grid-Connected Photovoltaic Systems and Case Studies,” 2007.

[46] G. Blaesser, “PV system measurements and monitoring the European experience,” *Sol. Energy Mater. Sol. Cells*, vol. 47, no. 1–4, pp. 167–176, Oct. 1997.

[47] A. Athienitis, *Thermal Analysis and Design of Passive Solar Buildings*, 1st ed. London, UK: James and James LTD, 2002.

[48] EnergySage, “Local Data on Solar panels in North Carolina,” 2019. [Online]. Available: https://www.energysage.com/solar-panels/nc/.

[49] DSIRE, “Residential Renewable Energy Tax Credit,” 2018. [Online]. Available: http://programs.dsireusa.org/system/program/detail/1235.

[50] Duke Energy Progress LLC, “Residential Service Schedule RES-53,” 2019. [Online]. Available: https://www.duke-energy.com/_/media/pdfs/for-your-home/rates/electric-nc/r1ncscheduleresdep.pdf?la=en.

[51] SunPower Corporation, “Home Solar System Warranty.” [Online]. Available: https://us.sunpower.com/home-solar-system-warranty.

[52] D. W. Christy, “An Experimental Evaluation of the Performance of the Amorphous Silicon PV Array on the NCSU AFV Garage,” North Carolina State University, 2007.

[53] SunPower Corporation, “225 Solar Panel,” 2007. [Online]. Available: http://sunlightsolar.com/img/spwr-225-spec-sheet.pdf.

[54] S. Rodrigues *et al.*, “TESLA POWERWALL: ANALYSIS OF ITS USE IN PORTUGAL AND UNITED STATES,” *Int. J. Power Energy Syst.*, vol. 36, no. 1, 2016.

[55] Tesla Inc., “Powerwall,” 2019. [Online]. Available: https://www.tesla.com/powerwall.

[56] Tesla Inc., “Tesla Powerwall 2 Datasheet,” 2018. [Online]. Available: https://www.tesla.com/sites/default/files/pdfs/powerwall/Powerwall 2_AC_Datasheet_en_northamerica.pdf.

[57] Tesla Inc., “Mobile App Overview,” 2019. [Online]. Available: https://www.tesla.com/support/energy/powerwall/mobile-app/mobile-app-overview.

[58] Database of State Incentives for Renewables and Efficiency (DSIRE), “Net Metering,” 2017. [Online]. Available: http://programs.dsireusa.org/system/program/detail/1246.

[59] R. L. Fares and M. E. Webber, “The impacts of storing solar energy in the home to reduce reliance on the utility,” *Nat. Energy*, vol. 2, no. 2, 2017.

[60] Duke Energy Progress LLC, “Net Metering for Renewable Energy Facilities Rider NM-4B,” 2019. [Online]. Available: https://www.duke-energy.com/_/media/pdfs/rates/rr3-nc-rider-nm-dep.pdf?la=en.

[61] J. Heeter, R. Gelman, and L. Bird, “Status of Net Metering: Assessing the Potential to Reach Program Caps,” Golden, CO, 2014.

[62] I. Gheorghiu, “Duke region hits South Carolina net metering cap,” *Utility Dive*, 2018. [Online]. Available: https://www.utilitydive.com/news/duke-region-hits-south-carolina-net-metering-cap/527718/.

[63] C. Truong *et al.*, “Economics of Residential Photovoltaic Battery Systems in Germany: The Case of Tesla’s Powerwall,” *Batteries*, vol. 2, no. 2, p. 14, May 2016.

[64] M. A. Serag-Eldin, “Design of a chilled-water storage unit for solar air-conditioning,” *Int. J. Sustain. Energy*, vol. 32, no. 5, pp. 385–405, Oct. 2013.

[65] The German Solar Energy Society, *Planning and Installing Solar Thermal Systems: A Guide for Installers, Architects, and Engineers*, 1st ed. London, UK: James and James LTD, 2005.

[66] S. P. Sukhatme, *Solar Energy: Principles of Thermal Collection and Storage*, 2nd ed. New Delhi, India: Tata McGraw-Hill, 1998.

[67] P. Fairey and D. Parker, “Review of Hot Water Draw Profiles Used in Performance Analysis of Residential Domestic Hot Water Systems,” Cocoa, FL, 2004.

[68] B. Becker and K. Stogsdill, “Development of a Hot Water Use Data Base,” in *Annual Meeting of the American Society of Heating, Refrigeration, and Air-Conditioning Engineers (ASHRAE)*, 1990.

[69] T. J. Merrigan, “Residential Hot Water Use in Florida and North Carolina,” *ASHRAE Trans.*, vol. 94 Part 1, 1988.

[70] E. Shaviv, A. Yezioro, and I. Capeluto, “Thermal mass and night ventilation as passive cooling design strategy,” *Renew. Energy*, vol. 24, no. 3–4, pp. 445–452, 2001.

[71] C. Booten and P. C. Tabares-Velasco, “Using EnergyPlus to Simulate the Dynamic Response of a Residential Building to Advanced Cooling Strategies,” in *2nd International Conference on Building Energy and Environment*, 2012.

APPENDICES

Appendix A

SPR-225 Specification Sheet

SUNPOWER™

225 SOLAR PANEL

EXCEPTIONAL EFFICIENCY AND PERFORMANCE

BENEFITS

Highest Efficiency
SunPower™ Solar Panels are the most efficient photovoltaic panels on the market today.

Attractive Design
Unique design combines high efficiency and a sleek, black appearance to blend elegantly with the roof.

More Power
Our panels produce more power in the same amount of space—up to 50% more than conventional designs and 100% more than thin film solar panels.

Reliable and Robust Design
Proven materials, tempered front glass, and a sturdy anodized frame allow panel to operate reliably in multiple mounting configurations.

SPR-225-BLK-U

The SunPower™ 225 Solar Panel provides a revolutionary combination of high efficiency and attractive, sleek appearance. Utilizing 72 back-contact solar cells and a black backsheet, the SunPower 225 blends elegantly with the roof and delivers a total panel conversion efficiency of 18.1%. The panel's reduced voltage-temperature coefficient and exceptional low-light performance attributes provide outstanding energy delivery per peak power watt.

SunPower's High Efficiency Advantage - Up to Twice the Power

	Thin Film	Conventional	SunPower
Peak Watts / Panel	65	170	225
Efficiency	9.0%	13.0%	18.1%
Peak Watts / ft² (m²)	**8 (90)**	**12 (130)**	**17 (181)**

About SunPower

SunPower designs, manufactures and delivers high-performance solar electric technology worldwide. Our high-efficiency solar cells generate up to 50% more power than conventional solar cells. Our high-performance solar panels, roof tiles and trackers deliver significantly more energy than competing systems.

c UL us

Figure A.1: SPR-225 specification sheet, page 1 [12].

SUNPOWER

225 SOLAR PANEL

EXCEPTIONAL EFFICIENCY AND PERFORMANCE

Electrical Data

Measured at Standard Test Conditions (STC): irradiance of 1000W/m², AM 1.5, and cell temperature 25° C

Peak Power (+/-5%)	P_{max}	225 W
Rated Voltage	V_{mpp}	41.0 V
Rated Current	I_{mpp}	5.49 A
Open Current Voltage	V_{oc}	48.5 V
Short Circuit Current	I_{sc}	5.87 A
Maximum System Voltage	UL	600 V
Temperature Coefficients		
	Power	-0.38% / K
	Voltage (V_{oc})	-132.5mV / K
	Current (I_{sc})	3.5mA / K
NOCT		46° C +/-2° C
Series Fuse Rating		20 A

I-V Curve

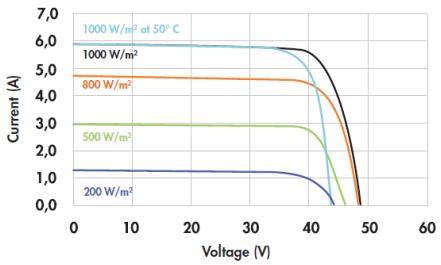

Current/voltage characteristics with dependence on irradiance and module temperature.

Mechanical Data

Solar Cells	72 SunPower all-back contact monocrystalline
Front Glass	High transmission tempered glass
Junction Box	IP-65 rated with 3 bypass diodes Dimensions: 32 x 155 x 128 (mm)
Output Cables	1000mm length cables / MultiContact (MC4) connectors
Frame	Anodized aluminum alloy type 6063 (black)
Weight	33.1 lbs. (15.0 kg)

Tested Operating Conditions

Temperature	-40° F to +185° F (-40° C to + 85° C)
Max load	113 psf 550kg/m² (5400 Pa) front – e.g. snow; 50 psf 245kg/m² (2400 Pa) front and back – e.g. wind
Impact Resistance	Hail 1 in (25 mm) at 52mph (23 m/s)

Warranties and Certifications

Warranties	25 year limited power warranty
	10 year limited product warranty
Certifications	Tested to UL 1703. Class C Fire Rating

Dimensions

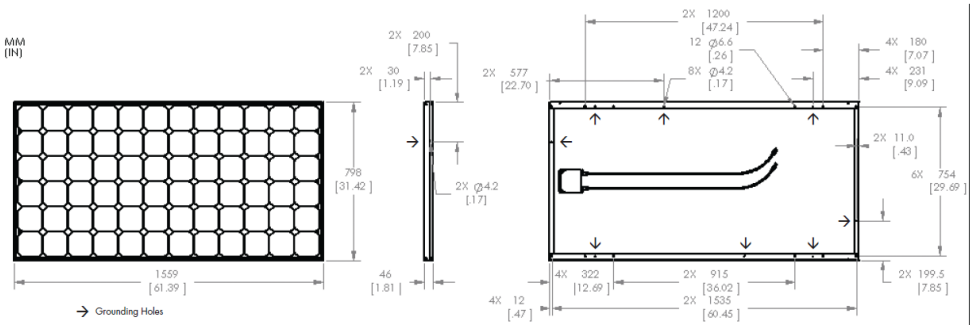

CAUTION: READ SAFETY AND INSTALLATION INSTRUCTIONS BEFORE USING THE PRODUCT.
Visit sunpowercorp.com for details

sunpowercorp.com

Document #001-42188 Rev*B / LTR_EN

Figure A.2: SPR-225 specification sheet, page 2 [12].

Appendix B

SPR-6000m Specification Sheet

SUNPOWER

BENEFITS

Reliable and Robust Design
Proven track record for durability and longevity

Effective Power Range
Enables most systems to use a single inverter rather than multiple units

Commercial Use
Flexible AC voltage output and scalable building blocks create an easy solution for commercial applications

High Efficiency
Weighted CEC efficiency over 95.5% and peak efficiency over 97%

Reduced Installation Cost
Integrated AC-DC disconnect with fuses lowers material costs and labor requirements

Attractive Aesthetics
Integrated disconnect eliminates need for visible conduits to inverter

SPR-5000m, SPR-6000m & SPR-7000m

5000m, 6000m & 7000m INVERTERS

EXCEPTIONAL RELIABILITY AND PERFORMANCE

The SunPower inverters 5000m, 6000m & 7000m provide exceptional reliability and market-leading design flexibility. The SPRm line of Solar Inverters can be easily applied in residential or commercial installations. All models come with a 10-year warranty.

www.sunpowercorp.com

Figure B.1: SPR-6000m specification sheet, page 1 [15].

SUNPOWER

5000m, 6000m & 7000m INVERTERS

EXCEPTIONAL RELIABILITY AND PERFORMANCE

Electrical Data

	SPR–5000m	SPR–6000m	SPR–7000m
AC Power	5000 W	6000 W	7000 W
AC Max Output Current (@ 208V, 240V, 277V):	24A, 20.8A, 18A	29A, 25A, 21.6A	34A, 29A, 25.3A
AC Nominal Voltage / Range	183 – 229 V @ 208 VAC 211 – 264 V @ 240 VAC 244 – 305 V @ 277 VAC	183 – 229 V @ 208 VAC 211 – 264 V @ 240 VAC 244 – 305 V @ 277 VAC	183 – 229 V @ 208 VAC 211 – 264 V @ 240 VAC 244 – 305 V @ 277 VAC
AC Freq / Range	60 Hz / 59.3 Hz – 60.5 Hz	60 Hz / 59.3 Hz – 60.5 Hz	60 Hz / 59.3 Hz – 60.5 Hz
Power Factor	1	1	1
Peak Inverter Efficiency	96.8%	97.0%	97.1%
CEC Weighted Efficiency	95.5 % @ 208 V 95.5 % @ 240 V 95.5 % @ 277 V	95.5 % @ 208 V 95.5 % @ 240 V 96.0 % @ 277 V	96.0 % @ 208 V 96.0 % @ 240 V 96.0 % @ 240V
Recommended Array Input Power (DC @ STC)	5300 W	6400 W	7500 W
DC Input Voltage Range	250 – 600 V	250 – 600 V	250 – 600 V
Peak Power Tracking Voltage	250 – 480 V	250 – 480 V	250 – 480 V
DC Max. Input Current	21 A	25 A	30 A
DC Voltage Ripple	< 5%		
No. of Fused String Inputs	4		
Power Consump: Standby / Nighttime	< 7 W / 0.25 W		
Fused DC & AC Disconnect	Standard; Complies with NEC Standards		
Grounding	Positive Ground		

SPRm Efficiency Curves

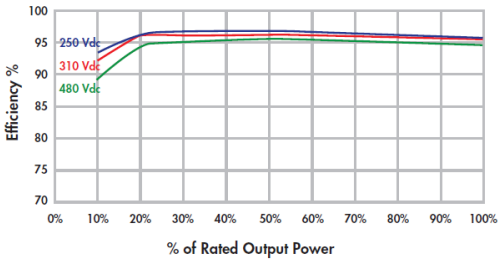

Mechanical Data

Shipping Dimensions W x H x D inches	23.5" x 31.0" x 16.0"
Unit Dimensions W x H x D inches	18.4" x 24.1" x 9.5"
Inverter Weight	143 lbs
Shipping Weight	154 lbs
Cooling	Forced Air / Sealed Electronics Enclosure
Enclosure	NEMA 3R
Mounting	Wall Mount Bracket Standard
Ambient Temperature Range	–13 to +113 °F

Warranty and Certifications

Warranty	10 year limited warranty
Certifications	Compliance: IEEE–929, IEEE–1547, UL 1741–2005, UL 1998, FCC Part 15 A & B

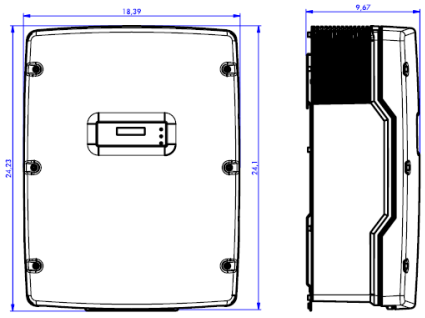

About SunPower

SunPower designs, manufactures and delivers high-performance solar electric technology worldwide. Our high-efficiency solar cells generate up to 50 percent more power than conventional solar cells. Our high-performance solar panels, roof tiles and trackers deliver significantly more energy than competing systems.

Document # 001–16967 Rev **

www.sunpowercorp.com

Figure B.2: SPR-6000m specification sheet, page 2 [15].

Appendix C

Slim V Plus Specification Sheet

Figure C.1: Slim V Plus specification sheet, page 1 [19].

Technical Data

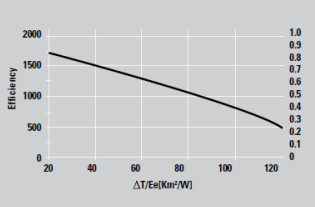

Performance Characteristics

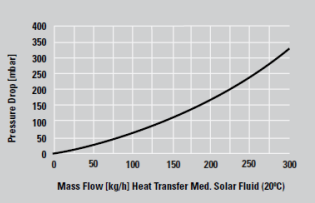

Pressure Drop Characteristics

Thousands of Btu Per Panel Per Day

Category (Ti-Ta)	Clear Day 2000 Btu/ft²·d	Mildly Cloudy 1500 Btu/ft²·d	Cloudy Day 1000 Btu/ft²·d
A (-9°F)	34	25	17
B (9°F)	31	23	15
C (36°F)	27	19	11
D (90°F)	18	10	3
E (144°F)	9	3	

A – Pool Heating (Warm Climate), **B** – Pool Heating (Cool Climate)
C – Water Heating (Warm Climate), **D** – Water Heating (Cool Climate)
E – Air Conditioning

SRCC Collector Thermal Performance Rating

Size:
80.3 x 44.9 x 2.2 in. (2039 x 1140 x 56 mm)
Collector surface area (Ag):
25 sq. ft. (2.32 m²)
Weight (empty): 88 lbs. (40kg)
Efficiency: η_o = 76.7%
Heat loss coefficient:
k_1 = 3.71 W/m²K; k_2 = 0.016 W/m²K²
Incident angle modifier: $k_{(50)}$ = 0.90
Thermal output: 1.64 kW_{th}

Piping configuration: Serpentine
Absorber long-wave emissivity:
ε = 5.0%
Absorber short-wave absorptivity:
α = 95%
Net aperture area:
23.1 sq. ft. (2.148 m²)
Aperture surface area:
23.0 sq. ft. (2.137 m²)
Absorber material: Copper
Absorber Coating:
High selectivity

Heat transfer fluid volume:
0.42 gal. (1.6 L)
Minimum volume flow:
0.66 gal./min (2.5 L/min)
Maximum number of collectors in series: 5

Pressure drop (0.66 gal./min solar fluid):
1.1 psi (78.0 mbar)
Connection:
12.0 mm Cu pipe, serpentine
Connector type:
Compression fitting
Operating pressure:
46.4 psi (3.2 bar)
Maximum operating pressure: 145 psi (10 bar)
Test pressure: 290 psi (20 bar)
Stagnation temperature:
381°F (194°C)
Maximum operating temperature: 248°F (120°C)

Solar glazing:
Low-iron, high-transparency
Transmittance: >91.0%
Thickness: 0.16 in. (4 mm)

Frame Material: Aluminum
Gaskets: EPDM
Thermal Insulation:
0.79 in. (20 mm) mineral wool

Schüco article:
Slim V 232 364
Schüco installation system:
SolarEZ

Specifications subject to change without notice.

Schüco USA L.P.
www.schuco-usa.com

P3252/USA/12.08/Printed in USA

Figure C.2: Slim V Plus specification sheet, page 2 [19].

Appendix D

Solaraide HE 81V80HE-1 Specification Sheet

Solaraide™ HE Solar Heat Exchanger, Solar Tank, or Electric Storage Water Heater

Available in 80 and 120 Gallon Models

▶ **6-Year Limited Tank and Parts Warranty***

- Brass drain valve
- Choice of two models…storage tank or single element water heater specifically engineered for installation with residential indirect solar systems
- Temperature and pressure relief valve included
- Collector feed and return fittings located at front of tank for convenient installation
- Isolated tank design for better heat retention
- High efficiency heating element
- Rheemglas® tank lining resists corrosion and prolongs tank life
- Heat exchanger: copper tubing wrapped around and secured to the tank. Double wall, vented design for positive leak detection
- Cold water inlet brings cold water to tank bottom to prevent mixing with heated water
- Anode rod equalizes aggressive water action for prolonged tank life
- Cold water inlet, hot water outlet, relief valve and anode rod at top of tank for easy access and fast, economical installation
- Automatic temperature control
- Over temperature protector

* See Residential Warranty Information Brochure for complete warranty information.

DESCRIPTION				ROUGHING IN DIMENSIONS (SHOWN IN INCHES)			ENERGY INFORMATION
TYPE	GAL. CAP.	MODEL NUMBER	ELEMENT WATTAGE UPPER	HEIGHT A	DIAMETER B	APPROX. SHIP WT. (LBS.)	APPROX. R-FACTOR
	80	81V80HE-1	4500 W*	58-3/4	24-1/2	222	R-17.3
	80	81V80HE-T	Storage only	58-3/4	24-1/2	222	R-17.3
	120	82V120HE-1	4500 W*	62	28-1/4	380	R-17.3
	120	82V120HE-T	Storage only	62	28-1/4	380	R-17.3

* Heaters furnished with standard 240 volt AC, single phase non-simultaneous wiring and 4500 watt heating element.
- **If heating elements of different wattages than those shown are demanded by zone requirements, they must be specifically requested.**
- To prevent corrosion, proper pH levels in transfer fluid must be maintained.
- Solaraide models meet all current state requirements for solar storage tanks.
- The tanks are Rheemglas lined and are designed to operate up to 150 PSI.

A special 1/2" NPT opening is provided for installation of a "probe type" thermostat.

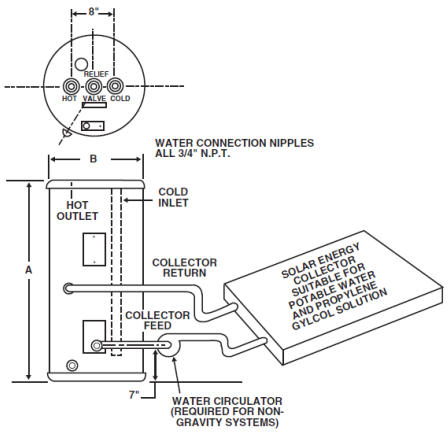

COPPER COIL DATA (Type L Copper)

Maximum pressure = 150 PSI
Maximum temperature = 185° F
Tube I.D. = 5/8"

Solaraide HE Tank Capacity	Coil Capacity Gallons	Length of Tubing Around Tank (Ft)
80 Gallons	2.2	120
120 Gallons	2.6	143

PRESSURE DROP THROUGH COIL (Feet of H_2O)		
	Head Loss (Feet)	
Flow Rate	80 Gallon	120 Gallon
1 GPM	1.3	1.6
2 GPM	4.8	5.7
3 GPM	10.0	12.0

In keeping with its policy of continuous progress and product improvement, Rheem reserves the right to make changes without notice.

Rheem Water Heating • 101 Bell Road, Montgomery, Alabama 36117 • www.rheem.com

PRINTED IN U.S.A 06/08 WP FORM NO. 101-16 Rev. 13

Figure D.1: Solaraide HE 81V80HE-1 specification sheet [30].